UNIVERSITY OF COPENHAGEN
FACULTY OF SCIENCE

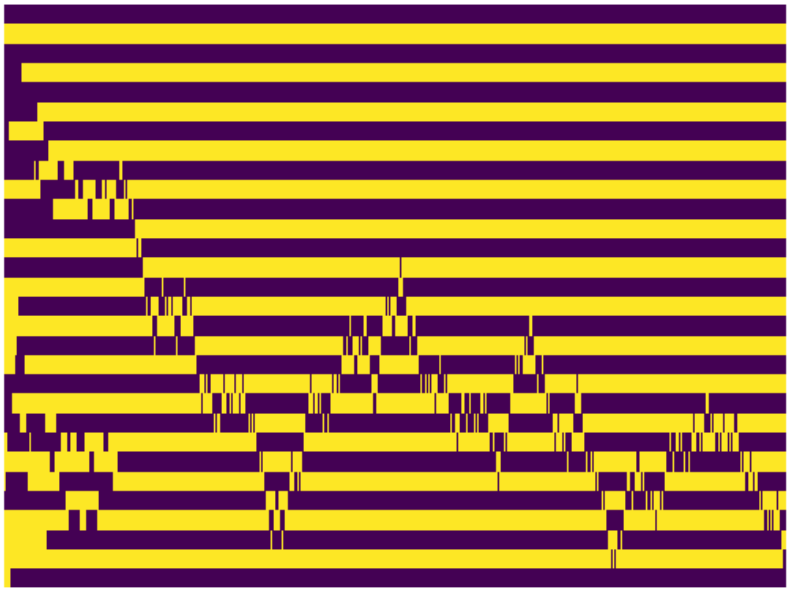

Master thesis

Emil Lytthans Boesen

The (2,N)-Quantum-dot cellular automaton

A study of non-equilibrium dynamics in the Kinetic Ising model

Supervisor: Jens Paaske

Handed in: 03. September - 2021

Abstract (English)

In this master thesis, a special kind of quantum-dot cellular automaton, know as the (2,N)-QDCA, are described and mapped to an anti ferromagnetic, nearest neighbour, quantum Ising model with open boundary conditions. Ignoring the quantum dynamics, the system acts as a classical Ising model in a longitudinal field. The equilibrium properties of the classical Ising model are therefore explored. From statistical average calculations it is shown that for small temperatures and small field, the system localizes around an zero-field AFM ground state. Increasing the field over a certain threshold is predicted to cause the system to localize around a zero-field FM ground state with a magnetization opposite to the field.

To describe the non-equilibrium dynamics of the classical model, the kinetic Ising model is introduced. This allows one to simulate how a given initial configuration will act when coupled to a Glauber heat bath. To simulate this, the Gillespie algorithm is implemented using Cython code and can be using in Python. From numerical results, it is shown that for zero longitudinal fields and zero temperature, the system randomly picks a zero-field AFM ground state, which it decays into. The average decay time is measured to be independent of the initial state in general, and depends on the system size via a power law with an exponent of 2.05188 ± 0.00006. When the field is non-zero but less than a given threshold, any given initial state decays into a disordered state with domain wall in the bulk. At the threshold, domain wall pairs can be created and annihilated spontaneous which introduces an enormous amount of disorder. For fields over the threshold, the system decays into the zero-field FM ground with magnetizations opposite to the field.

In the end of the thesis, the eigenvalues of the quantum Hamiltonian is evaluated semi-analytical.

Resumé (Dansk)

I dette speciale, en type kvant-dot cellulære automater, kaldet (2,N)-QDCA er beskrevet og afbildet til en antiferromagnetisk, nærmest nabo, kvante Ising model med åbne grænse betingelser. Hvis kvantedynamikken ignoreres vil systemet opføre sig som en klassik Ising model i et longitudinalt felt. Ligevægtsegenskaber for denne model er undersøges. For lave temperature og små feltstyrker vil det klassiske systemet lokaliserer sig omkring en de to nul-felts antiferromagnetiske grundtilstands konfigurationer. Er feltet stærkt nok, vil systemet i stedet lokaliserer sig omkring den nul-felts ferromagnetiske grundtilstand, hvis magnetisering er modsat feltet.

Til at beskrive ikke-ligevægtsdynamikken at den klassiske Ising model, introduceres den kinetisk Ising mode. Denne model tillader en af simulerer hvordan en given begyndelsestilstand opfører sig, når den er koblet til et Glauber varmebad. Til simuleringer bruges Gillespie algoritmen, def er implementeret i Cython og kan frit benyttes i Python koder. From numeriske resultater ses det, at for nul temperatur og feltet slået fra, vil system vælge en tilfældig nul-felts antiferromagnetisk grundtilstand, som den henfaldet til. Den gennemsnitlige henfaldstid afhænger generelt ikke af begyndelsestilstande men i stedet systemstørrelsen, der afspejles via en potensfunktion. Eksponenten for denne lov er estimeret til 2.05188 ± 0.00006. Er feltet ikke er nul, men i stedet er mindre end en bestemt værdi, da vil systemet henfalde til en ikke-ordnet tilstand med domænevæge i hovedparten af system. Skrues feltstyrken op, så den rammer den bestemte værdi, da vil domænevæge kunne skabes og tilintetgøres spontant. Systemet vil da indeholde meget uorden. Skrues feltet endnu højere op, vil enhver begyndelseskonfiguratio henfalde til den nul-felts ferromagnetisk grundtilstands hvis magnetisering er modsat feltet.

Tilsidst i specialet regnes egenværdierne af kvantemodellens Hamilton ud halvanalytisk.

Contents

Chapter 1

Introduction

Quantum cellular automata[1] (QCA) are quantum mechanical systems which have the ability to describe many interesting phenomena such as the dynamics of topological phases in Floquet systems[1], quantum Turing machines[2], and quantum random walks[1, 3, 4]. All three phenomena are super interesting with the first two being different approaches to build a quantum computer[1, 5]. This, for now, theoretical machine will exploit quantum mechanics to make the computers of today look pathetic because of the quantum computer's tremendously large computing power.

Since the dynamics of a quantum random walk has been shown to be similar to that of excitons in photosynthetic systems[3, 4, 6], the applications of QCA extends to areas other than material science. Also in the technology industry, a class of QCA called quantum-dot cellular automata (QDCA) shows potential for creating ultra-small circuits that can be used to create better and more compact computer chips[7, 8].

1.1 But what is a quantum cellular automaton?

1.1.1 Starting classical

A QCA is a generalization of the classical cellular automaton (CA) which was invented by John von Neumann to describe self-replicating phenomena [1, 2, 9]. The CA consists of a discrete, and sometimes infinite, d-dimensional lattice evolving in discrete time steps. Each site can be in any k different states which are updated each time step depending on the state of its neighbouring sites[9]. These "update rules" are local and homogeneous across the system and classifies the overall dynamics of the system. For different "update rules", the automaton will act in different ways. Demonstrations of this can easily be found on Youtube[10, 11, 12] where cellular automata with different dimensions and update rules are simulated. These models are very interesting for biologist and physicist specializing in complex systems, because they are able to simulate complex phenomena such as forest fires, starfish outbreaks in coral reefs, and formal languages[13, 14, 15].

An example of a 1D, $k = 2$, cellular automaton can be seen in figure 1.1.1. The two states are here represented by black and white squares which are updated using selection

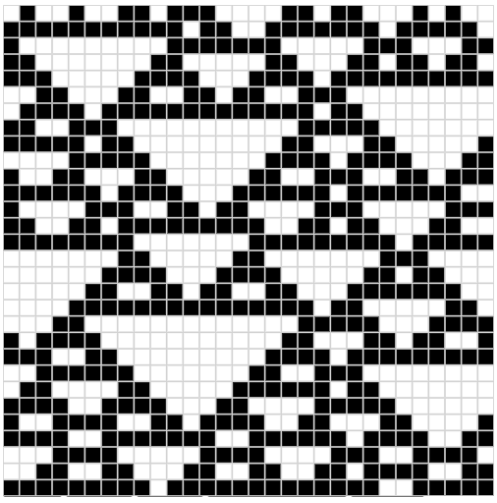

Figure 1.1.1: Simulation of a 1D, $k = 2$ cellular automaton with random initial configuration and selection rule 126. Time propagates in the downward direction.

[1] Single: Automaton - Plural: Automata

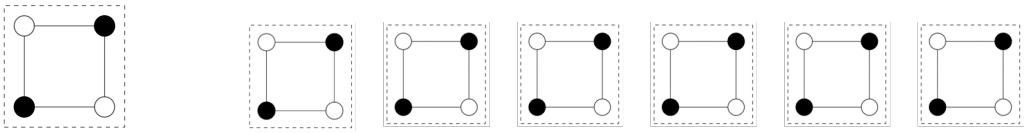

(a) (b)

Figure 1.1.2: The standard cell and the binary wire for Quantum-dot cellular automata based architectures.

rule 126[16]. Its initial state has been chosen randomly. Even so, "triangles" appear in the time directions, demonstrating order from simple local rules. This is why cellular automata are studied by complex physicist since many complex phenomena can emerge from simple local rules. For a quantum physicist's point of view, these cellular automata would be interesting to quantize.

1.1.2 The Quantum-dot cellular automata

[2]Through the history, different attempts of quantizing the cellular automaton have been made. Some attempts were good and some gave non-physical results[2]. One example of the quantization going well is referred to as a quantum-dot cellular automata (QDCA). This is a CA where the cells are replaced by quantum dots whose state can be any superposition of k basis states. The lattice is build from unit cells consisting of four or five quantum dots, see fig. 1.1.2a, which are named standard cells. On each standard cell, two electrons are placed. These electrons are able to tunnel between the dots, thereby creating some internal dynamics in the cell. Due to the Coulomb interaction, the electrons will move in ways such that the distance between them is maximized. If the tunnelling rates between the quantum dots are sufficiently small, the Hilbert space of the cell reduces to a two-level system where electrons occupies antipodal quantum dots denoted

$$\left|\begin{matrix}\bullet & \circ \\ \circ & \bullet\end{matrix}\right\rangle \quad \text{and} \quad \left|\begin{matrix}\circ & \bullet \\ \bullet & \circ\end{matrix}\right\rangle. \tag{1.1.1}$$

Here $\bullet$ represents a dot occupied by an electron, while $\circ$ represents an empty dot. It is standard to define a polarization $P \in \{-1, 1\}$ to the two antipodal states in eq. 1.1.1. Here the left state in eq. (1.1.1) is defined to have polarization $P = 1$, while the right state has polarization $P = -1$. Using linear superpositions, one can create a state with a given polarization $p \in [-1, 1]$ by choosing the coefficients picked so that

$$|\psi;\phi\rangle = \sqrt{\frac{1+p}{2}}\left|\begin{matrix}\bullet & \circ \\ \circ & \bullet\end{matrix}\right\rangle + \sqrt{\frac{1-p}{2}}e^{i\phi}\left|\begin{matrix}\circ & \bullet \\ \bullet & \circ\end{matrix}\right\rangle \quad \text{with} \quad \phi \in [0, 2\pi[. \tag{1.1.2}$$

Assuming the two states of eq. 1.1.1 to be orthonormal, the expectation value of a state $|\psi;\phi\rangle$ is p.

When placing two cells in close proximity of each other, this degeneracy between the two antipodal states are lifted. This is due to the Coulomb interaction between electrons of different cells. This means that if the polarization of one cell is fixed to a non-zero value, one of the antipodal states of the other cell will be energetically favourable over the other. This is reflected by the cell-cell response function[7], which is almost takes the form of a sign function,

$$P_2(P_1) \approx \operatorname{sgn}(P_1). \tag{1.1.3}$$

This response function in what the binary wire architecture is build upon. This structure can be constructed from a long string of standard cells placed close to each other, fig 1.1.2b. The ground state of such wire is the state, where all the cells have the same polarization. Fixing the polarization of the

[2]This section is based on articles [7, 8, 17]

first cell to any positive polarization $p > 0$, the rest of the cells in the wire will acts accordingly and shift to the $|\begin{smallmatrix}\bullet & \circ\\ \circ & \bullet\end{smallmatrix}\rangle$ state. If the polarization of the first cell is then changed to a negative polarization, the rest of the cells will change to the $|\begin{smallmatrix}\circ & \bullet\\ \bullet & \circ\end{smallmatrix}\rangle$ state. In this way, the binary wire allows transport of binary information, hence the name "binary wire", which can be done super fast[8].

Logical gates can also be constructed from standard cells. Gates such as inverters and Majority gates can be build using QDCA standard cells[17]. The latter is a logical gate that takes three inputs via binary wires, (a, b, c), and outputs, via a fourth wire, the polarization of the majority of the inputs. If one of the inputs are fixed to either 0 or 1, the Majoranty gate becomes a permanent AND or OR gate respectively. From these logic gates, larger architectures, such as the full adders and shift registers, can be realized. Experts hope to use this QDCA representation of binary information to build both small and fast processors that will work at room temperature[17]. Inspired by this, one can analyse the dynamics of other QDCA structures like the one described in the next section.

1.2 The (2,N) quantum-dot cellular automata

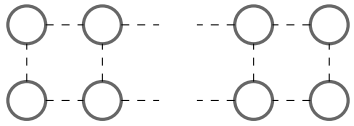

Figure 1.2.1: Sketch of (2,N) quantum-dot cellular automata. Dashes lines represents tunnelling coefficients $t_{i,j}$ between two dots.

To continue the idea of building QCAs from quantum dots, one can consider the $(2, N)$ QDCA. This system consists of a 2-dimensional array of quantum dots with N columns and 2 rows, fig. 1.2.1. The dots are filled to a certain occupation-level, using a chemical potential μ, such that the occupation of a single dot is given by the Fermi-Dirac distribution $\langle \hat{n}_{i,j,\sigma} \rangle = n_F(E_{i,j} - \mu)$. Here $\hat{n}_{i,j,\sigma}$ is the number operator of the j'th electronic eigenstate of the i'th dot. $\sigma \in \{\uparrow, \downarrow\}$ denotes the spin degrees of freedom, which is assumed not to influence the energy levels. Since $n_F(x) = [e^{x/T} + 1]^{-1}$ then, for small enough temperatures T, the Fermi Dirac distribution approaches the steps function

$$\Theta(x) := \lim_{T \to 0^+} n_F(x) = \begin{cases} 1 & \text{for} \quad x < 0 \\ \frac{1}{2} & \text{for} \quad x = 0 \\ 0 & \text{for} \quad x > 0 \end{cases}. \tag{1.2.1}$$

Assuming each quantum dot has a spectrum that mimics fig. 1.2.2a, and assuming that $T \ll \mu$ then all energy-level under the chemical potential will be fully occupied. This defines the Fermi surface in fig. 1.2.2a. In addition, if the spacing between the Fermi surface and the next energy level is Δ_1 and satisfies $(\Delta_1 - \mu) \ll T$, then all states above the Fermi surface are completely empty. This state is denoted $|\Omega\rangle$. The state of the complete quantum-dot array can then be written as the direct product $\bigotimes_{i=1}^{N} |\Omega\rangle$.

1.2.1 Adding extra electrons to $|\Omega\rangle$

To make the system a bit more interesting, a few additional electrons can be added to the system. Since all energy levels under the chemical potential are fully occupied, the only place to put the electrons are on the levels above the Fermi surface. Putting the electrons on the first levels above the Fermi level at temperatures also satisfying $\Delta_2 \ll T$, each quantum dot will now have a four dimensional Hilbert space of

$$\mathbb{H}_{\text{dot}} = \text{span}\{|\Omega\rangle, |\uparrow\rangle, |\downarrow\rangle, |\uparrow\downarrow\rangle\}. \tag{1.2.2}$$

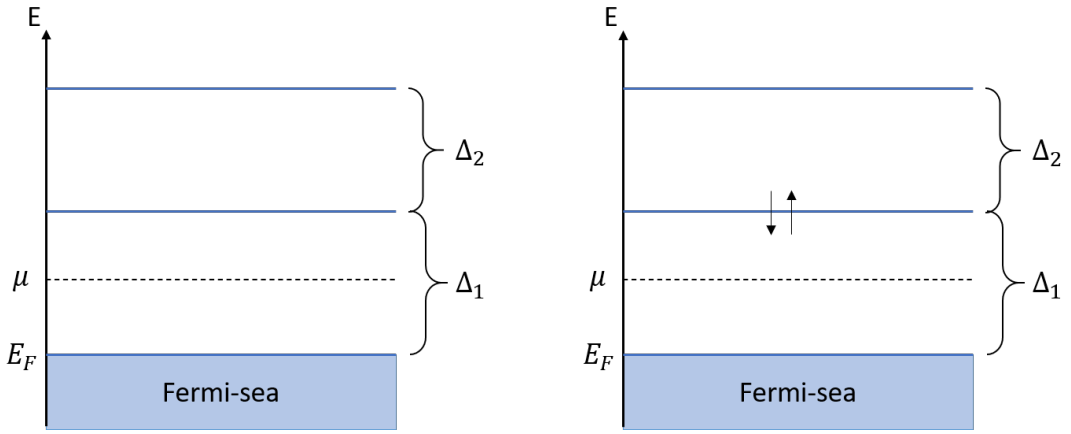

Figure 1.2.2: Graphical representation of the occupation of a single quantum dot for small temperatures. **a)** Occupation of dot with chemical potential μ. Because of the small temperature, all energy levels under the chemical potential is 100 % occupied, while higher states are empty. This state is labelled $|\Omega\rangle$. **b**) Two extra electrons are added to $|\Omega\rangle$ and placed on the first energy level over μ. Due to the Pauli exclusion principle, the spins of the electrons must anti-align. This state is labelled $|\uparrow\downarrow\rangle$.

Here $|\uparrow\rangle$ and $|\downarrow\rangle$ are the state $|\Omega\rangle$ dressed with an additional spin up or down electron on the first levels above Fermi level. Using second-quantized operators, one can write $|\uparrow\rangle = c_\uparrow^\dagger|\Omega\rangle$ and $|\downarrow\rangle = c_\downarrow^\dagger|\Omega\rangle$, where $c_\sigma^\dagger$ is the creation operator of an electron with spin σ having energy $E_F + \Delta_1$. The last state, $|\uparrow\downarrow\rangle = c_\uparrow^\dagger c_\downarrow^\dagger|\Omega\rangle$, is the state where both a spin up and spin down electron are added to $|\Omega\rangle$. They anti-align because of Pauli's exclusion principle. This state is depicted in fig. 1.2.2b. The requirement for $\Delta_2 \ll T$ is necessary to avoid electrons on the $E_F + \Delta_1$ levels being excited to the $E_F + \Delta_1 + \Delta_2$ by thermal excitations. If this were not the case, electrons would be able to move between energy levels, which would result in a more complicated Hilbert space. To keep the dynamics of system simple, the assumption is necessary.

1.2.2 Hamiltonian of multiple dots

Assuming that all dots in the (2,N) QDCA are roughly equivalent and have a Hilbert space $\mathbb{H}_{\text{dot}}$, the Hilbert space of the total system can be written in the direct product basis

$$\mathbb{H} = \text{span}\left\{\{|\Omega\rangle, |\uparrow\rangle, |\downarrow\rangle, |\uparrow\downarrow\rangle\}^{\otimes 2N}\right\}. \tag{1.2.3}$$

This Hilbert space has a dimension of 16^N, which is quite enormous even for just a few columns. Placing the quantum dots in close proximity of each other, the extra electrons on different dots are able to interact with each other. The Hamiltonian describing these interactions can be written as a sum of the following terms:

A zero-point energy This term describes the total interaction between all electrons of the QDCA that lay under the Fermi surface of the individual dots. Assuming this energy doesn't change when adding the extra electrons, the energy can be view as a constant on the Hilbert space $\mathbb{H}$. The zero-point energy therefore takes the form of

$$\mathcal{H}_0 = E_0\mathbb{I}. \tag{1.2.4}$$

Here $\mathbb{I}$ is the identity operator acting on $\mathbb{H}$. Since the only consequence of this term is a shift in the total energy of the system, it can be ignored for all practice purposes here.

On-site energy term Given the energy cost of putting an extra electron on the i'th dot, E_i, the on-site energy term of the Hamiltonian can be written as

$$\mathcal{H}^{\text{dot}} = \sum_i E_i(\hat{n}_{i\uparrow} + \hat{n}_{i\downarrow}) \tag{1.2.5}$$

Here $\hat{n}_{i,\sigma}$ is the number operator corresponding to an electron with spin $\sigma \in \{\uparrow, \downarrow\}$ sitting on the i'th dot.

Tunnelling Allowing electrons to jump from one dot to another via tunnelling processes. If $t_{i,j}$ is the coefficient associated of an electron tunnelling between the i'th and j'th dot, the tunnelling Hamiltonian can be written as

$$\mathcal{H}^{\text{tunnel}} = \sum_{<i,j>,\sigma} t_{i,j} \left(c^\dagger_{i\sigma} c_{j\sigma} + c^\dagger_{j\sigma} c_{i\sigma} \right). \tag{1.2.6}$$

Here $c^\dagger_{i\sigma}$ and $c_{i\sigma}$ are the electron creation and annihilation operators of the i'th dot. Again, $\sigma \in \{\uparrow, \downarrow\}$ represents the electron spin. The tunnelling processes are restricted so electrons only are allowed to hop between neighbouring sites. One therefore sums over all pairs $\langle i, j \rangle$ where i and j are neighbouring dots. For each dot, there are three kinds of neighbours. One being along the rows, one along the columns, and one being a combination of both. Each type of neighbour have an associated tunnelling coefficient being $t_i^\perp$, $t_i^\parallel$, and $t_i^\perp$. For the i'th dot, then the coefficient $t_i^\perp$ describes tunnelling in the same column, $t_i^\parallel$ describes tunnelling in the same row, and t_i^d is for diagonal tunnelling, 1.2.3. This part of the Hamiltonian makes the electrons move around the system and delocalizes them.

Inter-dot Coulomb repulsion If two electrons are placed on the same dot, each with different spins, then a repulsive Coulomb interaction, Q_i is present.

$$\mathcal{H}^{\text{Inter}} = \sum_i Q_i \hat{n}_{i\uparrow} \hat{n}_{i\downarrow}. \tag{1.2.7}$$

This interaction forces electrons to occupy different dots.

Extra-dot Coulomb repulsion Between all the extra electrons, a Coulomb repulsion is present described by the Hamiltonian

$$\mathcal{H}^{\text{Extra}} = \frac{1}{2} \sum_{i \neq j} \sum_{\sigma,\sigma'} V_{ij} \hat{n}_{i\sigma} \hat{n}_{j\sigma'}. \tag{1.2.8}$$

Here $V_{ij} = \frac{V}{\|\mathbf{r}_i - \mathbf{r}_j\|}$ is the Coulomb potential between two electrons with coordinates $\mathbf{r}_i$ and $\mathbf{r}_j$. Because of this interaction, the extra electrons move so they maximize the distance between them.

Adding the above terms, excluding the irrelevant zero-point energy, one get a Hubbard-like Hamiltonian describing the QDCA

$$\mathcal{H} = \sum_i E_i(\hat{n}_{i\uparrow} + \hat{n}_{i\downarrow}) + \sum_{\langle i,j \rangle,\sigma} t_{i,j} \left(c^\dagger_{i\sigma} c_{j\sigma} + c^\dagger_{j\sigma} c_{i\sigma} \right) + \sum_i Q_i \hat{n}_{i\uparrow} \hat{n}_{i\downarrow} + \frac{1}{2} \sum_{i \neq j} \sum_{\sigma,\sigma'} V_{ij} \hat{n}_{i\sigma} \hat{n}_{j\sigma'}. \tag{1.2.9}$$

Due to the large dimension of the Hilbert space, and therefore also the matrix representation of the Hamiltonian, the dynamics of the system cannot be evaluated numerical for large N's. It is therefore necessary to do some analytical work first. This is not trivial in any way because of the tunnelling and the extra-dot Coulomb interaction, which makes the eigenstates complicated. The Hilbert space is therefore restricted even more to make the Hamiltonian more manageable to work with.

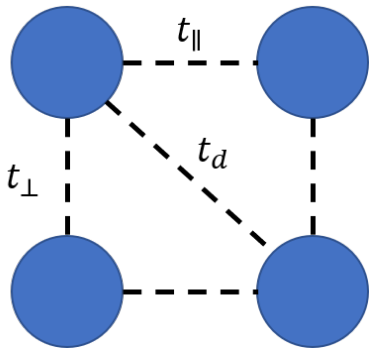

Figure 1.2.3: Graphical representation of the different ways electrons can tunnel between dots.

1.3 Restricting to a single electron pr. column

Assuming that the tunnelling rates between dots in the same column is much larger than the tunnelling rates between dots in different columns, $t_\perp \gg t_\parallel, t_d$, electrons will stay in their columns. If one at the same time assumes that only a single extra electron is put into every column, the Hilbert space of each column will reduce to a simple two-levels system,

$$\tilde{\mathbb{H}}_{\text{single}} = \text{span}\left\{\left|\begin{smallmatrix}\bullet\\\circ\end{smallmatrix}\right\rangle, \left|\begin{smallmatrix}\circ\\\bullet\end{smallmatrix}\right\rangle\right\}. \tag{1.3.1}$$

Here, $\left|\begin{smallmatrix}\bullet\\\circ\end{smallmatrix}\right\rangle$ is the state of a single column with the extra electron being on the top dot. In the same way, $\left|\begin{smallmatrix}\circ\\\bullet\end{smallmatrix}\right\rangle$ is the state of a single column, where the electron is on the bottom dot. The total, reduced Hilbert space of the system can then be written as

$$\tilde{\mathbb{H}} = \text{span}\left\{\left\{\left|\begin{smallmatrix}\bullet\\\circ\end{smallmatrix}\right\rangle, \left|\begin{smallmatrix}\circ\\\bullet\end{smallmatrix}\right\rangle\right\}^{\otimes N}\right\}. \tag{1.3.2}$$

When restricting the Hilbert space in this way, the inter-dot interaction $\mathcal{H}^{\text{Inter}}$ can be ignored since no process allows for two electrons to be on the same dot, given the initial configuration. Also, since the energy levels of the quantum dots are assumed to independent of spin, the spin degrees of freedom can be ignored. The Hamiltonian therefore reduces to

$$\mathcal{H} = \sum_{(i,j)} E_{(i,j)}\hat{n}_{(i,j)} + \sum_i t_i\left(c^\dagger_{(i,1)}c_{(i,2)} + c^\dagger_{(i,2)}c_{(i,1)}\right) + \sum_{(i,j),(i',j')} \frac{V}{\|\mathbf{r}_{(i,j)} - \mathbf{r}_{(i',j')}\|}\hat{n}_{(i,j)}\hat{n}_{(i',j')}. \tag{1.3.3}$$

Here (i,j) labels the coordinates of the dots with $i \in \{1,\cdots,N\}$ and $j \in \{1,2\}$. $j = 1$ refers to the bottom dot while $j = 2$ refers to the top. This two-level system has another representation, which will make it easier to work with. Since a system of N spin-1/2 particles have a Hilbert space of the same dimension as $\tilde{\mathbb{H}}$, one could imagine that a map between the them should exist. This turns out to be correct and is shown in the next section.

1.4 Mapping to the quantum Ising model

To map the Hilbert space of the restricted QDCA to the Hilbert space of a chain of N spin-1/2 particles, one does so column by column. If $M : \tilde{\mathbb{H}} \to \mathbb{H}_{\text{spin-1/2}}$ maps the restricted single column Hilbert space to the Hilbert space of a single quantum spin, one can chose M so that

$$\left|\begin{smallmatrix}\bullet\\\circ\end{smallmatrix}\right\rangle \leftrightarrow |\uparrow\rangle \quad \text{and} \quad \left|\begin{smallmatrix}\circ\\\bullet\end{smallmatrix}\right\rangle \leftrightarrow |\downarrow\rangle. \tag{1.4.1}$$

For this to be valid, one must ensure that the fermion anticommutator and spin commutator relation holds.

First, the fermion operator $c^\dagger_{(i,2)}c_{(i,1)}$ maps to the spin ladder operator σ^+_i. One observes this by using that

$$c^\dagger_{(i,2)}c_{(i,1)} = |{}^{\bullet}_{\circ}\rangle\langle{}^{\circ}_{\bullet}| \quad \text{and} \quad \sigma^+ = |\uparrow\rangle\langle\downarrow|. \tag{1.4.2}$$

Since the operators $c^\dagger_{(i,2)}c_{(i,1)}$ and σ^+_i acts in the same way on their respective basis states, then they must map to each other. σ^-_i must then represent the operator $c^\dagger_{(i,1)}c_{(i,2)}$, since $\sigma^- i = (\sigma^+_i)^\dagger$. From this, it is possible to shown that both the commutator relation, $[\sigma^+_i, \sigma^-_j] = \delta_{ij}\sigma^z_i$, and the anti-commutator relation, $\{c^\dagger_i, c^\dagger_j\} = \{c_i, c_j\} = 0$ and $\{c^\dagger_i, c_j\} = \delta_{ij}$, are satisfied simultaneous. This can be shown by expanding the commutator

$$[\sigma^+_i, \sigma^-_j] \leftrightarrow [c^\dagger_{(i,2)}c_{(i,1)}, c^\dagger_{(j,1)}c_{(j,2)}] = c^\dagger_{(i,2)}c_{(i,1)}c^\dagger_{(j,1)}c_{(j,2)} - c^\dagger_{(j,1)}c_{(j,2)}c^\dagger_{(i,2)}c_{(i,1)}. \tag{1.4.3}$$

Using the fermion anti-commutators one can show that

$$c^\dagger_{(i,2)}c_{(i,1)}c^\dagger_{(j,1)}c_{(j,2)} = \delta_{ij}\left(\hat{n}_{(i,2)} - \hat{n}_{(i,1)}\right) + c^\dagger_{(j,1)}c_{(j,2)}c^\dagger_{(i,2)}c_{(i,1)}, \tag{1.4.4}$$

which implies

$$[\sigma^+_i, \sigma^-_j] \leftrightarrow \delta_{ij}\left(\hat{n}_{(i,2)} - \hat{n}_{(i,1)}\right). \tag{1.4.5}$$

this operator can then be mapped to $\delta_{ij}\sigma^z_i = [\sigma^+_i, \sigma^-_j]$. By using the spin commutators relations, one can also show that the anti-fermion commutators are satisfied. The map M therefore maps the two Hilbert spaces correctly. From this, the spin representation of the Hamiltonian in eq. (1.3.3) can be found. This is done term by term. First, the on-site energy term can be written Zeemann term from a field pointing along the z-direction.

$$\sum_{i=1}^{N} E_{(i,2)}\hat{n}_{(i,2)} + E_{(i,1)}\hat{n}_{(i,1)} = \sum_{i=1}^{N} \frac{E_{(i,2)} + E_{(i,1)}}{2}(\hat{n}_{(i,2)} + \hat{n}_{(i,1)}) + \frac{E_{(i,2)} - E_{(i,1)}}{2}(\hat{n}_{(i,2)} - \hat{n}_{(i,1)}) \tag{1.4.6}$$

$$\leftrightarrow \sum_{i=1}^{N} \frac{E_{(i,2)} + E_{(i,1)}}{2}\mathbb{I} + h^z_i\sigma^z_i. \tag{1.4.7}$$

The first term can again be ignored, since it just shifts the energy levels by a constant. The field strength is directly proportional with the energy difference between the dots. In the same way, the tunnelling part of the Hamiltonian can be mapped to Zeemann term in the x-direction

$$\mathcal{H} = \sum_{i=1}^{N} t_i\left(c^\dagger_{(i,2)}c_{(i,1)} + c^\dagger_{(i,1)}c_{(i,2)}\right) \leftrightarrow \sum_{i=1}^{N} t_i\left(\sigma^+_i + \sigma^-_i\right) = \sum_{i=1}^{N} h^x_i\sigma^x_i. \tag{1.4.8}$$

Here the tunnelling coefficient directly maps to the magnetic field along the x-direction. This reflects the fact that for large t_i, the electron delocalizes and occupies the dots equality, resulting in $\left|\langle\hat{n}_{(i,2)}\rangle\right|^2 = \left|\langle\hat{n}_{(i,1)}\rangle\right|^2 = 0.5$. This is analogous to a transverse magnetic field that forces the spin to point in the x-direction so $|\langle\uparrow | \uparrow_x\rangle|^2 = |\langle\downarrow | \uparrow_x\rangle|^2 = |\langle\uparrow | \downarrow_x\rangle|^2 = |\langle\downarrow | \downarrow_x\rangle|^2 = 0.5$

For the extra-dot Coulomb repulsion, the interaction between the i'th and j'th column can be written in terms of four parts

$$\mathcal{H}^{\text{Coulomb}}_{i,j} = V_{i,j}\left(\hat{n}_{(i,1)}\hat{n}_{(j,1)} + \hat{n}_{(i,2)}\hat{n}_{(j,2)}\right) + V'_{i,j}\left(\hat{n}_{(i,1)}\hat{n}_{(j,2)} + \hat{n}_{(i,2)}\hat{n}_{(j,1)}\right) \tag{1.4.9}$$

Here $V_{i,j}$ are the Coulomb interaction between electrons in the same row, while $V'_{i,j}$ are the Coulomb interaction between electron is different rows. Adding and subtracting a few cross terms, which adds

to a total zero, one gets

$$\mathcal{H}_{i,j}^{\text{Coulomb}} = \frac{V_{i,j}+V'_{i,j}}{2}(\hat{n}_{(i,2)}+\hat{n}_{(i,1)})(\hat{n}_{(j,2)}+\hat{n}_{(j,1)}) + \frac{V_{i,j}-V'_{i,j}}{2}(\hat{n}_{(i,2)}-\hat{n}_{(i,1)})(\hat{n}_{(j,2)}-\hat{n}_{(j,1)}) \tag{1.4.10}$$

$$\leftrightarrow \frac{V_{i,j}+V'_{i,j}}{2}\mathbb{I} + J_{i,j}\sigma_i^z\sigma_j^z \tag{1.4.11}$$

The first term here can again be ignored, since it is a constant. The second term is an interaction term, which depends on the separation between the dots. This interaction constant J_{ij} will always be positive for these kind of systems. Due to the nature of the Coulomb interactions, the nearest neighbour interaction energy dominates eq. (1.4.11). One can show this by denoting the distance between rows by b, and the distance between columns a. The interaction energy $J_{i,j}$ will then takes the form of

$$J_{i,j} = \frac{V_{i,j}-V'_{i,j}}{2} = \frac{V}{2}\left(1 - \frac{a|i-j|}{\sqrt{(i-j)^2a^2+b^2}}\right). \tag{1.4.12}$$

The ratio between nearest neighbour interactions, J_{nn} and the interactions between spins separated by n columns are then

$$\frac{J_n}{J_1} = \frac{1}{x}\frac{1-\frac{n}{\sqrt{n^2+\left(\frac{b}{a}\right)^2}}}{1-\frac{1}{\sqrt{1+\left(\frac{b}{a}\right)^2}}}. \tag{1.4.13}$$

For $a = b$, this ratio is around 18% for $x = 2$ and around 3% for $x = 3$. Because of this, only the nearest neighbour interaction is considered throughout this thesis. Since $J_{nn} > 0$, then spins will therefore tend to anti-align with their neighbours. This makes the total Hamiltonian, acting on the reduced Hilbert space $\tilde{\mathbb{H}}$, take the form of

$$\mathcal{H} \leftrightarrow \sum_{i=1}^{N-1} J_i\sigma_i^z\sigma_{i+1}^z + \sum_{i=1}^{N} h_i^z\sigma_i^z + h_i^x\sigma_i^x. \tag{1.4.14}$$

which is a quantum Ising Hamiltonian. The (2,N)-QDCA will therefore have the same dynamics of the quantum Ising model, given the assumptions presented in the chapter.

1.5 Structure of the thesis

Now that the (2,N) QDCA has been mapped to a quantum Ising model, the next step is to analyse the dynamics of the system. Since the system is not isolated, but can interact with the environment, it can be interesting to study its non-equilibrium dynamic. If the coupling to between the "spins" and the environment are strong enough, the thermal dynamics of the system will dominate, and the quantum dynamics can be ignored for now. Doing so leads one to consider a classical Ising model coupled to heat baths each with their own temperature. This allows the classical system to experience thermal dynamics, which will be described in chapter 3.

Before delving into non-equilibrium dynamics of the classical Ising model, the language used to describe them are explain. The equilibrium dynamics is then analysed to gain some intuition about the long-term behaviour of the classical system for both zero, small, and high temperatures. All this is in chapter 2.

Chapter 3 describes the kinetic Ising model. Here the classical Ising model is coupled to a Glauber heat bath, which flips single spins randomly. The rates for which these spin-flip processes happens at can be used to simulate the non-equilibrium dynamics using stochastic simulations. The algorithm

used in these simulations, as well as the implementation in code, are described in chapter 4. The code is written in Cython, which is a Python/C hybrid language. Running the simulations yields results which will be analysed in chapter 5.

In the chapters 6, the first steps in the analytical framework using to described the quantum dynamics are taken. The open boundary, nearest neighbour, transverse field quantum Ising Hamiltonian is diagonalized using analytical methods.

To end the thesis a description on how the code could be improved, are written in chapter 7.

Chapter 2

Classical Ising model

To study simply magnetic systems, the classical Ising model is an all time classic. It describes a classical system of magnetic dipoles, often referred to as classical spins, on a D dimensional lattice. These spins can either point along or opposite to a special axis, which often is set to be the z-axis. These spins interacts with each other trough an exchange interaction, described via a matrix $\mathbf{J}$. Other than that, each spins interacts individually with a space dependent, longitudinal, magnetic field h. For different lattice types and values of $\mathbf{J}$ and h, the overall behaviour of the system changes.

The first iteration of this model was first set up by William Lenz to describe ferromagnetism in one-dimensional magnets[18]. It was then solved by Ernest Ising[19] for whom the model was named after. Ising calculated the magnetization of a one-dimensional chain with periodic boundary conditions, given that every spin interacts only with its nearest neighbours via a homogeneous exchange coupling J. The value of this interaction was picked so that the energy was minimized, if all spins pointed in the same direction. h was also chosen to be homogeneous along the chain. For different values of J and h, as well as the temperature of the environment T, he found the system's magnetization as a function of h/J and T/J.

The simplicity of the Ising model makes it a good toy model for studying many-body system. This includes magnets, but also lattice gas models[18] and even market modelling[20]. Even thou the model is simple, only a few cases can be solved exactly, even for homogeneous field and coupling constants. Numerical methods, such as Monte Carlo simulations, are therefore necessary if one needs to calculate statistical properties such as magnetization, correlation functions, and critical points.

In this chapter, the notation used to describe the one-dimensional, classical, Ising model with homogeneous J and h is described first section. Here, the different terms in the energy function is also descried as well as the term "domain wall excitations". In the second section, the equilibrium properties of this model analysed, is calculated. This includes the magnetic properties, the nearest neighbour correlation function, and the entropy, for different values of J/T and h/T. From this, a phase diagram of the 1D classical Ising model can be made.

2.1 Notation and definitions

To describe a given configuration consisting of N spins, one labels each spin by an integer $i \in \{1, \cdots, N\}$. The projection of each spin on the z-axis, which is here picked as the special axis, are written as σ_i and can be either plus or minus one,

$$\sigma_i \in \{1, -1\}. \tag{2.1.1}$$

Here, $\sigma_i = 1$ represents the spin pointing along the z-axis, while $\sigma_i = -1$ represents the spin pointing opposite to the z-axis. A given configurations is therefore written as $\{\sigma_i\}$. Graphically, one can represent $\{\sigma\}$ either as a collection of arrows, or as in fig. 2.1.1, a set of grey and white dots.

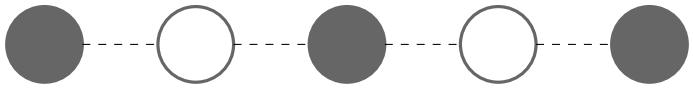

Figure 2.1.1: Cartoon of the configuration $\{\sigma\} = \{-1, 1, -1, 1, -1\}$ of a classical Ising model with five sites. The filled dots represents a site with value -1 while an empty site represents a site with value 1.

2.1.1 Interaction energy

Between two spins in the vicinity of each other, an interaction energy proportional to the spins orientations exists. Given two spins, labelled i and j, this interaction energy takes the form of $J_{ij}\sigma_i\sigma_j$, where J_{ij} a an element of $\mathbf{J}$. Summing over all unordered spin pairs (i, j), the total spin-spin interaction energy of a given configuration $\{\sigma\}$ takes the form of

$$E_{\text{spin-spin}}(\{\sigma\}) = \sum_{(i,j)} J_{ij}\sigma_i\sigma_j = \sum_{i<j} J_{ij}\sigma_i\sigma_j. \tag{2.1.2}$$

For different values of J_{ij}, pairs of spins act differently. Given two isolated spins, who interacts with coupling strength J, one gets the following behaviour depending on the sign of J:

- $J < 0$: If the coupling is negative, the spins can minimize their energy by aligning with each other. The ground state configurations are therefore $\{1, 1\}$ and $\{-1, -1\}$. Both of these have an overall non-zero magnetic field, since the sum of spins will be either be 1 or -1 respectively. Negative coupling constants are therefore said to be ferromagntic (FM), since they tend to create non-zero overall magnetic fields, just like ferromagnetic materials do.

- $J > 0$: If the coupling is positive, the spins can minimize their energy by anti-aligning with each other. The ground state configurations are therefore $\{1, -1\}$ and $\{-1, 1\}$. The magnetic moment of the two spins will then cancel, resulting in no overall magnetic field. Negative coupling constants are therefore said to be antiferromagntic (AFM), since they tends to prevent non-zero magnetic field, exactly like antiferromagnetic materials do not have an overall magnetic field.

- $J = 0$: Here the spins do not interact with each other. One does not care what the other is doing and all configurations have the same energy. One therefore says that the spins are non-interacting.

[1] If all non-zero coupling constants all have the same sign, the models is said to be either a pure ferromagnetic or a pure antiferromagnetic system. In some systems, such as the model analysed in this thesis, the interacting between spins decays rapidly with distance. Nearest neighbour interactions will therefore be much stronger than interactions between next-nearest neighbours and beyond. This reduces the total spin-spin interaction energy to

$$E_{\text{spin-spin,nn}}(\{\sigma\}) = \sum_{\langle i,j\rangle} J_{ij}\sigma_i\sigma_j. \tag{2.1.3}$$

In eq. (2.1.3), $\{\langle i, j\rangle\}$ refers to the set of nearest neighbouring pairs. On a $D = 1$, regular, and equally separated lattice, each site in the system's bulk have two neighbours. For $D = 2$, this number increases to four. For different boundary conditions, the number of neighbours a edge spin has, can vary from site to site. If periodic boundary conditions (PBC) are assumed, there will be no edge sites, so all spins have the same number of neighbours. For open boundary conditions (OBC), the edge spins of a chain will always have one neighbour. For a 2D, regular, square lattice with straight edges, the edge spins on the side have three nearest neighbours, while the corner spins have two. This can be seen in fig. 2.1.3.

[1] In other literature, the interacting energy is defined with an overall sign, meaning $J > 0$ is FM and $J < 0$ AFM. This is just a question of convention. Since this thesis will mostly work with antiferromagnetic interactions, the convention described here is used throughout this thesis. This is to minimize the number of potential sign error.

Due to the interaction being quadratic in spin, the energy functions in eq. (2.1.2) and eq. (2.1.3) are $\mathbb{Z}_2$ symmetric. This is because one can flip all spins, $\sigma_i \to -\sigma_i$, without changing the energy of the system. This implies that all energy states must be at least two-fold degenerate. For pure FM systems, the ground state configurations are the configurations where all spins align. For AFM system, it is not immediately clear how the ground state configurations look like. This is because, for some lattices, a spin can sometimes be flipped without changing the energy. An example of this can be seen for an 1D nearest neighbour Ising model with periodic boundary conditions and $N = 3$, fig. 2.1.2. Here, if either the left of the middle spin is flipped, the energy does not change, since it will still align with one and anti-align with the other. That is of course if the nearest coupling constants are homogeneous. For one dimensional system, the AFM ground state are the states where the spin projection alternates from spin to spin, such as the configuration depicted in fig. 2.1.1.

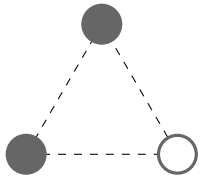

Figure 2.1.2: One of the ground states configurations of a 1D AFM Ising model with periodic boundary conditions and $N = 3$

2.1.2 Magnetizations and sub lattices

To characterize the overall behaviour of a system, one can use the total magnetization $M(\{\sigma_i\}) = \sum_{i=1}^{N} \sigma_i$ as an order parameter. This is often normalized with the number of sites N, such that

$$m(\{\sigma\}) = \frac{1}{N} \sum_{i=1}^{N} \sigma_i. \tag{2.1.4}$$

For a pure FM, the ground state configurations have $m = 1$ or $m = -1$, since all spins point in the same direction. Therefore, if one measures a magnetization with magnitude $|m| = 1$, one knows for sure that the system is in a FM ground state. For AFM systems, this is unfortunately not that simple. For a D-dimensional cubic lattice, both AFM ground state configurations have a very small magnetization of order $\mathcal{O}\left(N^{-\frac{1}{D}}\right)$. The reason for this is that the number of edge sites scales proportional to $x^{1-1/D}$ when the number of spin is scaled by a factor x. Because the magnetic moment of the edge sites are not necessary cancelled by other spins, they can all contribute to a non-zero overall magnetic field. Normalizing the magnetization, results in it scaling proportional to $x^{-1/D}$. An example of this can be seen by noticing that the number of edge sites of a $D = 1$ chain is always two. Also a $D = 2$ square lattice, with side length ℓ, has 4ℓ edge sites. In both cases, the "area to volume" ratio scales proportional to $N^{-1/D}$.

Due to the normalized magnetization being vanishingly small for large AFM ground state configurations, it is not a good order parameter. One can do something else. If the lattice is split into an even and an odd sub lattice,

$$\mathbb{L} = \mathbb{L}_{\text{even}} \cup \mathbb{L}_{\text{odd}}, \tag{2.1.5}$$

then one can define a magnetization for each part. Denoting the number of sites in the sub lattice $\mathbb{L}_\alpha$ by $|\mathbb{L}_\alpha|$, one defines

$$m_{\text{even}} = |\mathbb{L}_{\text{even}}|^{-1} \sum_{i \in \mathbb{L}_{\text{even}}} \sigma_i \quad \text{and} \quad m_{\text{odd}} = |\mathbb{L}_{\text{odd}}|^{-1} \sum_{i \in \mathbb{L}_{\text{odd}}} \sigma_i. \tag{2.1.6}$$

For a 1D chain, the even sub lattice is the collection of all spins labelled with an even i. The rest is in the odd sub lattice. Using this, the AFM ground state configurations will have magnetizations $(m_{\text{even}}, m_{\text{odd}})$ being either $(1, -1)$ or $(-1, 1)$. This donation does also work for FM ground state configurations, because $(m_{\text{even}}, m_{\text{odd}})$ will either be $(1, 1)$ or $(-1, -1)$. In this way, the even and odd sub lattice magnetization are better at describing order in AFM systems than the total magnetization. This will be important in chapter 5.

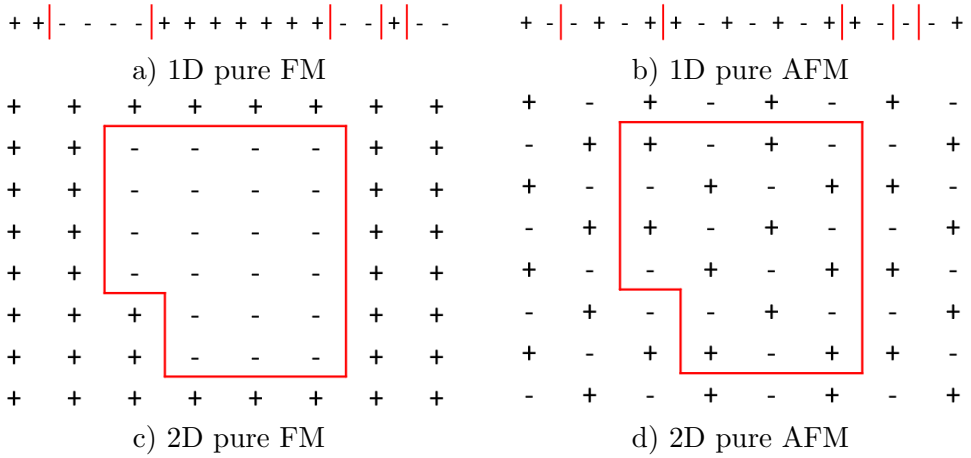

Figure 2.1.3: Graphical representation of ferromagnetic and anti-ferromagnetic states in one and two dimensions. For each state, domain walls are drawn as red bars. For a FM couplings, domains walls are drawn between sites where $\sigma_i\sigma_j = -1$ and for AFM couplings, domain walls are drawn between sites where $\sigma_i\sigma_j = -1$.

2.1.3 Domain wall excitations in classical nearest neighbour Ising model

Because each spin only has to worry about their nearest neighbours, one can divide a D-dimensional, cubic, classical, nearest neighbour, Ising system into different domains using the following rules:

1. All spins are in the same domain as themselves.
2. Given to nearest neighbouring spins, σ_i and σ_j, if their interaction energy is positive, $J_{ij}\sigma_i\sigma_j > 0$, then the spins are in different domains.
3. Given to nearest neighbouring spins, σ_i and σ_j, if their interaction energy is negative, $J_{ij}\sigma_i\sigma_j < 0$, then the spins are in the same domain.
4. Given three spins; σ_i, σ_j, and σ_k, then if σ_i is in the same domain as σ_j, and σ_j is in the same domain as σ_j, then σ_i and σ_k are also in the same domain.
5. Between two domains, a domain wall is said to be present.

Four examples of the rules can be seen in fig. 2.1.3. Here, both one and two dimensional systems are shown for both FM and AFM coupling constants with the red lines denote domain walls. When a spin is flipped the domains will change and domain walls will move. It can therefore sometimes be easier look at how domain walls move, instead of looking at which spins are flipped. Mapping the domain walls to particles on a discrete lattice, the dynamics of spin flips can be translated into motion, creating, and/or annihilation of the domain wall particles. For instance, if one uses the configuration of fig. 2.1.3a, one maps the domain walls to particles via

$$\uparrow\downarrow\downarrow\uparrow\downarrow\uparrow\uparrow\downarrow\uparrow\downarrow\uparrow\downarrow\uparrow\uparrow\downarrow\downarrow\downarrow\uparrow \longrightarrow \circ\bullet\circ\circ\circ\bullet\circ\circ\circ\circ\circ\bullet\circ\bullet\bullet\circ \tag{2.1.7}$$

Here a $\bullet$ represents a domain wall while $\circ$ represents a lack of domain walls. Note that the number of sites is reduces by one, since domain walls live in the space between spins. For a 1D, classical, nearest neighbour Ising model, the possible domain wall moves are relatively simple. To first order in spin flips, meaning only one spin is flipped at a time, every move can be divided into only five categories. These categories are listed in table 2.1.4. From here, one observes that if two walls meet, they can annihilate each other via pair annihilation. In spin space, this translates to a domain being collapsed between two other domains. These two domains are then combined into one big domain. This releases

List of single spin flip actions					
Action	Realization (DW)	Realization (AFM)	Realization (FM)	ΔE	$\sigma_{i-1}\sigma_{i+1}$
Pair creating	$\circ\circ \Rightarrow \bullet\bullet$	$\uparrow\downarrow\uparrow \Rightarrow \uparrow\uparrow\uparrow$ $\downarrow\uparrow\downarrow \Rightarrow \downarrow\downarrow\downarrow$	$\uparrow\uparrow\uparrow \Rightarrow \uparrow\downarrow\uparrow$ $\downarrow\downarrow\downarrow \Rightarrow \downarrow\uparrow\downarrow$	$4\lvert J\rvert$	1
Pair annihilation	$\bullet\bullet \Rightarrow \circ\circ$	$\uparrow\uparrow\uparrow \Rightarrow \uparrow\downarrow\uparrow$ $\downarrow\downarrow\downarrow \Rightarrow \downarrow\uparrow\downarrow$	$\uparrow\downarrow\uparrow \Rightarrow \uparrow\uparrow\uparrow$ $\downarrow\uparrow\downarrow \Rightarrow \downarrow\downarrow\downarrow$	$-4\lvert J\rvert$	1
Moving left/right	$\circ\bullet \Leftrightarrow \bullet\circ$	$\downarrow\uparrow\uparrow \Leftrightarrow \downarrow\downarrow\uparrow$ $\uparrow\downarrow\downarrow \Leftrightarrow \uparrow\uparrow\downarrow$	$\uparrow\uparrow\downarrow \Leftrightarrow \uparrow\downarrow\downarrow$ $\downarrow\downarrow\uparrow \Leftrightarrow \downarrow\uparrow\uparrow$	0	-1
Edge creation	$\circ\cdots \Rightarrow \bullet\cdots$	$\uparrow\downarrow\cdots \Rightarrow \downarrow\downarrow\cdots$ $\downarrow\uparrow\cdots \Rightarrow \uparrow\uparrow\cdots$	$\uparrow\uparrow\cdots \Rightarrow \downarrow\uparrow\cdots$ $\downarrow\downarrow\cdots \Rightarrow \uparrow\downarrow\cdots$	$2\lvert J\rvert$	0
	$\cdots\circ \Rightarrow \cdots\bullet$	$\cdots\uparrow\downarrow \Rightarrow \cdots\uparrow\uparrow$ $\cdots\downarrow\uparrow \Rightarrow \cdots\downarrow\downarrow$	$\cdots\uparrow\uparrow \Rightarrow \cdots\uparrow\downarrow$ $\cdots\downarrow\downarrow \Rightarrow \cdots\downarrow\uparrow$	$2\lvert J\rvert$	0
Edge annihilation	$\bullet\cdots \Rightarrow \circ\cdots$	$\downarrow\downarrow\cdots \Rightarrow \uparrow\downarrow\cdots$ $\uparrow\uparrow\cdots \Rightarrow \downarrow\uparrow\cdots$	$\downarrow\uparrow\cdots \Rightarrow \uparrow\uparrow\cdots$ $\uparrow\downarrow\cdots \Rightarrow \downarrow\downarrow\cdots$	$-2\lvert J\rvert$	0
	$\cdots\circ \Rightarrow \cdots\bullet$	$\cdots\uparrow\downarrow \Rightarrow \cdots\uparrow\uparrow$ $\cdots\downarrow\uparrow \Rightarrow \cdots\downarrow\downarrow$	$\cdots\uparrow\uparrow \Rightarrow \cdots\uparrow\downarrow$ $\cdots\downarrow\downarrow \Rightarrow \cdots\downarrow\uparrow$	$-2\lvert J\rvert$	0

Figure 2.1.4: List over possible moves of single domain walls from single dipole moment flips. In column 2, the full circles, $\bullet$, represents a site with a domain wall, while white circles, $\circ$, represents sites with no domain wall. In column 3 and 4, the corresponding action in Ising picture is given for a pure AFM and a pure FM. The change in energy, when a given action is performed, is given by the column 5 for a homogeneous system with no longitudinal field. The last column set the value of products of the nearest neighbouring spin $\sigma_{i-1}\sigma_{i+1}$. For Edge creation/annihilation this product is set to zero since one of spin does does not exist.

an energy of $4|J|$ for homogeneous coupling constants. A pair of domain walls can also be created, which splits one domain in two by created a small domain between them. This has an energy cost of $4|J|$ for homogeneous coupling constants. If the system has open boundary conditions, then single domain walls can be create/annihilated on the edge of the chain. This only cost/releases an energy of $2|J|$. In spin space, this translated to one of the edge spins being flipped. The last move on the list is domain wall motion. Because a spin on the edge of a domain goes from being in one to be in the other when flipped, domain walls can be moved. If the nearest neighbour coupling is homogeneous, this move is free in terms of energy cost. These action becomes important in chapter 3, when the non-equilibrium behaviour of the classical Ising model is considered. Other higher order spin-flip process can also be translated into domain wall motions, but will not be done so in this thesis. Note that these process are symmetric w.r.t the $\mathbb{Z}_2$ transformation mentioned earlier. This means that each action in the domain wall picture can be related to two different processes in spin space. This changes when a longitudinal magnetic field is added over the system.

2.1.4 Adding a longitudinal magnetic field over the system

An isolated classical spin will have an energy degeneracy between the $\sigma_i = 1$ and $\sigma_i = -1$ state. This changes when it is placed in a longitudinal magnetic field. Just like the Zeeman effect for quantum spins, the energy levels split proportional to the magnetic field strength. For electrons in a magnetic field $\mathbf{B}$, the eigenstates will have energy $E = \pm\frac{g\mu_B}{2}|B|$ with μ_B being the Bohr mangeton, and g being the g-factor of electrons.

In the same way, when a classical Ising spin is placed in a longitudinal magnetic field, which is set to point along the z-direction, the energy of spin is

$$E_{\text{single,field}}(\sigma) = \sigma h. \tag{2.1.8}$$

This means, that if a nearest neighbour Ising model is placed in a space dependent, longitudinal, magnetic field $h(x)$, the energy of the system becomes

$$E(\{\sigma\}) = \sum_{\langle i,j \rangle} J_{i,j}\sigma_i\sigma_j + \sum_{i=1}^{N} h_i\sigma_i. \tag{2.1.9}$$

Here $h_i = h(x_i)$ is the field strength at the i'th site. This extra term breaks the $\mathbb{Z}_2$ symmetry, since if all the spin in a configuration $\{\sigma\}$ is flipped, the energy changes by

$$\Delta E_{\text{Flip all}}(\{\sigma\}) = -2\sum_{i=1}^{N} h_i\sigma_i. \tag{2.1.10}$$

Notice that if the field is homogeneous, then $\Delta E = -2hM$ with M being to total magnetization of the system. Some of the degeneracies are therefore lifted, but not all of them. If $\sum_{i=1}^{N} h_i\sigma_i = 0$ for a configuration $\{\sigma\}$, the two-fold degeneracy is still present.

The effect of this magnetic field is that for pure FM systems, one of the zero-field ground states will have a lower energy than the other. In equilibrium, this means that the system will have a higher probability of being in a state with a magnetization $M \approx -h$. Even for small field strengths, one would expect the system to prefer states with $M \approx -h$, since the nearest neighbour interaction helps with aligning the spins. For pure AFM systems, because the magnetization of the zero-field ground states is small, the field does not influence the equilibrium properties very much for small fields. One would therefore excepts the system behaving much like the zero-field case, when $h \ll J$ for pure AFM systems. On the other hand, if $h \gg J$, then the magnetization dominates the energy of the system. One would therefore expects then $M \approx -h$ states to be preferred, even for pure AFM systems. The threshold values this seem to be $|h| = 2J$ for homogeneous fields and coupling constants. At this value spin configuration such as $\downarrow\uparrow\downarrow$ with $h = 2J > 0$ can have its middle spin flipped with no energy cost. One would therefore except a crossover around $|h| = 2J > 0$ between a system preferring configurations with vanishing magnetization to systems that prefers configurations with high magnetization.

Another important thing to note is that the longitudinal field divides the single spin-flip processes, listed in table 2.1.4, into two subcategories. All process that flips a spin from 1 to -1 now changes the energy by an extra of $-2h$, and will therefore be labelled by a minus sign. In the same way, all spin flip processes that flips a spin from -1 to 1, will be labelled by a plus sign. This distinction will becomes important in chapter 3, where the non-equilibrium dynamics of the classical Ising model is described. Before going into details with non-equilibrium dynamics, it can be useful to have some intuition about the equilibrium properties of the system.

2.2 Equilibrium properties of 1D classical Ising model

To get the equilibrium properties of the 1D, nearest neighbour, classical Ising model, one first needs to calculate the partition function as usual. To do this, one labels the non-zero elements of $\mathbf{J}$ with an integer i, such that $J_i = J_{i,i+1}$. In doing so, the energy function reduces to

$$E(\{\sigma\}) = \sum_{i=1}^{N} J_i\sigma_i\sigma_{i+1} + \sum_{i=1}^{N} h_i\sigma_i. \tag{2.2.1}$$

For OBC, $J_N = 0$. When coupling the system to a heat bath with a temperature T, the partition function takes the form of

$$Z = \sum_{\{\sigma\}} e^{-\beta E(\{\sigma\})} = \sum_{\{\sigma\}} \prod_{i=1}^{N} e^{-\beta[J_i\sigma_i\sigma_{i+1} + h_i\sigma_i]}, \tag{2.2.2}$$

with $\beta = 1/T$. For homogeneous nearest neighbour couplings and homogeneous longitudinal fields, the equilibrium properties of system can be evaluated using the transfer matrix $\mathbf{T}$. This is a 2x2, real matrix, whose elements are given by

$$T_{ab} = e^{\beta(Jab+hb)} \quad \text{so that} \quad \mathbf{T} = \begin{pmatrix} e^{-\beta(J+h)} & e^{\beta(J-h)} \\ e^{\beta(J+h)} & e^{-\beta(J-h)} \end{pmatrix}. \tag{2.2.3}$$

$\mathbf{T}$ is designed in this way to make partition function reduce to a sum over products of the elements of $\mathbf{T}$. The exact form of Z will then be

$$Z = \sum_{\{\sigma\}} \prod_{i=1}^{N} T_{\sigma_i \sigma_{i+1}}. \tag{2.2.4}$$

For periodic boundary conditions, then σ_N and σ_1 are nearest neighbours. This implies that the product in eq. 2.2.4 simplifies to the trace over $\mathbf{T}^N$. one sees this to writing the product out explicit and observing that the sums corresponds to matrix products.

$$Z_{\text{PBC}} = \sum_{\{\sigma\}} \underbrace{T_{\sigma_1\sigma_2} \cdots T_{\sigma_{N-1}\sigma_N} T_{\sigma_N\sigma_1}}_{N \text{ factor matrix product}} = \sum_{\sigma_1} (\mathbf{T}^N)_{\sigma_1\sigma_1} = \text{tr}\{\mathbf{T}^N\}. \tag{2.2.5}$$

For open boundary conditions then, because there is no interaction between the first and last spin, the partition function takes the form of

$$Z_{\text{OBC}} = \sum_{\{\sigma\}} \underbrace{T_{\sigma_1\sigma_2} \cdots T_{\sigma_{N-1}\sigma_N}}_{N-1 \text{ factor matrix product}} e^{-\beta h \sigma_N} = \sum_{\sigma_1, \sigma_N} (\mathbf{T}^{N-1})_{\sigma_1\sigma_N} e^{-\beta h \sigma_N}. \tag{2.2.6}$$

The matrix products are easiest to evaluate in the eigenbasis of $\mathbf{T}$, which requires knowledge of its eigenvectors and eigenvalues. These can be found using standard techniques. If $\lambda_\pm$ denotes the eigenvalues of $\mathbf{T}$ and $\mathbf{v}_\pm$ denotes the eigenvectors, then

$$\lambda_\pm = e^{-\beta J}\left[\cosh(\beta h) \pm \sqrt{\sinh^2(\beta h) + e^{4\beta J}}\right] \quad \text{with correspoding eigenvectors} \tag{2.2.7}$$

$$\mathbf{v}_\pm = (a, b_\pm)^T = \left(e^{\beta(J-h)}, e^{-\beta J}\left[\sinh(\beta h) \pm \sqrt{\sinh^2(\beta h) + e^{4\beta J}}\right]\right)^T. \tag{2.2.8}$$

In the eigenbasis of $\mathbf{T}$, then $\mathbf{T}^M$ is simply the diagonal matrix with elements being $\lambda_\pm^M$. Transforming back to the standard basis, one gets that $\mathbf{T}^{N-1}$ evaluates to

$$\mathbf{T}^M = \mathbf{P}\begin{pmatrix} \lambda_+^M & 0 \\ 0 & \lambda_-^M \end{pmatrix}\mathbf{P}^{-1} = \frac{\lambda_+^M}{a(b_- - b_+)}\begin{pmatrix} a & a \\ b_+ & b_- \end{pmatrix}\begin{pmatrix} 1 & 0 \\ 0 & \kappa^M \end{pmatrix}\begin{pmatrix} b_- & -a \\ -b_+ & a \end{pmatrix}. \tag{2.2.9}$$

Here $\mathbf{P} = (\mathbf{v}_+, \mathbf{v}_-)$ is the matrix whose columns are the eigenvector $\mathbf{v}_+$ and $\mathbf{v}_-$, and is used in the basis transformation. Because $\lambda_+ + \lambda_- > 0$ and $\lambda_+ - \lambda_- > 0$, then $\kappa = \lambda_-/\lambda_+ \in]-1, 1[$. This is true for all non-zero temperatures and implies that $|\kappa|^M \ll 1$ for $M \gg 1$. The κ^M factor can then be ignored in eq. (2.2.9) for large systems. This results in a an open boundary condition partition function of

$$Z_{\text{OBC}} = \frac{\lambda_+^{N-1}}{a(b_- - b_+)}\left[a(b_- e^{-\beta h} - b_+ e^{\beta h}) + b_+ b_- e^{-\beta h} - a^2 e^{\beta h}\right] \tag{2.2.10}$$

The four terms in eq. (2.2.10) can be written in term of two sums, which evaluates to

$$b_+ b_- e^{-\beta h} - a^2 e^{\beta h} = -e^{\beta(2J-h)} - e^{\beta(2J-h)} = -2e^{\beta(2J-h)} \tag{2.2.11}$$

$$a(b_- e^{-\beta h} - b_+ e^{\beta h}) = -2e^{-\beta h}\left[\sinh^2(\beta h) + \sqrt{\sinh^2(\beta h) + e^{4J\beta}}\cosh(\beta h)\right] \tag{2.2.12}$$

At the same time, the denominator of eq. (2.2.10) will reduce to

$$a(b_- - b_+) = -2e^{-\beta h}\sqrt{\sinh^2(\beta h) + e^{4J\beta}} \tag{2.2.13}$$

Putting it all together, the partition function takes the form of

$$Z_{\text{OBC}} = \lambda_+^{N-1} g\left(\frac{J}{T}, \frac{h}{T}\right) \quad \text{with} \quad g\left(\frac{J}{T}, \frac{h}{T}\right) = \frac{\sinh^2(\beta h) + e^{2J\beta}}{\sqrt{\sinh^2(\beta h) + e^{4J\beta}}} + \cosh(\beta h) \tag{2.2.14}$$

Since $g(x, y) > 1$ for all $x, y \in \mathbb{R}$, then $\ln g(x, y)$ is positively defined. The free energy pr. site can then be evaluated in the thermodynamic limit, where $N \gg 1$. This evaluates to

$$f = -\frac{N-1}{N\beta}\ln\lambda_+ - \frac{1}{\beta N}\ln g(x, y) \to J - \frac{1}{\beta}\ln\left[\cosh(\beta h) + \sqrt{\sinh^2(\beta h) + e^{4\beta J}}\right]. \tag{2.2.15}$$

Compared to the partition function for periodic boundary conditions, the trace can be evaluated in the eigenbasis, which results in

$$Z_{\text{PBC}} = \lambda_+^N + \lambda_-^N = \lambda_+^N\left(1 + \kappa^N\right) \approx \lambda_+^N \quad \text{for} \quad N \gg 1. \tag{2.2.16}$$

Evaluating the free energy pr. site in the thermodynamic limit yields the same results for both PBC and OBC. The effect of the boundary conditions vanishes in the thermodynamics limit. For non-zero temperatures, then $f(J/T, h/T)$ is an infinitely differentiable function. This means that any derivative of f to any k is continuous. This implies that no phase transitions are present in the phase space $(J/T, h/T) \in \mathbb{R}^2$. The fact that eq. 2.2.15 is an infinitely differentiable function is proven using a theorem described in appendix A.1.

2.2.1 Magnetic properties

It can be demonstrated that for AFM couplings, a crossover between two phase occurs around $|h| = 2J$. This can be shown by calculating the magnetic susceptibility as a function of $h\beta$ for fixed $J\beta$. Starting with the magnetization, one gets

$$m = -\frac{1}{\beta N}\frac{\partial \ln Z}{\partial h} = -\frac{\sinh(\beta h)}{\sqrt{\sinh^2(\beta h) + e^{4\beta J}}}. \tag{2.2.17}$$

Here, it doesn't matter which partition function is used, since the boundary conditions are ignored. Differentiating again, the magnetic susceptibility will be

$$\chi T = T\frac{\partial M}{\partial h} = -e^{4J\beta}\frac{\cosh(\beta h)}{(\sinh^2(\beta h) + e^{4\beta J})^{3/2}} = \frac{e^{4J\beta}\coth(\beta h)}{\sinh^2(\beta h)}m^3. \tag{2.2.18}$$

Both the magnetization and the magnetic susceptibility are plotted in fig. 2.2.1 for both AFM and FM coupling constants. It is observed that the magnetization for a AFM are zero for small fields, $|h| < 2J$. When $|h| \to 2J$ from below, the strength of the magnetization increases drastically. Continuing in the same direction, when the field becomes stronger, $|h| > 2J$, the magnetization approaches $-\text{sgn}(h)$. This is reflected in the magnetic susceptibility, which peaks at $|h| = 2J$. The AFM side of the phase space $(J/T, h/T)$ is therefore divided into three regimes; One with $m \approx 1$, one with $m \approx -1$, and one with $m \approx 0$.

For FM coupling constants, the magnetization $m = -\text{sgn}(h)$ for non-zero field. Around $h\beta \approx 0$, the sign of the magnetization changes sign, reflected by the magnetic susceptibility that peaks. To explain how the system achieves there magnetizations, its is necessary to analyse the energy and the order of the system. To help with the order, entropy as well as the average expectation value of the nearest neighbour correlation function is used.

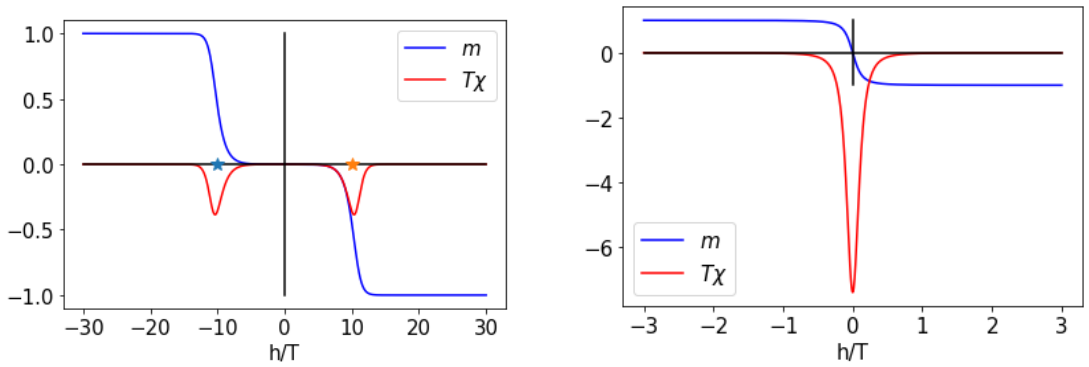

(a) AFM ($J/T = 5$) (b) FM ($J/T = -1$)

Figure 2.2.1: Magnetization and susceptibility of classical nearest neighbour Ising model with homogeneous coupling constant.

2.2.2 Entropy, energy, and correlation function

Given a canonical ensemble with a temperature of T, then the probability of being in a given configuration $\{\sigma\}$, given that the system is in equilibrium with the heat bath, is denoted $p(\{\sigma\})$. The entropy of the system will then be

$$S = -\sum_{\{\sigma\}} p(\{\sigma\}) \ln p(\{\sigma\}). \tag{2.2.19}$$

For some parameter J, h, and T, the system can localize in a given configuration $\{\tilde{\sigma}\}$. By "localization", it is here meant that the probability of the system being in a configuration $\{\tilde{\sigma}\}$ is close to one, while the probability of being in any other state is close to zero:

$$p(\{\sigma\}) \approx \begin{cases} 1 & \text{for} \quad \{\sigma\} = \{\tilde{\sigma}\} \\ 0 & \text{for} \quad \{\sigma\} \neq \{\tilde{\sigma}\} \end{cases}. \tag{2.2.20}$$

If this is the case, the entropy will be close to zero, since

$$x \ln x \to 0^- \quad \text{for both} \quad x \to 0^+ \quad \text{and} \quad x \to 1^-. \tag{2.2.21}$$

This statement is also true the other way around, so that if $S = 0$, then the system must be localized. Proof is in appendix A.2. One can therefore conclude that if $S \to 0$, then the system approaches a given configuration. The entropy of the Ising model is therefore calculated via $S = \ln Z + \beta E$. Here E is the statistical average of the energy. Calculating the two quantities, one gets the following

$$E/N = -\frac{\partial \ln \lambda_+}{\partial \beta} = J + \left(h + J \frac{2e^{3J\beta}}{\lambda_+ \sinh(\beta h)} \right) m(J\beta, h\beta) \tag{2.2.22}$$

$$S/N = \ln(\lambda_+) + \frac{E\beta}{N}. \tag{2.2.23}$$

The entropy is plotted in fig. 2.2.2a, which shows a flat landscape of $S = 0$, except around the origin and $|h| \approx 2J > 0$. The system must therefore localize around a few states when being on the AFM side of the phase diagram. The same is true for $J < 0$ but for all h values. The figure out which states the system approaches, one uses the statistical average of the nearest neighbour correlation function, averaged over all spins

$$C(J\beta, h\beta) = \frac{1}{Z} \sum_{\{\sigma\}} \left(\sum_{i=1}^{N-1} \frac{\sigma_i \sigma_{i+1}}{N-1} \right) e^{-\beta E(\{\sigma\})} = \frac{-1}{Z\beta(N-1)} \frac{\partial}{\partial J} \sum_{\{\sigma\}} e^{-\beta E(\{\sigma\})} = -\frac{1}{\beta} \frac{\partial \ln \lambda_+}{\partial J} \tag{2.2.24}$$

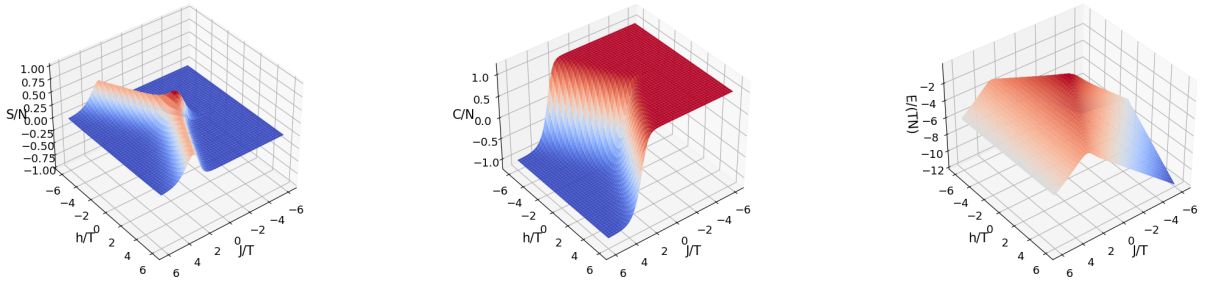

(a) (b) (c)

Figure 2.2.2: Statistical properties of the 1D. classical nn. Ising model. In **a)**, the entropy pr. site is shown, in **b)**, the average nearest neighbour correlation functions is shown, and in **(c)**, the energy of the system is shown.

Performing the differentiation, one gets

$$C(J\beta, h\beta) = 1 + \frac{2e^{3J\beta}}{\lambda_+ \sinh(h\beta)} m(J\beta, h\beta) \tag{2.2.25}$$

which is plotted in fig. 2.2.2b. Looking at the plot, one observes that the correlation between nearest neighbours are 1 for $|h| > 2J$, which implies that the system is in a FM ground state. From the energy plotting in fig. 2.2.2c one observes that $E = J - |h|$ for $|h| > 2J$ implying a diamagnetic ground state. For AFM couplings and $2J > |h|$, the entropy nearest neighbour correlation functions C takes the value of -1 implying an AFM ground state reflected by the $C = -1$ from fig. 2.2.2b. The exact ground state is not possible to determine since the energy difference between the two AFM ground states are pr. site $|h|/N$. For $2J \not\approx |h|$ the system is in an ordered state for non-zero finite temperatures. This is also reflected in the energy plot, fig. 2.2.2c, since it goes as $-2J$ in this region.

Around $2J = |h|$ the entropy increases dramatically since the energy required to create a domain wall pairs becomes so small that domains can be created from thermal excitations. This introduces disorder to the system reflected by the increase in entropy. This is reflected in the average correlation function C going smoothly between -1 and 1.

FM side - Low temperature - non-zero field

One the FM side of the phase diagram, the square root of the eigenvalues will be dominated by the $\sinh^2(h\beta)$ term, since $e^{4J\beta} \in]0; 1[$. The low temperature behaviour of the positive eigenvalue and the magnetization will therefore be

$$\lambda_+ \sim e^{-J\beta}\left[\cosh(h\beta) + \sinh(|h|\beta)\right] = e^{(-J+|h|)\beta} \quad \text{and} \quad m \sim -\frac{\sinh(h\beta)}{\sinh(|h|\beta)} = -\text{sgn}(h) \tag{2.2.26}$$

for $T \ll |J|, |h|$. The entropy will then takes the form

$$\frac{E}{N} \sim J + \left(h + J\frac{2e^{3J\beta}}{e^{(-J+|h|)\beta}\left(-\frac{\text{sgn(h)}}{2}\right)e^{|h|\beta}}\right)(-\text{sgn}(h)) = J - |h| + 4Je^{2[2J-|h|]\beta} \tag{2.2.27}$$

$$\sim J - |h|. \tag{2.2.28}$$

This reflects correctly that the system localized into the zero-field FM ground state. The average nearest neighbour correlation function also reflects this behaviour, since $C \sim 1$ as seen in fig. 2.2.2b. To shown this localization is correct, the entropy can be evaluated in this limit, which results in

$$\frac{S}{N} = \ln \lambda_+ + \beta E \sim (-J + |h|)\beta + \beta(J - |h|) = 0. \tag{2.2.29}$$

In conclusion, for any non-zero longitudinal field and $J \neq 0$, the system localizes into a zero-field FM ground state, which have all its spins pointing opposite to magnetic field.

AFM side - Low temperature behaviour - non-zero field

For low temperature $T \ll J, |h|$, the square root in the eigenvalues $\lambda_\pm$ will have low temperature behaviour

$$\sqrt{\sinh^2(\beta h) + e^{4\beta J}} \sim \begin{cases} \sinh(\beta|h|) & \text{for} \quad |h| > 2J \\ \frac{\sqrt{5}}{2} e^{2\beta J} & \text{for} \quad |h| = 2J \\ e^{2\beta J} & \text{for} \quad |h| < 2J \end{cases}. \tag{2.2.30}$$

As expected, some of the quantities used in calculations if statistical properties have different behaviours depending on $|h| > 2J$, $|h| < 2J$, or $|h| = 2J$. These different behaviours results in the positive eigenvalue and the magnetization having the following low temperature behaviour

$$\lambda_+ \sim \begin{cases} e^{(-J+|h|)\beta} & \text{for} \quad |h| > 2J \\ \varphi e^{J\beta} & \text{for} \quad |h| = 2J \\ e^{J\beta} & \text{for} \quad |h| < 2J \end{cases} \quad \text{and} \quad m \sim \begin{cases} -\text{sgn}(h) & \text{for} \quad |h| > 2J \\ -\frac{\text{sgn}(h)}{\sqrt{5}} & \text{for} \quad |h| = 2J \\ -\frac{\text{sgn}(h)}{2} e^{-(2J-|h|)\beta} & \text{for} \quad |h| < 2J \end{cases}. \tag{2.2.31}$$

The special value $\varphi = \frac{1+\sqrt{5}}{2} \approx 1.618$ is knows as the golden ratio. The energy, correlation function, and entropy will are then

$$\frac{E}{N} \sim \begin{cases} J - |h| & \text{for} \quad |h| > 2J \\ -J & \text{for} \quad |h| = 2J \\ -J & \text{for} \quad |h| < 2J \end{cases}, \quad C \approx \begin{cases} 1 & \text{for} \quad |h| > 2J \\ -0.106 & \text{for} \quad |h| = 2J \\ -1 & \text{for} \quad |h| < 2J \end{cases}, \quad \text{and} \quad \frac{S}{N} \approx \begin{cases} 0 & \text{for} \quad |h| > 2J \\ 0.481 & \text{for} \quad |h| = 2J \\ 0 & \text{for} \quad |h| < 2J \end{cases}. \tag{2.2.32}$$

For fields strength $|h| > 2J$, the system localized since $S \approx 0$. It does so by decaying into a zero-field FM ground state with magnetization opposite to the field, since $C = 1$ and $E = J - |h|$. For small fields$|h| < 2J$, the energy pr. spin, the nearest neighbour correlation function, and the magnetization all matches a zero-field AFM ground state. At first, one could falsely make the conclusion that the system must localize into one of the zero-field AFM ground states. To show that this is false, one needs to consider the open boundary partition function. For AFM couplings and small fields $|h| < 2J$, the partition function takes the form of the following sum

$$Z_{\text{OBC}} = \underbrace{2e^{\beta(N-1)J} \cosh(h\beta\delta_{\text{mod}(N,2),1})}_{\text{zero-field AFM ground states}} + \underbrace{\mathcal{O}\left(e^{\beta[(N-3)J+|h|]}\right)}_{\text{Rest}} \tag{2.2.33}$$

The first term is a result of zero - field ground states having energy

$$E_{\text{zero-field AFM groundstate}}(\pm) = -(N-1)|J| \pm |h|\delta_{\text{mod}(N,2),1}. \tag{2.2.34}$$

Her, the Kronecker delta function appears because for odd system, the last spin will contribute with a small magnetic moment which, when interacting with the field, causes the energy levels to split. Summing over the Boltzmann factors of the two lowest energy levels gives the first term in eq. (2.2.34). The next term reflect that fact that the Boltzmann factors of all higher energy levels grows slower than the the Boltzmann factors of the two lowest energy levels. The free energy is therefore

$$F = -T \ln Z_{\text{OBC}} = -T \ln 2 - (N-1)J + \ln\cosh\left(h\beta\delta_{\text{mod}(N,2),1} + \mathcal{O}\left(e^{(|h|-2J)\beta}\right)\right). \tag{2.2.35}$$

From this, the magnetization, energy, correlation function, and entropy can be calculated in the low-field, low-temperature limit

$$M = -\frac{1}{\beta}\frac{\partial \ln Z}{\partial h} \sim -\tanh(h\beta)\delta_{\mathrm{mod}(N,2),1} \sim -\mathrm{sgn}(h)\delta_{\mathrm{mod}(N,2),1} \tag{2.2.36}$$

$$E = -\frac{\partial \ln Z}{\partial \beta} \sim -(N-1)J + Mh \tag{2.2.37}$$

$$C = -\frac{1}{(N-1)\beta}\frac{\partial \ln Z}{\partial J} \approx -1 \tag{2.2.38}$$

$$S = \ln Z + \beta E \sim \ln 2 + \ln\cosh(h\beta\delta_{\mathrm{mod}(N,2),1}) - Mh\beta \tag{2.2.39}$$

For even N, then $M \approx 0$, $E \sim -(N-1)J$, $C \approx -1$, and $S \approx \ln 2$. Both zero-field AFM ground states are therefore equality likely to be visited, since the energy of the two are equal. This is reflected by the entropy being $S \approx \ln 2$, which can occur if the system has an equal probability of being in two states and a zero probability for all other states. There two states must be the zero-field AFM ground states to produce the given values of M, E, and C. Note that this effect cannot be seen from the thermodynamic limit since the $\ln 2$ vanishes when divided by a large N.

For odd N, then one of the zero-field AFM ground states will have a lower energy than the other. Because of this,

$$p_{\text{zero-field AFM groundstate}}(\pm) = \frac{e^{-(|h|\pm|h|)\beta}}{1 + e^{-2|h|\beta} + \mathcal{O}\left(e^{(|h|-2J)\beta}\right)} \approx \begin{cases} 0 & \text{for } + \\ 1 & \text{for } - \end{cases} \tag{2.2.40}$$

in the low temperature limit. The system will therefore localize in the lowest energy level, which is reflected in $S = 0$.

High temperature

In the high temperature limit, $T \gg |J|, |h|$, then the positive eigenvalue can be expanded around $\beta \approx 0$. To second order in β, one gets

$$\lambda_+ = e^{-J\beta}\left[2 + 2J\beta + (2J^2 + h^2)\beta^2 + \mathcal{O}\left(\beta^3\right)\right]. \tag{2.2.41}$$

From this, the different statistical quantities can be calculated. Starting with the magnetization, one gets that

$$m = -\frac{1}{\beta}\frac{\partial \ln \lambda_+}{\partial h} = -\frac{1}{\lambda_+}\left(2h\beta + \mathcal{O}\left(\beta^2\right)\right) \to 0 \tag{2.2.42}$$

In the same way, the limiting behaviour of the energy, entropy, and the correlation function, can be calculated.

$$E \approx 0, \quad C = 0 \quad \text{and} \quad S = N\ln 2. \tag{2.2.43}$$

This is expected since when the temperature dominates, all Boltzmann factors approaches 1. The partition function are therefore simply the number of different configurations, which here is 2^N. This makes all derivatives of Z zero, so $M = E = C$, and $S = N\ln 2$. Around the origin of the phase diagram, one would therefore expect a rise in entropy, which is confirmed in fig. 2.2.2a.

Summary of results

In summary, the system will for FM couplings magnetize opposite to the longitudinal field,

$$\{\sigma\} \to \{-\mathrm{sgn}(h), \cdots, -\mathrm{sgn}(h)\}, \tag{2.2.44}$$

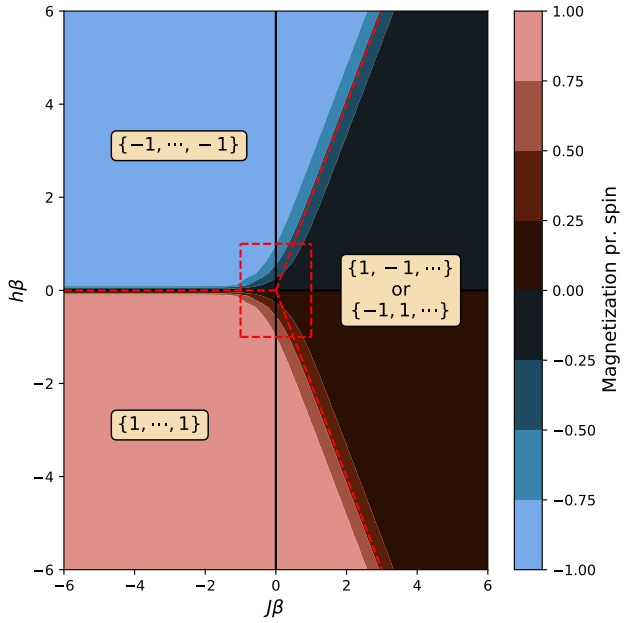

Figure 2.2.3: Phase diagram of the classical Ising model. The red lines marks the crossover lines $|h| = 2J$ while red box marks the area where $\beta < |J|, |h|$

in the low temperature limit $T \ll |J|, |h|$. This is reflected in the energy pr. spin and the average nearest neighbour correlation function, which matches the properties of this configuration. Form the entropy, it can be concluded that the system localizes into a single state, since $S = 0$.

On the AFM side of the phase diagram, if $|h| > 2J$, the system still magnetized opposite to the field. Again, this is based on the energy pr. spin, the average nearest neighbour correlation function, and the entropy pr. spin, which takes the same value as for FM couplings. If $|h| < 2J$, then the system changes its characteristics. If the number of spins is even, the configurations with the lowest energy are the zero-field AFM ground states. Both states have the same energy, which implies that the system has an equal probability of visiting both states. This is reflected in the entropy $S = \ln 2$ in the low temperature limit. On the other hand, if the number of spins is odd, one zero-field AFM ground state has a lower energy than the other. As a result, the system localizes in the configuration with the lowest energy, reflected by $S = 0$. For fields satisfying $|h| = 2J$, then the system experience a crossover between high and low magnetization. The entropy pr. site becomes of order $\mathcal{O}(1)$, which reflects that a low of configurations will have the same probability of being visited.

Around the origin of the phase diagram, where the temperature dominates the energy scales, $T \gg |J|, |h|$, all configurations becomes equality likely to be visited. This is reflected in the entropy taking the value of $S = N \ln 2$.

The behaviour of the system is summarized in the phase diagram depicted in fig 2.2.3. On the axis, the parameters J/T and h/T are shown while the colours indicates the magnetization pr. site.

Chapter 3

Kinetic Ising model

The calculations performed in section 2.2 were done so, assuming that the system was in equilibrium with a heat bath with a given temperature T. In doing so, all details about how the systems initial state and the time it took to get to equilibrium was not included. The statistical averages over the magnetizations, the energy, and the correlation function can therefore not be completely trusted, if the non-equilibrium properties of a system is to be analysed. It can therefore be necessary to perform numerical simulation of the system to get its exact properties and dynamics. For classical systems, there are no intrinsic mechanisms that can drive it, so a pure classical system will remain static on its own. One therefore needs to get classical dynamics from somewhere else. One way of doing this, is to couple the system to one or more heat baths[21, 22]. Each heat bath can be labelled by an index $\alpha \in \{1, \cdots, M\}$, where M is the number of heat baths, and is assigned a temperature T_α. These temperatures can, in principle, take any non-negative values, including $T_\alpha = 0$. The system can now exchange energy with the baths, which occurs at time scales τ_α, which results in the classical being dynamical. Each heat bath are allowed to perform a different set of mores, which alters the configuration of the system.

If $T_\alpha = 0$, then heat bath α is frozen. This means that the classical system can be give energy to the heat bath, but not receive any. If the classical system is only coupled to heat baths with $T_\alpha = 0$, then its energy will decrease steadily. That is, until it hits a ground state configuration and cannot decrease its energy further. In that case, only energy conserving moves can be performed, if any is available. If not, the system will become static and does not evolve further.

When coupling a classical Ising model to a set of heat baths in this way, and is know as the Kinetic Ising model (KIM). To describe the dynamics of the KIM, one uses the Master equation, which is the topic of the next section.

3.1 Master equation approach

Give a general classical system coupled to set of heat bath denoted by α, then the Master equation describes time evolution the probabilities $P(s|I,t)$. These are the probabilities of the system being in a state s to time $t \in \mathbb{R}_+$, given the a priori knowledge I. It does so using the rates the set of rates $\{\omega_\alpha(s \to s')\}$ which are probabilities pr. unit time, that the system transitions from a state s to a state s' by interacting with heat bath α. All together, the time evolution $\dot{P}(s|I,t)$ can be described by the linear differential equation

$$\dot{P}(s|I,t) = \sum_{\alpha=1}^{M} \sum_{s' \in \mathcal{S} \setminus \{s\}} \left[\omega_\alpha(s' \to s, I) P(s'|I,t) - \omega_\alpha(s \to s', I) P(s|I,t) \right], \tag{3.1.1}$$

which is the Master equation. Here $\mathcal{S}$ denotes the total state space of the classical system. In appendix B.1, eq. (3.1.1) is derived from first principles. Applied to the classical Ising model, the Master equation

is written as

$$\dot{P}(\{\sigma\},t) = \sum_{\alpha=1}^{M} \sum_{\{\sigma'\}\neq\{\sigma\}} \left[\omega_\alpha(\{\sigma'\}\to\{\sigma\})P(\{\sigma'\},t) - \omega_\alpha(\{\sigma\}\to\{\sigma'\})P(\{\sigma\},t)\right]., \tag{3.1.2}$$

From this equation, given the set of rates $\{\omega_\alpha\}$, the dynamics of the KIM can be described.

Some of the key actors in describing the dynamics of the KIM, were Glauber and Kawasaki[23, 24]. In Glaubers original work[23], he assumed the present of only a single heat bath. This heat bath could alter the 1D, classical, nearest neighbour, Ising model by flipping one spin at the time. The types of moves are now know as Glauber dynamics and does not conserve the magnetization of the system. If one wishes dynamics that conserves the magnetization, then Kawasaki dynamics is the way to go[24]. Here, two nearest neighbouring spins, whose projections are opposite to each other, can flip simultaneous, which conserving the overall magnetization.

In the thesis, Glauber dynamics will be studies primarily. Kawasaki dynamics will be mentioned and discussed, but will not be analysed further.

3.1.1 Detailed balance

One way of determining the set of transitions rate $\{\omega\}$, is to consider the system in equilibrium with a given heat bath. When this is the case, and the system if not coupled to any other heat baths, one gets a master equation of

$$0 = \sum_{\{\sigma'\}\neq\{\sigma\}} \left[\omega_\alpha(\{\sigma'\}\to\{\sigma\})P^{\text{equilibrium}}(\{\sigma'\},t) - \omega_\alpha(\{\sigma\}\to\{\sigma'\})P^{\text{equilibrium}}(\{\sigma\},t)\right]. \tag{3.1.3}$$

This is of course assuming that the equilibrium distribution $P^{\text{equilibrium}}(\{\sigma\},t)$ is a steady state solution to the Master equation. In eq. (3.1.3), the probability flow into any state is perfectly cancelled out by the probability flow out of the state. One solution to eq. (3.1.3) is to also balance the probability flow between any pair of configurations $(\{\sigma\},\{\sigma'\})$. If true, then

$$\omega_\alpha(\{\sigma'\}\to\{\sigma\})P_\alpha^{\text{equilibrium}}(\{\sigma'\}) = \omega_\alpha(\{\sigma\}\to\{\sigma'\})P_\alpha^{\text{equilibrium}}(\{\sigma\}). \tag{3.1.4}$$

This condition is know as detailed balance[21]. Given that $P^{\text{equilibrium}}(\{\sigma\})$ allows the equilibrium distribution of a canonical ensemble, then

$$P_\alpha^{\text{equilibrim}}(\{\sigma\}) = Z^{-1}e^{-\beta_\alpha E(\{\sigma\})} \quad \text{with} \quad \beta_\alpha = 1/T_\alpha. \tag{3.1.5}$$

This implies that for non-zero rates, the detailed balance condition in eq. 3.1.4 can be rewritten as

$$\frac{\omega_\alpha(\{\sigma\}\to\{\sigma'\})}{\omega_\alpha(\{\sigma'\}\to\{\sigma\})} = \frac{P_\alpha^{\text{equilibrium}}(\{\sigma'\})}{P_\alpha^{\text{equilibrium}}(\{\sigma\})} = \exp\left(-\frac{E(\{\sigma'\})-E(\{\sigma\})}{T_\alpha}\right). \tag{3.1.6}$$

One of the solution to eq. (3.1.6), is to use the Fermi function

$$n_F(x) = \frac{1}{1+e^x}, \quad \text{because} \quad \frac{n_F(x)}{n_F(-x)} = \frac{1+e^{-x}}{1+e^x} = \frac{1+e^x}{1+e^x}e^{-x} = e^{-x}. \tag{3.1.7}$$

Using this, the solutions of eq. (3.1.6) can be written as

$$\omega_\alpha(\{\sigma\}\to\{\sigma'\}) = \tau_\alpha^{-1} n_F\left(\frac{E(\{\sigma'\})-E(\{\sigma\})}{T_\alpha}\right). \tag{3.1.8}$$

The τ_α in eq. 3.1.8 is a time scaled associated with how often the heat bath interacts with the system. This is necessary to include, since $\omega_\alpha(\{\sigma\})$ must have units of 1/time. This is not the only solution to

the detailed balance, since one can scale it by any positive scalar and still have it satisfy detail balance. One can even scale the solution by a function of the parts of the configuration, that does not change under the transition $\{\sigma\} \leftrightarrow \{\sigma'\}$. An example of this will be seen later, when Glauber dynamics are considered in section 3.1.2. It should also be noted, that the Fermi function does not appear here because of any relation to Fermions. It just happens to be a function that satisfies eq. (3.1.6).

For small temperatures, $T_\alpha \ll |J|, |h|$, the rate of processes that increases the energy of the system, will be exponentially small since

$$\omega_{\text{Energy gain}}\tau_\alpha = e^{-\beta\Delta E} + \mathcal{O}\left(e^{-2\beta\Delta E}\right) \approx 0 \quad \text{for} \quad T \ll \Delta E = \mathcal{O}\left(|J|, |h|\right). \tag{3.1.9}$$

At the same time, processes that decreases the energy of the system will occur at time scales of τ_α, since

$$\omega^{-1}_{\text{Energy loss}} = \tau_\alpha\left(1 + e^{-\beta\Delta E}\right) \approx \tau_\alpha \quad \text{for} \quad T \gg -\Delta E = \mathcal{O}\left(|J|, |h|\right) > 0. \tag{3.1.10}$$

For moves that neither decrease nor increase the energy, the rates are $1/(2\tau_\alpha)$. At $T_\alpha = 0$, the limits becomes exact and energy increasing moves will always have their rates equal to zero. If at any point in time, the system is in a configuration where all rates are zero, then the system has become static. This can happen if the temperatures of all heat baths are zero and the system is in a configuration where all moves requires energy to perform.

From these considerations, Glauber dynamics can be studied.

3.1.2 Glauber dynamics

If the KIM is coupled to a heat bath, that interacts with the spins by flipping them one at a time, the resulting dynamics is known as Glauber dynamics. As mentioned earlier, these single spin-flip processes do not conserve the overall magnetization, since each move change it by a ± 2. For a KIM with N spins, N different moves can be performed on the system. All of these are listed in table 2.1.4 from chapter 2. One labels these processes corresponding to which spin is flipped, so that process i flips the i'th spin. Assuming no longitudinal field is present, the spin-flip rates takes the form of[21, 23, 22]

$$\omega_j(\{\sigma\}) = \frac{1}{2\tau}\left[1 + \sigma_i(\gamma_i^+\sigma_{i-1} + \gamma_i^-\sigma_{i+1})\right](1 - \delta\sigma_{i-1}\sigma_{i+1}) \quad \text{with} \tag{3.1.11}$$

$$\gamma_i^\pm = \frac{1}{2}\left[\tanh\left(\frac{J_{i-1} + J_i}{T}\right) \pm \tanh\left(\frac{J_{i-1} - J_i}{T}\right)\right]. \tag{3.1.12}$$

Note that the tanh terms in eq. (3.1.12) are in agreement with eq. (3.1.8), since $2n_F(x) = 1 - \tanh(x/2)$. The $1 - \delta\sigma_{i-1}\sigma_{i+1}$ term is an extra term originally introduced by Glauber[23] which, as will be seen later, can be used to tune the ratio between domain wall motion and domain wall creation/annihilation. The parameter $\delta \in [-1, 1]$ and the product $\sigma_{i-1}\sigma_{i+1}$ is set to be zero for $i = 1$ and $i = N$ for OBC. On the topic of OBC, when satisfied the nearest neighbour couplings J_0 and J_N are both set to be zero. This results in the $\gamma_i^\pm$ coefficient for $i = 1$ and $i = N$ satisfying

$$\gamma_1^\pm = \begin{cases} 0 & \text{for} \quad + \\ \tanh\left(\frac{J_1}{T}\right) & \text{for} \quad - \end{cases} \quad \text{and} \quad \gamma_N^\pm = \begin{cases} \tanh\left(\frac{J_{N-1}}{T}\right) & \text{for} \quad + \\ 0 & \text{for} \quad - \end{cases}, \tag{3.1.13}$$

which implies

$$\omega_1(\{\sigma\}) = \frac{1}{2\tau}\left[1 + \sigma_1\sigma_2\tanh\left(\frac{J_1}{T}\right)\right] = \tau^{-1}n_F\left(\frac{-2J_1\sigma_1\sigma_2}{T}\right) \quad \text{and} \tag{3.1.14}$$

$$\omega_N(\{\sigma\}) = \frac{1}{2\tau}\left[1 + \sigma_{N-1}\sigma_N\tanh\left(\frac{J_{N-1}}{T}\right)\right] = \tau^{-1}n_F\left(\frac{-2J_{N-1}\sigma_{N-1}\sigma_N}{T}\right). \tag{3.1.15}$$

The rest of the $\gamma_i^{\pm}$ coefficients are defined so that the first term of eq. (3.1.11) reduces to eq. (3.1.8) for general, space-dependent, nearest neighbour couplings J_i. This can be shown by setting $\sigma_{i-1} = \pm\sigma_{i+1}$, which implies an energy difference of

$$\Delta E_i^{\text{int}} = E^{\text{int}}(\{\sigma'\}) - E^{\text{int}}(\{\sigma\}) = -2J\sigma_i\sigma_{i-1}(J_{i-1} \pm J_{i+1}). \tag{3.1.16}$$

Here $\{\sigma'\}$ and $\{\sigma\}$ differ only by the sign of σ_i. Eq. (3.1.8) will therefore take the form of

$$n_F\left(\frac{\Delta E_i^{\text{int}}}{T}\right) = \frac{1}{2}\left(1 - \tanh\left(\frac{\Delta E_i^{\text{int}}}{2T}\right)\right) = \frac{1}{2}\left(1 + \tanh\left(\frac{J_{i-1} \pm J_{i+1}}{T}\right)\sigma_i\sigma_{i-1}\right) \tag{3.1.17}$$

$$= \frac{1}{2}\left[1 + \sigma_i\sigma_{i-1}\left(\gamma_i^+ \pm \gamma_i^-\right)\right] = \frac{1}{2}\left[1 + \sigma_i\left(\gamma_i^+\sigma_{i-1} + \gamma_i^-\sigma_i^-\right)\right]. \tag{3.1.18}$$

In the first equality, the fermi function is simply expanded as a tanh. In the second equality, the energy difference in eq. (3.1.16) is written explicit, while the $\sigma_i\sigma_{i-1}$ factor can be taken out of the tanh, since it only contributes with a sign. In equality three, the tanh term is expanded in terms of the $\gamma_i^{\pm}$ coefficients, and in the last equality, σ_{i-1} is distributes into the parenthesis and $\sigma_{i-1} = \pm\sigma_{i+1}$ is used. For homogeneous nearest neighbour coupling, $J_i = J$, then $\gamma_i^{\pm} = \frac{1}{2}\tanh(2J/T)$ for $1 \neq i \neq N$.

3.1.3 Evolution of statistical averages of spin projections

In general, Glauber dynamics can be used to calculate the time evolution of statistical averages of the spin projections on the z-axis. One does by considering the statistical average of σ_i, with is denoted by m_i, which satisfies

$$m_i(t) = \langle\sigma_i\rangle(t) = \sum_{\{\sigma\}}\sigma_i P(\{\sigma\}, t). \tag{3.1.19}$$

There quantities can be put into a vector $\mathbf{m}(t)$ whose elements are $m_i(t)$, which referred to as the magnetization vector. The exact dynamics of such quantity can be determined by using a rewritten version of the Master equation in eq. (3.1.2), which includes the spin-flip operator $\hat{p}_i$. This operator is defined such that given a function $f(\{\sigma\})$, then

$$\hat{p}f(\{\sigma\}) = f(\hat{p}\{\sigma\}). \tag{3.1.20}$$

$\hat{p}\{\sigma\}$ is the same configuration as $\{\sigma\}$, with the exception that the i'th spin has been flipped. This allows one to rewrite the Master equation in eq. (3.1.2), which only includes Glauber dynamics, to

$$\dot{P}(\{\sigma\}, t) = -\sum_j(1 - \hat{p}_j)\omega_j(\{\sigma\}, t)P(\{\sigma\}, t). \tag{3.1.21}$$

The elements of the magnetization vector will then evolve via

$$\dot{m}_i(t) = \sum_{\{\sigma\}}\sigma_i\dot{P}(\{\sigma\}, t) = -\sum_{\{\sigma\}}\sigma_i\sum_j(1 - \hat{p}_j)\omega_j(\{\sigma\})P(\{\sigma\}, t) \tag{3.1.22}$$

To make this a bit easier to work with, the sum over spin configurations can be expressed in terms of spin flip operators via

$$\sum_{\{\sigma\}} = \prod_{\ell=1}^{N}(1 + \hat{p}_\ell) \tag{3.1.23}$$

This results in eq. (3.1.22) taking the form of

$$\dot{m}_i = -\sum_j\left[\prod_{\ell=1}^{N}(1 + \hat{p}_\ell)\right]\Big(\sigma_i(1 - \hat{p}_j)\omega_j(\{\sigma\})P(\{\sigma\}, t)\Big) \tag{3.1.24}$$

Now because $(1+\hat{p}_i)\sigma_i(1-\hat{p}_j) = 2(1+\hat{p}_i)\sigma_i\delta_{i,j}$ and the spin flip operators commutes, $[\hat{p}_i, \hat{p}_j] = 0$, then eq. (3.1.24) reduces to

$$\dot{m}_i = -2\sum_j \left[\prod_{\ell=1}^{N}(1+\hat{p}_\ell)\right]\Big(\sigma_i\omega_i(\{\sigma\})P(\{\sigma\},t)\delta_{i,j}\Big) = -2\sum_{\{\sigma\}}\sigma_i\omega_i(\{\sigma\})P(\{\sigma\},t). \tag{3.1.25}$$

Expanding the spin-flip rates $\omega_i(\{\sigma\})$ one gets the following differential equation describing the magnetization of each site

$$\dot{m}_i\tau = -\left[m_i + \gamma_i^+ m_{i-1} + \gamma_i^- m_{i+1} - \delta\left(\gamma_\ell^+ m_{i+1} + \gamma_i^- m_{i-1} + \langle\sigma_{i-1}\sigma_i\sigma_{i+1}\rangle\right)\right] \tag{3.1.26}$$

Solving this differential equation is possible for $\delta \neq 0$. This is because eq. (3.1.26) depends on the 3-point correlation function $\langle\sigma_{i-1}\sigma_i\sigma_{i+1}\rangle$. One must therefore also include the three-point correlation functions in the system of coupled differential equation before $\mathbf{m}(t)$ can be evaluated. Since the differential equations describing the n-point correlation functions depends on correlation functions up to $n+1$'th order, the system of coupled differential equation needed is of size $2^N - 1$ which includes all correlation function up to N'th order. The size of the system of differential equation therefore gets out of hand fast, even for only a few sites N. The same problem occurs for non-zero longitudinal fields. For some cases thou, the magnetization vector $\mathbf{m}$ can be solved analytical, which is done in the next section.

3.2 Special cases of Glauber dynamics with analytical solutions

In some special cases, the evolution of the magnetization vector $\mathbf{m}(t)$ can be found analytically. For $h_i = \delta = T = 0$, then $\mathbf{m}$'s time derivative can be expressed as

$$\dot{\mathbf{m}}(t) = -\frac{1}{\tau}\mathcal{A}\mathbf{m}(t). \tag{3.2.1}$$

Here $\mathcal{A}$ is an $N \times N$ matrix, which generates the time evolution, and can be written explicit as

$$\mathcal{A} := \begin{pmatrix} 1 & \gamma_1^- & 0 & \cdots & 0 \\ \gamma_2^+ & 1 & \gamma_2^- & \ddots & \vdots \\ 0 & \ddots & \ddots & \ddots & 0 \\ \vdots & \ddots & \gamma_{N-1}^+ & 1 & \gamma_{N-1}^- \\ 0 & \cdots & 0 & \gamma_N^+ & 1 \end{pmatrix}. \tag{3.2.2}$$

This will from now on be refer to as the classical time evolution matrix. If $\mathcal{A}$ is diagonalizable, one can expand the vector $\mathbf{m}$ in terms $\mathcal{A}$'s eigenvectors. If $\mathbf{v}_\ell$ is the ℓ'th eigenvector of $\mathcal{A}$, with eigenvalue λ_ℓ, then

$$\mathbf{m}(t) = \sum_\ell c_\ell \mathbf{v}_\ell e^{-\lambda_\ell(t-t_0)/\tau} \tag{3.2.3}$$

is a solution to eq. (3.2.1). Here $t_0 \in \mathbb{R}$ is some initial time, where the magnetization vector $\mathbf{m}$ is known. The coefficients $\{c_\ell\}$ are the scalar product between the initial magnetization vector $\mathbf{m}_0 = \mathbf{m}(t_0)$ and the ℓ'th eigenvector $\mathbf{v}_\ell$:

$$c_\ell = \langle\mathbf{m}_0, \mathbf{v}_\ell\rangle. \tag{3.2.4}$$

Since $m_i \in [-1, 1]$, then the eigenvalues of $\mathcal{A}$ must satisfy $\lambda_\ell \geq 0$, so that the exponential in eq. (3.2.3) does not increase. The exponentials with negative eigenvalue will decay to zero, while those with zero

eigenvalues will not evolve. In the limit of $(t-t_0)/\tau \to \infty$, the only terms left in eq. (3.2.3) will be the terms involving eigenvectors with $\lambda_\ell = 0$. The number of these eigenvalues depends on the specific case. If non exists, the magnetization vector $\mathbf{m}(t) \to 0$ and the statistical average of the magnetization will be zero.

Using the method described above, one can start analysing the dynamics of a 1D AFM KIM with $h_i = \delta = T = 0$.

3.2.1 Zero field, zero temperature, homogeneous AFM coupling

For a system with zero field $h_i = 0$, homogeneous coupling constant $J_i = J(1-\delta_{i,N})$, and $T = 0$, the off-diagonal elements $\mathcal{A}$ reduces to $\gamma_i^{\pm} = \frac{1}{2}$ for $1 < i < N$, $\gamma_1^+ = \gamma_N^- = 0$, and $\gamma_1^- = \gamma_N^+ = 1$. $\mathcal{A}$ will therefore take the form of

$$\mathcal{A} = \begin{pmatrix} 1 & 1 & 0 & \cdots & 0 \\ \frac{1}{2} & 1 & \frac{1}{2} & \ddots & \vdots \\ 0 & \ddots & \ddots & \ddots & 0 \\ \vdots & \ddots & \frac{1}{2} & 1 & \frac{1}{2} \\ 0 & \cdots & 0 & 1 & 1 \end{pmatrix}. \tag{3.2.5}$$

For a vector $\mathbf{v}$ to be an eigenvector of $\mathcal{A}$, with a given eigenvalue λ, then the elements of $\mathbf{v}$ must satisfy the following linear difference equation:

$$0 = xv_1 + v_2, \tag{3.2.6a}$$
$$0 = \frac{1}{2}v_i + xv_{i+1} + \frac{1}{2}v_{i+2}, \tag{3.2.6b}$$
$$0 = v_{N-1} + xv_N, \tag{3.2.6c}$$

with $x = 1-\lambda$. The exact values of set $\{v_i\}$ can be evaluated using the method described in [25]. Here it is stated, that the elements of $\mathbf{v}$ should satisfy $v_i = A[r_+^i + Br_-^i]$ to be a solution of eq. (3.2.6) with A and B being general complex numbers. For this to be true, the coefficient r_+ and r_- must be roots of the polynomial

$$P(z) = \frac{1}{2}z^2 + xz + \frac{1}{2}, \tag{3.2.7}$$

where the coefficients of P matches the those of eq. (3.2.6b). The roots of P can easily be evaluated and takes the form of

$$r_\pm = -x \pm \sqrt{x^2-1}. \tag{3.2.8}$$

Note that r_+ and r_- are reciprocal to each other, since $r_+r_- = 1$. For eigenvalues $\lambda \in]0,2[$, then $r_\pm$ both lays on the complex unit circle and forms complex conjugate pair. If $\lambda < 0$ or $\lambda > 2$, then $r_\pm$ are both real non-zero numbers.

From the boundary conditions, eq. (3.2.6a) and eq (3.2.6c), the allowed values of x and B are determined. A will work as a normalization constant, which is determined afterwards. From the first boundary condition, eq. (3.2.6a), then

$$0 = xv_1 + v_2 = Ax[r_+ + Br_-] + A[r_+^2 + Br_-^2] = A\left[r_+(x+r_+) + Br_-(x+r_-)\right]. \tag{3.2.9}$$

Since $(x+r_\pm) = \pm\sqrt{x^2-1}$ and $r_+r_- = 1$ is true, then

$$0 = A\sqrt{x^2-1}\left[r_+ - Br_-\right] = \frac{A\sqrt{x^2-1}}{r_+}\left[r_+^2 - B\right] \Leftrightarrow A = 0 \quad \text{or} \quad |x| = 1 \quad \text{or} \quad B = r_+^2. \tag{3.2.10}$$

The first possibility, being $A = 0$ is not considered because if $A = 0$, then $\mathbf{v}$ is the zero vector $\mathbf{0}$, which can never be an eigenvector of a matrix. The second possibility of $|x| = 1$ can be considered, which gives a valid eigenvector. This ends up being covered by the last condition $B = r_+^2$, so for the rest of the calculations, $B = r_+^2$.

The choice causes $v_i = Ar_+[r_+^{i-1} + r_-^{i-1}]$. From the last boundary conditions, x can be determined. This extra factor of r_+ can be absorbed into the normalization constant, by redefining $A \to Ar_+$. Doing so makes the last boundary condition, eq. (3.2.6c), take the form of

$$0 = A\left[r_+^{N-2} + r_-^{N-2} + x(r_+^{N-1} + r_-^{N-1})\right] = \frac{A\sqrt{x^2-1}}{r_+^{N-1}}\left(1 - r_+^{2(N-1)}\right). \tag{3.2.11}$$

Do get this, one uses $r_\pm^{N-2} + xr_\pm^{N-1} = r_\pm^{N-1}(r_\mp + x) = \mp r_\pm^{N-1}\sqrt{x^2-1}$ together with $r_+r_- = 1$. From this condition, it can be concluded the allowed values of r_+ must be roots of the polynomial $Q(z) = 1 - z^{2(N-1)}$. This has $2(N-1)$ solutions, which all are equally distributed on the complex unit circle.

$$z_\ell = e^{i\frac{\ell\pi}{N-1}} \quad \text{with} \quad \ell \in \{-(N-2), \ldots, -1, 0, 1, \cdots, N-2, N-1\} \tag{3.2.12}$$

For the ℓ eigenvector, then $r_+ = z_\ell$, which implies $r_- = z_{-\ell}$, again since $r_+r_- = 1$. The corresponding eigenvector $\mathbf{v}_\ell$ will then have elements

$$(\mathbf{v}_\ell)_i = A\left[(r_+)_\ell^{i-1} + (r_-)_\ell^{i-1}\right] = 2A\cos\left(\frac{\ell\pi}{N-1}(i-1)\right) \tag{3.2.13}$$

Normalizing the vector defines A, which gives the following expressions for the eigenvectors.

$$(\mathbf{v}_\ell)_i = \begin{cases} \sqrt{\frac{2}{N+1}}\cos[(i-1)\theta_\ell] & \text{for} \quad \ell \in \{\pm 1, \cdots, \pm(N-2)\} \\ \frac{1}{\sqrt{N}} & \text{for} \quad \ell = 0 \\ \frac{1}{\sqrt{N}}(-1)^i & \text{for} \quad \ell = N-1 \end{cases}. \tag{3.2.14}$$

Since cosine is an even function, then $\mathbf{v}_{-\ell} = \mathbf{v}_\ell$. There are therefore only N distinct eigenvectors of $\mathcal{A}$, as expected. The corresponding eigenvalues can also be calculated, which simply yields

$$\lambda_\ell = 1 - x_\ell = 1 + \frac{1}{2}\left[(r_+)_\ell + (r_-)_\ell\right] = 1 + \cos\left(\frac{\ell\pi}{N-1}\right). \tag{3.2.15}$$

All eigenvalues are positive except for $\lambda_0 = 0$. This implies that one of the exponentials will not decay when time increases. From this, the magnetization vector that solved eq. (3.2.1) with $\mathcal{A}$ taking the form of eq. 3.2.5, is

$$\mathbf{m}(t) = \langle \mathbf{m}_0, \mathbf{v}_{N-1}\rangle \mathbf{v}_{N-1} + \sum_{\ell=0}^{N-2} \langle \mathbf{m}_0, \mathbf{v}_\ell\rangle e^{-\left[1+\cos\left(\frac{\ell\pi}{N-1}\right)\right]\frac{t-t_0}{\tau}} \mathbf{v}_\ell. \tag{3.2.16}$$

For $t - t_0 \gg \tau/[1 - \cos\left(\frac{\pi}{N-1}\right)]$, the magnetization vector approaches

$$\mathbf{m}(t) \overset{(t\to\infty)}{\to} \langle \mathbf{m}_0, \mathbf{v}_{N-1}\rangle \mathbf{v}_{N-1} = \frac{1}{\sqrt{N}}\left(\sum_{i=1}^{N} (\mathbf{m}_0)_i(-1)^i\right)\mathbf{v}_{N-1}. \tag{3.2.17}$$

The exacts meaning of this result is unfortunately not clear. This is because the dot product $\langle \mathbf{m}_0, \mathbf{v}_{N-1}\rangle$ does not really relate to any physical quantity. One thing can be said thou. The long-term behaviour

of the statistical average of the total magnetization, can be evaluated.

$$\lim_{t\to\infty} m(t) = \frac{1}{N}\sum_{i=1}^{N}\lim_{t\to\infty}\left(\mathbf{m}(t)\right)_i = \sum_{i=1}^{N}\frac{1}{\sqrt{N}N}\left(\sum_{j=1}^{N}(\mathbf{m}_0)_j(-1)^j\right)(\mathbf{v}_{N-1})_i \tag{3.2.18}$$

$$= \begin{cases} -\frac{1}{\sqrt{N}N}\sum_{j=1}^{N}(\mathbf{m}_0)_j(-1)^j & \text{for odd } N \\ 0 & \text{for even } N \end{cases} \in [-N^{-1}, N^{-1}]. \tag{3.2.19}$$

At the same time, each element of $\mathbf{m}(t\to\infty)$ have the same absolute value and alternate sign along the chain. This could lead one to assume that the system decays into a random AFM ground states with an unknown probability of going into either. This can be tested in chapter 5, where the non-equilibrium dynamics of the system is simulated.

3.2.2 Field at first site, AFM homogeneous coupling, and zero temperature

Even thou (3.1.26) cannot be solved for general longitudinal fields, it is possible to find the dynamics for the system if a local field is placed on the first site $h_i = h\delta_{i,1}$. If the field is strong enough, a domain wall could be created between spin 1 and 2, which can be moves to the opposite side of the system. This allows the system to transition from one ground state to another. The threshold for this lays on the line $|h| = J$, with the sign of h determining which state is preferred.

When introducing a field on the first site, only the first rate $\omega_1(\{\sigma\})$ changes compared to before. Assuming $T = \delta = 0$ then $\omega_1(\{\sigma\})$ takes the form of

$$\omega_1(\sigma) = \frac{1}{\tau}n_F\left(-2\sigma_1\frac{J\sigma_2 + h}{T}\right) \overset{T\to 0^+}{=} \frac{1}{2\tau}\left[1 + \sigma_1 \mathrm{sgn}\left(J\sigma_2 + h\right)\right] = \frac{1}{2\tau}\left[1 + \sigma_1\left(a_+\sigma_2 + a_-\right)\right], \tag{3.2.20}$$

$$\text{with} \quad a_\pm = \frac{\mathrm{sgn}(J+h) \pm \mathrm{sgn}(J-h)}{2}. \tag{3.2.21}$$

The system of differential equation, describing the time evolution of $\mathbf{m}(t)$, will therefore gain an extra term compared to $h = 0$.

$$\dot{\mathbf{m}} = -\frac{1}{\tau}\left(\mathcal{A}\mathbf{m} + \mathbf{g}\right) \quad \text{with} \quad \mathcal{A} = \begin{pmatrix} 1 & a_+ & 0 & \cdots & 0 \\ \frac{1}{2} & 1 & \frac{1}{2} & \ddots & \vdots \\ 0 & \ddots & \ddots & \ddots & 0 \\ \vdots & \ddots & \frac{1}{2} & 1 & \frac{1}{2} \\ 0 & \cdots & 0 & 1 & 1 \end{pmatrix} \quad \text{and} \quad \mathbf{g}_i = \delta_{i,1}a_-. \tag{3.2.22}$$

The introduction of this extra term $\mathbf{g}$ makes the differential equation non-homogeneous. It must therefore be solved using the generalized Panzer formula[26] for systems of differential equations.

$$\mathbf{m}(t) = \Phi(t)\Phi(t_0)^{-1}\mathbf{m}_0 - \frac{1}{\tau}\Phi(t)\int_{t_0}^{t} dt'\ \Phi(t')^{-1}\mathbf{g}. \tag{3.2.23}$$

In the Panzer formula, the matrix $\Phi(t)$ is know as the fundamental matrix of the system. It is defined to be the solution of the homogeneous system

$$\dot{\Phi}(t) = -\frac{1}{\tau}\mathcal{A}\Phi(t). \tag{3.2.24}$$

If $\mathcal{A}$ is diagonalizable, then, in the eigenbasis of $\mathcal{A}$, Φ is also diagonal with elements $e^{-\lambda_\ell(t-t_0)/\tau}$. The boundary condition used here are $\Phi(t_0) = \mathbb{I}$. This reduces eq. (3.2.23) correctly to $\mathbf{m}(t_0) = \mathbf{m}_0$. Change

from $\mathcal{A}$'s eigenbasis to the canonical basis, using the transformation matrix $\mathbf{S}$, the fundamental matrix can be written as

$$\Phi(t) = \exp\left(-\mathcal{A}\frac{t-t_0}{\tau}\right) = \mathbf{S}\ \mathrm{diag}\left(e^{-\lambda_0\frac{t-t_0}{\tau}}, \cdots, e^{-\lambda_{N-1}\frac{t-t_0}{\tau}}\right)\mathbf{S}^{-1} \quad \text{with} \quad \mathbf{S} = \left(\mathbf{v}_0, \cdots, \mathbf{v}_{N-1}\right). \tag{3.2.25}$$

If the local field is time independent, then the vector $\mathbf{g}$ is time independent too. It can therefore be pulled from the integral in eq. (3.2.23), so that

$$\int_{t_0}^{t} dt'\ \Phi(t')^{-1}\mathbf{g} = \mathbf{S}\ \mathrm{diag}\left(\int_{t_0}^{t} dt' e^{\lambda_\ell\frac{t'-t_0}{\tau}}\right)\mathbf{S}^{-1}\mathbf{g}. \tag{3.2.26}$$

The integral over the exponential function depends on the value of eigenvalue λ_ℓ in question. If $\lambda_\ell = 0$, the integral becomes linear in $t - t_0$. This would make some of the elements in $\mathbf{m}(t)$ increase/decrease linear in time as well, which would, at some point, exceed allowed values of $\mathbf{m}$. For the system to act physical, all eigenvalues of $\mathcal{A}$ must be non-zero. Assuming this is to be the case, the integral in eq. (3.2.26) reduces to

$$\int_{t_0}^{t} dt'\ \Phi(t')^{-1}\mathbf{g} = -\tau\mathbf{S}\ \mathrm{diag}\left\{\left(e^{-\lambda_\ell\frac{t-t_0}{\tau}} - 1\right)\lambda_\ell^{-1}\right\}\mathbf{S}^{-1}\mathbf{g} = -\tau\left[\Phi^{-1}(t) - 1\right]\mathcal{A}^{-1}\mathbf{g}. \tag{3.2.27}$$

Inserting this back into the Panzer formula in eq. (3.2.23), that the magnetization evolves as

$$\mathbf{m}(t) = \Phi(t)(\mathbf{m}_0 - \mathcal{A}^{-1}\mathbf{g}) + \mathcal{A}^{-1}\mathbf{g}. \tag{3.2.28}$$

Since the eigenvalues of $\mathcal{A}$ are all assumed to be positive, then $\Phi(t)$ will vanish for $(t-t_0)/\tau \gg 1$. This makes $\mathbf{m}(t) \to \mathcal{A}^{-1}\mathbf{g}$. If any of $\mathcal{A}$'s eigenvalues are negative, some of the elements of the fundamental matrix will diverge and $\mathbf{m}$ becomes non-physical.

Using this scheme, the long-term behaviour of $\mathbf{m}$ can be calculated for different value of h_1.

Low positive field, AFM coupling

For positive local fields with $J > h_1 > 0$, then the two constants, a_+ and a_-, evaluates to 1 and 0 respectively. $\mathbf{g}$ will therefore evaluate to the zero vector, while $\mathcal{A}$ acts as if the field was zero. In summary,

$$\mathcal{A} = \begin{pmatrix} 1 & 1 & 0 & \cdots & 0 \\ \frac{1}{2} & 1 & \frac{1}{2} & \ddots & \vdots \\ 0 & \ddots & \ddots & \ddots & 0 \\ \vdots & \ddots & \frac{1}{2} & 1 & \frac{1}{2} \\ 0 & \cdots & 0 & 1 & 1 \end{pmatrix} \quad \text{and} \quad \mathbf{g} = \mathbf{0}. \tag{3.2.29}$$

The differential equation describing this system will therefore reduce to eq. (3.2.1). The dynamics will then be equivalent to if the field didn't exist at all. The reason for this is that even thou the field changed some energy levels, it is not strong enough to rearrange the energetic order of the configurations. At zero temperature, if the system has decays into the zero-field AFM ground state with $\sigma_1 = \mathrm{sgn}(h_1)$, a domain wall cannot be created between the first and second site. The system can therefore not transition to the true ground state configuration. This implies that the zero-field AFM ground state the system first decays into, is the one that it gets stuck in.

A last note to make here is that since $\mathbf{g} = \mathbf{0}$, then the integral in eq. (3.2.23) is zero. The condition stating that all eigenvalues of $\mathcal{A}$ must be non-zero is therefore not required any more. The magnetization vector will therefore have a long-term equivalent to that of $h_1 = 0$.

$$\mathbf{m}(t) \sim \langle\mathbf{v}_{N-1}, \mathbf{m}_0\rangle\mathbf{v}_{N-1} \quad \text{for} \quad \frac{t-t_0}{\tau} \gg 1. \tag{3.2.30}$$

Things becomes more interesting when $h_1 = J$.

Critical positive field, AFM coupling

If the field $h_1 = J$, then the nearest neighbour interaction and the field contributes equally to the energy of the first spin. This mean that if the system is in a configuration where the first two spin being $\uparrow\downarrow$, then a domain wall can be created between them without an energy cost. This implies that if the system is in the zero-field AFM ground state with $\sigma_1 = \mathrm{sgn}(h_1)$, then the system can transition into the true ground state using a single domain wall. This wall is created between site 1 and 2 and moves as a random walk until it hit the other edge, where it is annihilated. The system will therefore always end up in the true ground state, which the magnetization vector $\mathbf{m}$ should match. To check if this is true, a_+ and a_- are evaluated. Both of then evaluates to $1/2$ which makes $\mathcal{A}$ and $\mathbf{g}$ evaluate to

$$\mathcal{A} = \begin{pmatrix} 1 & \frac{1}{2} & 0 & \cdots & 0 \\ \frac{1}{2} & 1 & \frac{1}{2} & \ddots & \vdots \\ 0 & \ddots & \ddots & \ddots & 0 \\ \vdots & \ddots & \frac{1}{2} & 1 & \frac{1}{2} \\ 0 & \cdots & 0 & 1 & 1 \end{pmatrix} \quad \text{and} \quad \mathbf{g} = \frac{1}{2}\hat{e}_1. \tag{3.2.31}$$

Here $\hat{e}_1$ is the first unit vector with $(\hat{e}_1)_i = \delta_{i,1}$. If $\mathbf{v}$ is an eigenvector of $\mathcal{A}$, with eigenvalue λ, then the elements of $\mathbf{v}$ must satisfy the linear difference equation

$$0 = xv_1 + \frac{1}{2}v_2, \tag{3.2.32a}$$

$$0 = \frac{1}{2}v_i + xv_{i+1} + \frac{1}{2}m_{i+2}, \tag{3.2.32b}$$

$$0 = v_{N-1} + xv_N, \tag{3.2.32c}$$

with $x = 1 - \lambda$. This looks a bit like eq. (3.2.6), with the exception of the first boundary condition. v_i must therefore satisfy $v_i = A(r_+^i + Br_-^i)$ with $r_\pm = -x \pm \sqrt{x^2 - 1}$ as before. From the first boundary condition eq. (3.2.32a), B can again be determined. Doing so reveals

$$0 = A\left[x(r_+ + Br_-) + \frac{1}{2}(r_+^2 + Br_-^2)\right] = A\left[\left(x + \frac{1}{2}r_+\right)r_+ + \left(x + \frac{1}{2}r_-\right)r_-B\right]. \tag{3.2.33}$$

Since

$$\left(x + \frac{1}{2}r_\pm\right)r_\pm = \frac{1}{2}\left(2x - x \pm \sqrt{x^2 - 1}\right)r_\pm = -\frac{1}{2}r_\mp r_\pm = -\frac{1}{2}, \tag{3.2.34}$$

then eq. (3.2.33) reduces to

$$0 = -\frac{A}{2}(1 + B) \Leftrightarrow (A = 0 \quad \text{or} \quad B = -1). \tag{3.2.35}$$

Again, if $A = 0$, then $\mathbf{v}$ is the zero vector, which cannot be an eigenvector. Therefore, $B = -1$ must be the only solution. $\mathbf{v}$'s elements must therefore be $v_i = A[r_+^i - r_-^i]$ to satisfy the first boundary condition. From this, the second boundary condition eq. (3.2.32c) reduces to

$$0 = A\left[r_+^{N-1} - r_-^{N-1} + x\left(r_+^N - r_-^N\right)\right] = A\left[r_+^N(x + r_-) - r_-^N(x + r_+)\right] \tag{3.2.36}$$

As before, $(r_\pm + x) = \pm\sqrt{x^2 - 1}$, which implies

$$0 = -A\sqrt{x^2 - 1}\left[r_+^N + r_-^N\right] = -\frac{A\sqrt{x^2 - 1}}{r_+^N}\left(r_+^{2N} - 1\right). \tag{3.2.37}$$

What remains is that either; r_+ must be a root of the polynomial $Q(z) = z^{2N} + 1 = 0$, or $|x| = 1$. In the second case, with $|x| = 1$, then $r_+ = r_-$.

which have solutions

$$(r_+)_\ell = e^{i\frac{2\ell-1}{2N}\pi} \quad \text{for} \quad \ell \in \{-(N-1), \cdots, -1, 0, 1, \cdots, N\} \tag{3.2.38}$$

The eigenvectors of $\mathcal{A}$ are therefore on the form.

$$(\mathbf{v}_\ell)_i = \sqrt{\frac{2}{N-1}} \sin\left(\frac{2\ell-1}{2N}\pi i\right) \text{ for } \ell \in \{0, 1, \cdots, N-1\} \tag{3.2.39}$$

Note that the eigenvectors generated from negative ℓs are equal to the eigenvector generated from positive ℓ's since

$$\phi_{-\ell} = \frac{-2\ell-1}{2N}\pi = -\frac{2\ell+1}{2N}\pi = -\frac{2(\ell+1)-1}{2N}\pi = -\phi_{\ell+1} \tag{3.2.40}$$

when normalizing the eigenvector, the sign difference is removed and the $\mathbf{v}_{-\ell} = \mathbf{v}_{\ell+1}$ for $\ell \in \{1, \cdots, N-1\}$. The eigenvalues can also be evaluated which will be

$$\lambda_\ell = 1 - x = 1 + \frac{1}{2}(r_+ + r_-) = 1 + \cos\left(\frac{2\ell-1}{2N}\pi\right) > 0 \tag{3.2.41}$$

All eigenvalues are then greater than zero, which implies $\mathcal{A}^{-1}$ is well defined and the fundamental matrix does not diverge. The magnetization vector will therefore evolve via

$$\mathbf{m}(t) = \Phi(t)(\mathbf{m}_0 - \mathcal{A}^{-1}\vec{g}) + \mathcal{A}^{-1}\vec{g} \quad \text{with} \quad \Phi(t) = \exp(\mathcal{A}(t - t_0)) \tag{3.2.42}$$

which for $t - t_0 \gg \tau$, decays into $\mathcal{A}^{-1}\mathbf{g}$. The exact value of this vector-matrix product can be evaluated analytical, which is done in appendix B.2, the result of the calculations yields

$$\mathbf{m}(t) \sim \mathcal{A}^{-1}\mathbf{g} = (-1)^i \tag{3.2.43}$$

From this, one can conclude that the system must decay into the zero-field AFM ground state with the first spin being opposite to the field.

High positive field, AFM coupling

In the high field limit, $h > J > 0$ the field dominated over the nearest neighbour coupling. It is therefore expected that the system decays into the zero-field AFM ground state $\{\sigma\} = \{1, -1, \cdots, \}$. The same physics apply as for the critical field region, $h = J > 0$, but with the exception that field now dominated. This means that instead of the domain wall being able to be annihilated of both sides of the spin chain, it is now only possible for domain walls to be annihilated at the N'th site. The magnetization vector is therefore expected to again decay into the $(\mathbf{m}(t))_i \to (-1)^i$. To show this, the $a_\pm$ coefficients are evaluated. Since

$$a_+ = 0 \quad \text{and} \quad a_- = 1, \tag{3.2.44}$$

then $\mathcal{A}$ and $\mathbf{g}$ takes the form of

$$\mathcal{A} = \begin{pmatrix} 1 & 0 & 0 & \cdots & 0 \\ \frac{1}{2} & 1 & \frac{1}{2} & \ddots & \vdots \\ 0 & \ddots & \ddots & \ddots & 0 \\ \vdots & \ddots & \frac{1}{2} & 1 & \frac{1}{2} \\ 0 & \cdots & 0 & 1 & 1 \end{pmatrix} \quad \text{and} \quad \mathbf{g} = \delta_{i,1}. \tag{3.2.45}$$

This is actually a problem since the method described above does not work, because $\mathcal{A}$ is not diagonalizable. This will not be proven here, but one can prove it by evaluating the eigenvectors using the previous described method. When one is done, it can shown that the set of generated "eigenvectors" are not linear independent which implies $\det \mathbf{S} = 0$ and $\mathbf{S}^{-1}$ does not exists. $\mathcal{A}$ can therefore not be diagonalized since there does not exists a matrix $\mathbf{S}$ such that $\mathbf{S}^{-1}\mathcal{A}\mathbf{S}$ is diagonal. Luckily there is another way to solve eq. (3.2.22).

Writing the system of coupled differential equation out explicit, one get that the magnetization vector's elements must satisfy

$$\dot{m}_1 = -\frac{1}{\tau}(m_1 + 1) \tag{3.2.46a}$$

$$\dot{m}_i = -\frac{1}{2\tau}(m_{i-1} + m_{i+1}) - \frac{1}{\tau}m_i \quad \text{for} \quad 1 < i < N \tag{3.2.46b}$$

$$\dot{m}_N = -\frac{1}{2\tau}(m_{N-1} + m_N), \tag{3.2.46c}$$

one observes that the differential equation describing the evolution of m_1 is independent of all the other elements of $\mathbf{m}$. The time evolution of m_1 can therefore be evaluated using the one-dimensional Panzer formula[26].

$$m_1(t) = m_1(t_0)e^{-\frac{t-t_0}{\tau}} + e^{-\frac{t-t_0}{\tau}} \int_{t_0}^{t} dt' e^{\frac{t'-t_0}{\tau}} \left(-\frac{1}{\tau}\right) = (m_1(t_0) + 1)e^{-\frac{t-t_0}{\tau}} - 1 \tag{3.2.47}$$

For times $t - t_0 \gg \tau$, the magnetization on site one approaches the fix-point $m_1 = -1$ which minimizes hm_1. The rest of the system are described by the reduced magnetization vector $\mathbf{m}_{\text{red}}$ which is simply the magnetization vector $\mathbf{m}$ without the first site. The dynamics of $\mathbf{m}_{\text{red}}$ are

$$\dot{\mathbf{m}}_{\text{red}} = -\frac{1}{\tau}\left(\begin{pmatrix} 1 & \frac{1}{2} & 0 & \cdots & 0 \\ \frac{1}{2} & 1 & \frac{1}{2} & \ddots & \vdots \\ 0 & \ddots & \ddots & \ddots & 0 \\ \vdots & \ddots & \frac{1}{2} & 1 & \frac{1}{2} \\ 0 & \cdots & 0 & 1 & 1 \end{pmatrix} \mathbf{m}_{\text{red}} + \mathbf{g}_{\text{red}}(t)\right) \quad \text{with} \quad \mathbf{g}_{\text{red}}(t))_i = \frac{1}{2}m_1(t)\delta_{i,1} \tag{3.2.48}$$

This system of differential equations looks similar to that of the previous paragraph but with a time dependent $\mathbf{g}$ vector. The fundamental matrix corresponding to eq. (3.2.32) is therefore the same as for $h = J$ but with one less site.

$$\Phi(t) = \mathbf{S}\ \text{diag}\left(e^{-\lambda_0\frac{t-t_0}{\tau}}, \cdots, e^{-\lambda_{N-2}\frac{t-t_0}{\tau}}\right)\mathbf{S}^{-1} \quad \text{with} \tag{3.2.49}$$

$$S_{ij} = \sqrt{\frac{2}{N-2}}\sin\left((i-1)\frac{2j-1}{2(N-1)}\pi\right) \quad \text{and} \quad \lambda_\ell = 1 + \cos\theta_\ell \tag{3.2.50}$$

The Panzer formula, for the reduced magnetization vector can then be written as

$$\mathbf{m}_{\text{red}}(t) = \Phi(t)\Phi(t_0)^{-1}\mathbf{m}_{\text{red}}(t_0) - \frac{1}{\tau}\Phi(t)\int_{t_0}^{t} dt'\ \Phi(t')^{-1}\mathbf{g}_{\text{red}}(t') \tag{3.2.51}$$

Diagonalizing the fundamental matrix, the integral in eq. (3.2.51) can be written as

$$\left(\int_{t_0}^{t} dt'\ \Phi(t')^{-1}\mathbf{g}_{\text{red}}(t)\right)_i = \sum_\ell S_{i\ell}(\mathbf{S}^{-1})_{\ell 1}\int_{t_0}^{t} dt'\ e^{\lambda_\ell\frac{t'-t_0}{\tau}}[(m_1(t_0)+1)e^{-\frac{t'-t_0}{\tau}} - 1] \tag{3.2.52}$$

This integral acts different depending on if N is even of odd. If N is even, then $N/2$ in an integer. This mean that

$$\lambda_{N/2} = 1 + \cos\left(\frac{2\frac{N}{2}-1}{2(N-1)}\pi\right) = 1 + \cos\left(\frac{\pi}{2}\right) = 1 \tag{3.2.53}$$

The $\ell = \frac{N}{2}$ term of eq. (3.2.52) will therefore evaluated to

$$\int_{t_0}^{t} dt'\ e^{\frac{t'-t_0}{\tau}}\left[(m_1(t_0)+1)e^{-\frac{t-t_0}{\tau}} - 1\right] = (m_1(t_0)+1)\,(t-t_0) - \tau\left(e^{\frac{t-t_0}{\tau}} - 1\right) \tag{3.2.54}$$

$$= \tau e^{\frac{t-t_0}{\tau}}\left[(m_1(t)+1)\frac{t-t_0}{\tau}e^{-\frac{t-t_0}{\tau}} + e^{-\frac{t-t_0}{\tau}} - 1\right]. \tag{3.2.55}$$

For the other ℓs, the integral in eq. (3.2.52) can be expressed as

$$\int_{t_0}^{t} dt'\ e^{\lambda_\ell\frac{t'-t_0}{\tau}} m_1(t') = \tau e^{\lambda_\ell\frac{t-t_0}{\tau}}\left\{\frac{m_1(t)+1-(m_1(t_0)+1)\,e^{-\lambda_\ell\frac{t-t_0}{\tau}}}{\lambda_\ell - 1} + \frac{e^{-\lambda_\ell\frac{t-t_0}{\tau}}-1}{\lambda_\ell}\right\} \tag{3.2.56}$$

If N is odd, then for all ℓ, $\lambda_\ell \neq 1$, which implies eq. (3.2.56) work for all ℓ. Defining the matrix

$$\Xi(t) = \frac{1}{\tau}\Phi(t)\int_{t_0}^{t} dt'\ \Phi(t')^{-1} m_1(t'), \tag{3.2.57}$$

one can write time evolution of the magnetization vector as

$$\mathbf{m}(t) = \Phi(t)\mathbf{m}(t_0) - \Xi(t)\hat{e}_1 \tag{3.2.58}$$

Again, it is used that $\Phi(t_0) = \mathbb{I}$. For both even and odd system sizes, then for $t - t_0 \gg \tau$, the Ξ matrix approaches

$$\Xi(t) \to -\mathcal{A}^{-1} \tag{3.2.59}$$

The reduced magnetization vector will therefore approach

$$\mathbf{m}_{\text{red}}(t) \to \mathcal{A}^{-1}\hat{e}_1 = \begin{pmatrix}1 & -1 & 1 & -1 & \cdots\end{pmatrix}^T \tag{3.2.60}$$

using the results of appendix B.2. Since $m_1(t)$ approaches -1, then the limiting behaviour of the magnetization vector is

$$\mathbf{m}(t) \to \begin{pmatrix}-1 & 1 & -1 & 1 & \cdots\end{pmatrix}^T \tag{3.2.61}$$

As expected, the system decays into the zero-field AFM ground state that minimized the energy of the first site.

Other regimes with local field

For other combinations of J and h, the behaviour of the model can be related to cases described above. Keeping an AFM coupling while changing the sign of the field value, one observes that the sign of a_- since

$$a_\pm = \frac{1}{2}\left[\text{sgn}(J+h) \pm \text{sgn}(J-h)\right] = \frac{1}{2}\left[\text{sgn}(J-|h|) \pm \text{sgn}(J+|h|)\right] = \pm a_\pm \tag{3.2.62}$$

This results in $\mathbf{g}$ changing its sign, $\mathbf{g} \to -\mathbf{g}$ while the classical time-evolution matrix $\mathcal{A}$ stays the same as for $h > 0$. The system will therefore, again, decay into a random AFM ground state for

sub-critical field. For critical field and super critical fields, the system decays into the configuration $\{\sigma\} = (1, -1, 1, -1, \cdots)$. One can also get this result by constructing a new set of spins, $\{\tilde{\sigma}\}$ satisfying: $\tilde{\sigma}_i = -\sigma_i$. The energy functional of $\{\tilde{\sigma}\}$ are the same as for $\{\sigma\}$ with the field being flipped since

$$E(\{\sigma\})\Big|_{J>0,h<0} = \sum_{i=1}^{N-1} J\sigma_i\sigma_{i+1} + h\sigma_1 = \sum_{i=1}^{N-1} J\tilde{\sigma}_i\tilde{\sigma}_{i+1} + |h|\tilde{\sigma}_1 = E(\{\tilde{\sigma}\})\Big|_{J,h>0} \tag{3.2.63}$$

In the second to last equality it is used that $h < 0$ which implies $-h = |h| > 0$. This new set of spins have a local, positive field on the first site which implies the set $\{\tilde{\sigma}\}$ evolves as described in the previous section. This mean that for $0 > h > -J$, then the system decays into any of the two AFM ground states of $\{\tilde{\sigma}\}$ which translates into the AFM ground states of $\{\sigma\}$. For critical and super-critical fields, $0 > -J \geq h$, the system decays into $\{\tilde{\sigma}\} = (-1, 1, -1, 1, \cdots)$ which translates into $\{\sigma\} = (1, -1, 1, -1, \cdots)$.

Changing the sign of J makes the system ferromagnetic. Instead of redoing all the calculation, one can simply map the spin configuration $\{\sigma\}$ to a new spin configuration $\{\tilde{\sigma}\}$ by flipping all then even spins.

$$\{\tilde{\sigma}\} = \begin{cases} \tilde{\sigma}_i = \sigma_i & \text{for} \quad i \text{ being odd} \\ \tilde{\sigma}_i = -\sigma_i & \text{for} \quad i \text{ being even} \end{cases} \tag{3.2.64}$$

This new configuration has an energy function which act as a AFM energy function

$$E(\{\sigma\})\Big|_{J<0,h\neq 0} = \sum_{i=1}^{N-1} J\sigma_i\sigma_{i+1} + h\sigma_1 = \sum_{i=1}^{N-1} |J|\tilde{\sigma}_i\tilde{\sigma}_{i+1} + h\tilde{\sigma}_1 = E(\{\tilde{\sigma}\})\Big|_{J>0,h\neq 0} \tag{3.2.65}$$

The new spins $\{\tilde{\sigma}\}$ therefore evolves as if $J > 0$ which results in the $\{\tilde{\sigma}\}$ spin evolving into a random AFM ground state for $|J| > |h|$ and into the AFM configuration with the lower energy for $|h| > |J|$. Going back to the original spins, this limiting behaviour will be a randomly chosen FM zero-field ground state for $|J| > |h|$, and the zero-field FM groundstates which magnetizes opposite to the field for $|h| > |J|$.

One can also show then result by noticing that changing the spin of J results in $a_\pm \to \mp a_\pm$ and $\gamma_j^\pm \to \gamma_j^\pm$. The off-diagonal terms of $\mathcal{A}$ then change sign, which implies $\mathcal{A} \to 2\mathbf{I}_N - \mathcal{A}$ which further implies $\lambda_\ell \to 2 - \lambda_\ell = \lambda_{N-\ell-1}$. This changes the order in which eigenvectors are labelled, which changes long-term behaviour of the system.

The results of this section can be summarized in tabular 3.2.1.

3.3 Kawasaki dynamics

To end the chapter, the Kawasaki dynamics are described in short. Kawasaki dynamics are, as described earlier, dynamics resulting from spin exchange processes. Here two nearest neighbouring spin that are anti-aligned with each other can flip simultaneous, $\uparrow\downarrow \leftrightarrow \downarrow\uparrow$. These moves will therefore conserve the total magnetization ov the system and was first described in Kawasaki's original paper[24]. Since all moves does not change the total magnetization, a homogeneous longitudinal field would not influence rates $\omega(\{\sigma\} \to \{\sigma'\})$. For 1D systems with OBC, each allowed move can be written in the domain wall representation, which divides the set of all Kawasaki moves into three subsets. These are depicted in tabular 3.3.1. Note that in contrast with the Glauber moves, the domain wall representation of each move depends on the sign of J.

For AFM nearest neighbour couplings, domain walls can move left and right by skipping over one empty site. Domain walls can be created/annihilated in the bulk around an empty site, while on the edges a domain wall can be created the site next to the edge site, given that the edge site is empty. For FM nearest neighbour coupling, domain walls can be moved in pairs of two. The can be

J	h	Case	Solution	Changes w.r.t $J, h > 0$	$\lim_{t\to\infty} \mathbf{m}(t)$
$J > 0$	$h > 0$	$\|J\| > \|h\|$	Low	—	Random AFM ground state
		$\|J\| = \|h\|$	Critical	—	$(-1, 1, \cdots)$
		$\|J\| < \|h\|$	High	—	$(-1, 1, \cdots)$
	$h < 0$	$\|J\| > \|h\|$	Low	$\mathbf{g} \to -\mathbf{g}$	Random AFM ground state
		$\|J\| = \|h\|$	Critical	$\mathbf{g} \to -\mathbf{g}$	$(1, -1, \cdots)$
		$\|J\| < \|h\|$	High	$\mathbf{g} \to -\mathbf{g}$	$(1, -1, \cdots)$
$J < 0$	$h > 0$	$\|J\| > \|h\|$	Low	$\lambda_\ell \to \lambda_{N-\ell-1}$	Random FM ground state
		$\|J\| = \|h\|$	Critical	$\lambda_\ell \to \lambda_{N-\ell-1}$	$(-1, \cdots, -1)$
		$\|J\| < \|h\|$	High	$\lambda_\ell \to \lambda_{N-\ell-1}$	$(-1, \cdots, -1)$
	$h < 0$	$\|J\| > \|h\|$	Low	$\lambda_\ell \to \lambda_{N-\ell-1}$ and $\mathbf{g} \to -\mathbf{g}$	Random FM ground state
		$\|J\| = \|h\|$	Critical	$\lambda_\ell \to \lambda_{N-\ell-1}$ and $\mathbf{g} \to -\mathbf{g}$	$(1, \cdots, 1)$
		$\|J\| < \|h\|$	High	$\lambda_\ell \to \lambda_{N-\ell-1}$ and $\mathbf{g} \to -\mathbf{g}$	$(1, \cdots, 1)$

Figure 3.2.1: Behaviour of the different regimes of the classical Ising model for different values of (J, h). The dynamics are all compared with the $(J > 0, h > 0)$ regime. The difference between regimes, in terms of the dynamic, are, at most, a sign change of $\mathbf{g}$ and an offset of the eigenvalues λ_ℓ

created/annihilated around an occupied site, while on the edge, a domain wall can only be created next to the edge site, if and only if the edge site is occupied. For FM coupling, the system can never reach an FM ground state if only Kawasaki dynamics are present, since the last domain wall cannot be annihilated.

Given a system 1D KIM with N sites and OBC, there will be $N-1$ different nearest neighbour spin pairs. Each spin exchange process can therefore be associated to the lowest indexed site participating in the spin exchange. This means the first process is the process where spin 1 and 2 exchange spins, while the second process exchanges spins between spin 2 and 3. Given a general, space dependent, nearest neighbour coupling J_i and a homogeneous longitudinal field $h_i = h$, the rate of the i'th Kawasaki process can be written as

$$\tilde{\omega}_i(\{\sigma\}) = \frac{1}{2\tau}\left[1 + \sigma_i\left(\tilde{\gamma}_i^+\sigma_{i-1} - \tilde{\gamma}_i^-\sigma_{i+2}\right)\right]\frac{1-\sigma_i\sigma_{i+1}}{2} \quad \text{for} \quad i \in \{1, \cdots, N-1\} \quad \text{with} \tag{3.3.1}$$

$$\tilde{\gamma}_i^\pm = \frac{1}{2}\left[\tanh\left(\frac{J_{i-1}+J_{i+1}}{T_\alpha}\right) \pm \tanh\left(\frac{J_{i-1}-J_{i+1}}{T_\alpha}\right)\right] \tag{3.3.2}$$

This can be shown by setting $\sigma_i = -\sigma_{i+1}$ and $\sigma_{i-1} = \pm\sigma_{i+1}$ and observing that the r.h.s. of eq. (3.3.1) reduces to $\tau^{-1}n_F(\Delta E/T)$. Also, the $\frac{1-\sigma_i\sigma_{i+1}}{2}$ term is to ensure that for $\sigma_i = \sigma_{i+1}$, the rate is zero. From this, the magnetization vector of the system will still satisfy eq. (3.1.25), where $\hat{P}(\{\sigma\}, t)$ is described via the Master equation for Kawasaki processes

$$\dot{P}(\{\sigma\}, t) = -\sum_{j=1}^{N-1}(1 - \hat{p}_j\hat{p}_{j+1})\tilde{\omega}_j(\{\sigma\})P(\{\sigma\}, t) \tag{3.3.3}$$

Using the method described in section 3.1.3, it is possible to shown that

$$(1+\hat{p}_j)(1+\hat{p}_{j+1})(1-\hat{p}_j\hat{p}_{j+1}) = 0 \quad \text{and} \quad (1+\hat{p}_j)(1+\hat{p}_{j+1})(1+\hat{p}_j\hat{p}_{j+1}) = 2(1+\hat{p}_j)(1+\hat{p}_{j+1}) \tag{3.3.4}$$

Action	DW (AFM)	AFM	DW (FM)	FM	ΔE
Move left/right	$\circ\circ\bullet \leftrightarrow \bullet\circ\circ$	$\uparrow\downarrow\uparrow\uparrow \leftrightarrow \uparrow\uparrow\downarrow\uparrow$ $\downarrow\uparrow\downarrow\downarrow \leftrightarrow \downarrow\downarrow\uparrow\uparrow$	$\circ\bullet\bullet \leftrightarrow \bullet\bullet\circ$	$\uparrow\uparrow\downarrow\uparrow \leftrightarrow \uparrow\downarrow\uparrow\uparrow$ $\downarrow\downarrow\uparrow\downarrow \leftrightarrow \downarrow\uparrow\downarrow\downarrow$	0
Pair creation/annihilation	$\circ\circ\circ \leftrightarrow \bullet\circ\bullet$	$\uparrow\downarrow\uparrow\downarrow \leftrightarrow \uparrow\uparrow\downarrow\downarrow$ $\downarrow\uparrow\downarrow\uparrow \leftrightarrow \downarrow\downarrow\uparrow\uparrow$	$\circ\bullet\circ \leftrightarrow \bullet\bullet\bullet$	$\uparrow\uparrow\downarrow\downarrow \leftrightarrow \uparrow\downarrow\uparrow\downarrow$ $\downarrow\downarrow\uparrow\uparrow \leftrightarrow \downarrow\uparrow\downarrow\uparrow$	$\pm 4\lvert J\rvert$
Edge creation/annihilation	$\circ\circ \leftrightarrow \circ\bullet$	$\uparrow\downarrow\uparrow \leftrightarrow \downarrow\uparrow\uparrow$ $\downarrow\uparrow\downarrow \leftrightarrow \uparrow\downarrow\downarrow$	$\bullet\circ \leftrightarrow \bullet\bullet$	$\uparrow\downarrow\downarrow \leftrightarrow \downarrow\uparrow\downarrow$ $\downarrow\uparrow\uparrow \leftrightarrow \uparrow\downarrow\uparrow$	$\pm 2\lvert J\rvert$

Figure 3.3.1: Table describing the allowed moved for spin-exchange dynamics in both spin and domain wall picture. In the last column, creation of domain walls costs energy while annihilation frees energy.

which implies that

$$\dot{m}_1(t) = -2\sum_{\{\sigma\}} \sigma_1 \left(\omega_1\{\sigma\} + \omega_2(\{\sigma\})\right) P(\{\sigma\}, t) \tag{3.3.5a}$$

$$\dot{m}_i(t) = -2\sum_{\{\sigma\}} \sigma_i \left(\omega_{i-1}(\{\sigma\}) + \omega_i\{\sigma\} + \omega_{i+1}(\{\sigma\})\right) P(\{\sigma\}, t) \quad \text{for} \quad i \in \{2, \cdots, N-2\} \tag{3.3.5b}$$

$$\dot{m}_{N-1}(t) = -2\sum_{\{\sigma\}} \sigma_{N-1} \left(\omega_{N-2}\{\sigma\} + \omega_{N-1}(\{\sigma\})\right) P(\{\sigma\}, t) \tag{3.3.5c}$$

$$\dot{m}_N(t) = -2\sum_{\{\sigma\}} \sigma_N \omega_{N-1}\{\sigma\} P(\{\sigma\}, t) \tag{3.3.5d}$$

Writing the spin exchange rate out explicit, one gets that three point correlation functions enter the system of differential equations eq. 3.3.5, which makes an analytical solution to the problem hard. Solving the dynamics of the magnetization vector will not be attempted here.

3.4 Summary and conclusion

When the equilibrium properties of the classical Ising model is not sufficient to describe the behaviour of the system, the non-equilibrium dynamics must be considered. Coupling the classical Ising model to heat baths that are each allowed to perform different changes to the system, one gets the Kinetic Ising Model (KIM), whose probability distribution $P(\{\sigma\}, t)$ evolves via the Master equation, eq. (3.1.21). When only Glauber dynamics are considered, which only alters the system via single spin-flip processes, the statistical average of the magnetization can be found analytical for some conditions. The conditions are homogeneous nearest neighbour couplings, zero temperature, and zero longitudinal field up to a local field on the first site. Here the system decays exponentially into either a zero-field FM or AFM ground state configuration given the value of the J and the local field strength.

Kawasaki dynamics are also introduces, but it is not possible to analyse the resulting dynamic using analytical methods. They will therefore be ignored for some time, since nothing really can be concluded yet.

Chapter 4

Simulating the non-equilibrium dynamics of the KIM

Since the dynamics of the KIM only can be evaluated analytical for a few cases, if one wishes to get the complete picture, one must perform numerical simulation of the KIM. An algorithm that is well suited for this, is the Gillespie algorithm[27]. This allows one to simulate the KIM using the rates described in the section about the Master equation, 3.1.

To explore the properties of the KIM for general condition, a Cython implementation of the Gillespie Algorithm is written. The design of the code is described in the chapter as well as the theory behind Gillespie's original work[27]. The code is written in Cython 0.29.21 and implemented in Python 3.7.3. The reason for using Cython, which is a hybrid between C and Python, are described in the first part of this chapter. In section two, the Gillespie algorithm is described, and in section three, its Cython implementation is described.

4.1 Why Cython?

Cython is a language which uses the high-level aspects from Python together with elements from C and C++. The advantage of this being that the user can write fast functions at C-level, which can be used in Python codes. If done correctly, one can speed up algorithms by a few hundred times compared to pure Python. This high speed comes primarily from one thing, namely use of statically typed C variables[28, 29]. This is easily described using the following example.

4.1.1 1 + 2 = 3

In Python, everything is an object[1]. This means that a lot of code have be ran for Python to store simple things such as numbers. Mathematical operations on and with these objects are therefore also complicated and requires a lot of steps to performs. As an example, if one wishes to declare two integers; $i = 1$ and $j = 2$, then Python creates two integer objects in which 1 and 2 are stored respectively. If one wishes to add i and j and store the result in a variable k, then the command k = i + j is called. Under the hood, Python then has to go through the following steps[29]:

- First, Python checks what kind of object i is. In this example, i is an int.
- Then, Python checks if the int type has a build-in __add__ method, which is does.
- Python then calls i's __add__ method which takes j as an inputs.

[1] What an object means will be described later in sec. 4.3

- Inside __add__, the type of j is then checked. If the type is suitable for addition, then the values stored in i and j are added. Here, if j was not an integer, then either conversion between data types is done before the addition, or an error is raises.
- If nothing has gone wrong yet, an object k is created where the result of the addition is stored. The type of k will depend on the type of i and j. In this example, k is also an int.

This requires a lot of function calls and lookups which makes a simple instruction, such as $1 + 2 = 3$, take a long time[2]. Even thou this is slow compared to other languages such as C, it is much more flexible and easier to use. This method of adding allows one to do addition across data types. For example

- Integers and floating point numbers can be added resulting in a floating point: 1 + 1.0 = 2.0
- Integers and complex numbers can be added resulting in a complex number: 1 + 1.0j = (1.0 + 1.0j)
- Integers can be added to numpy arrays element wise: 1 + array([1.0,2.0,3.0]) = array([2.0,3.0,4.0])

Programmers can then use addition without worrying about data types which makes code easier to write. This trade-off between speed and flexibility makes code slow, but easier to develop and write. In Cython, one can do this much faster by first declaring i, j, and k as C-variables:

```
cdef int i = 1, j = 2          (4.1.1)
cdef int k = i + j             (4.1.2)
```

These instructions are then translated into C code which is compiled and ran. The first line allocates space for two C-ints in RAM where 1 and 2 are stored. The second line roughly translated into add two C-integers labelled i and j and place the results in a integer variable k allocated in RAM. This is much faster, but also comes with several caviares. If the type of j was instead a floating point number, then this addition would not be possible, and the program cannot be compiled. This means that if the data types are correctly typed, then when the code has been compiled, the computer does not need to check the data types of **i** and **j** when the code is ran. Also, if the numbers are large, so that i + j is greater that $2^{31} - 1 = 2,147,483,647$ then the sum overflows, which means that the numbers wrap around and starts counting from $-2,147,483,647$. Depending on the code, a warning is printed to the user indicating the addition resulted in an overflow, but is not guaranteed. The programmer therefore has to add another item to the list of things that can go wrong when programming. It can be worth the trouble thou, since a function written properly in Cython will perform faster than its Python equivalence. This is demonstrated in the next example.

4.1.2 Example of speed up

To demonstrate Cython's ability to speed up code, one can consider the following question: What is the sum of the integer from 1 to N? Without using the obvious method which is to use that $\sum_{i=1}^{N} \frac{N(N+1)}{2}$, the answer can be evaluated using loops. Implementing an algorithm that calculates the sum in both Python and Cython, one can compare the average runtime of the two, using the %timeit magic.

Starting with the Python implementation, fig. 4.1.1a, a function named summer_py is written that takes the number N as an input. Because of the flexibility, N can be any Python object. The "results = 0" command then creates a python int where 0 is stored in. The program then adds all the integers from "1" to "N" with a for loop.[3] At the beginning of the loop, when range is called, the type of the input N is check, which raises a TypeError if **N** is not a python int. At the end of the function

[2]Of course a long time is relative here. On my PC it takes (83 ± 7) ns to perform this.

[3]Note that upper limit of the range object is "N+1" since the range object excludes the upper limit.

```
def summmer_py(N) -> int:
  result = 0

  for i in range(1,N+1):
    result += i

  return result
```

a)Python implementation of summer

```
def summmer_cy(long long N):
  cdef long long result = 0, i

  for i in range(1,N+1):
    result += i

  return int(result)
```

b) Cython implementation of summer

Figure 4.1.2: Two different implementation of the same algorithm. One is written in pure Python **a)** while the other is written in Cython **b)**

	$N = 10^6$	$N = 10^7$	$N = 10^8$	$N = 10^9$
Python	91 ms	812 ms	10.1 s	-
Cython	423 μs	3.99 ms	45 ms	423 ms
Speed up	215	203	224	-

Figure 4.1.3: The performance of a Python and Cython implementation of the same algorithm. Run times are measure using the %timeit command.

results is returned. Timing this implementation for $N = 10^6$, $N = 10^7$, and $N = 10^8$, yields the results written in tabular 4.1.3. One observed that when summing from 1 to 10^8, the algorithm takes seconds to complete.

In the Cython implementation, fig. 4.1.1b, a function named summer_cy is created which takes a long long and store it in a variable called N. A long long is a C data type which allocated 64 bits of memory to represent a signed integer. This means that is can store integer value from $-(2^{32} - 1)$ to $2^{32} - 1$ which is necessary to avoid overflow errors for $N <= 10^9$. The results and i variables are then statically typed as long longs and results is set to "0". The for loop is then performed. Here, the simplicity of the C's +-operator really shines though, since the numbers are simply added. At the end of the Cython function, results is converted to a Python int which is returned. Timing this methods, one gets the results written in table 4.1.3. Compared to pure Python, the Cython implementation is around 200 times faster! From this example, it is clear that Cython dramatically can increase efficiently. Due to this, Cython is used to run the simulations of the KIM.s

4.2 The Gillespie algorithm

To simulate the KIM, the Gillespie algorithm[27, 30] is the way to go. The basic idea is that given a system whose state can change via different stochastic processes, its dynamics can be simulated using the rates at which each process happens. Given a system I that can react/change via M different processes, labelled by $\mu \in \{1, \cdots, M\}$, then one can defined the probability density function (PDF) $\mathcal{P}(\mu, \tau|I, t)$ as

$$\begin{aligned}\mathcal{P}(\mu, \tau|I, t)\Delta\tau = \; & \textit{The probability, to first orther in } \Delta\tau, \textit{ that the } \mu\textit{'th} \\ & \textit{process occures in the time interval }]t+\tau; t+\tau+\Delta\tau[, \\ & \textit{given that the system was in the configuration } I \textit{ at time } t. \end{aligned} \tag{4.2.1}$$

This PDF must then satisfy

$$\sum_{\mu=1}^{M} \int_0^\infty \mathcal{P}(\mu, \tau | I, t) d\tau = 1 \tag{4.2.2}$$

for the probabilities to sum one unity. It is here assumed that if the system can react via a given process, it is bound to do at some point. In Gillespie's original work[27], he used this PDF to describe an algorithm for which a chemical system can be simulation. In this section, the thoughts presented by Gillespie is used to get the PDF related to the KIM.

The basic idea of the algorithm is then to simulate a reaction event of a state I by picking an integer $\mu \in \{1, \cdots, M\}$ and a positive real number $\tau \in \mathbb{R}_+$ from the PDF $P(\mu\tau|I, t)$. The system I is then updated using the μ'th process after the time τ has passed. This procedure is iterated until either the system becomes static or a maximum number of iterations has been performed. This is described in greater details in section 4.2.3. For now, the exact form of the PDF $P(\mu, \tau|I, t)$ is determined.

4.2.1 Determining the PDF

The PDF $\mathcal{P}(\mu, \tau|I, t)$ can be evaluated using the rates in the master equation in eq. 3.1.1. Since these are the probability pr. unit time, that the system changes via a given process, one gets that[27, 30]

$$\begin{aligned} \omega_\mu(I)\Delta t = \; & \textit{Probability, to first order in } \Delta t, \textit{ that the system} \\ & \textit{changes via the } \mu\textit{'th process in a time interval of size } \Delta t, \\ & \textit{given the state of the system is } I. \end{aligned} \tag{4.2.3}$$

From this assumption, the probability that more than one reaction/process occurs in the this time interval is of order $\mathcal{O}\left((\Delta t)^2\right)$. Therefore, for small time intervals, one can assuming that no more than one reaction/process can occur in the interval. Therefore, the probability described in eq. (4.2.1) must satisfy

$$\mathcal{P}(\mu, \tau|I, t)\Delta\tau = P_0(\tau + t, t|I) \left(w_\mu \Delta\tau + \mathcal{O}\left((\Delta\tau)^2\right)\right) \tag{4.2.4}$$

Here $P_0(\tau + t, t|I)$ is the probability that the system does not changing in the time interval $]t; t + \tau]$, given that the system is in the state I at time t. $\omega_\mu \Delta d\tau$ is then the probability, to first order in $\Delta\tau$, that the system changes via the μ'th process in the interval $]t + \tau; t + \tau + \Delta\tau]$. To determine P_0, one splits in interval $]t; t + \tau]$ into N smaller intervals of size τ/N.

$$]t; t + \tau] = \bigcup_{n=0}^{N-1} \left]t + \frac{\tau}{N}n; t + \frac{\tau}{N}(n + 1)\right] \tag{4.2.5}$$

From this, one can say that if nothing must happen in $]t; t + \tau$ is the same as saying the nothing must happen in the interval $]t + \tau/N; t + \tau]$ given that nothing happened at $]t; t + t/N]$. In this way

$$P_0(\tau + t, t|I) = P_0\left(\tau + t, t + \frac{\tau}{N}\middle| I\right) P_0\left(t + \frac{\tau}{N}, t\middle| I\right) \tag{4.2.6}$$

Continuing this line of reasoning, one can write that

$$P_0(\tau + t, t|I, t) = \prod_{n=0}^{N-1} P_0\left(t + \frac{\tau}{N}(n + 1), t + \frac{\tau}{N}n\middle| I\right) \tag{4.2.7}$$

If N can be considered to be large, which can be chosen freely, the one can expand P_0 in the following way

$$P_0\left(t+\frac{\tau}{N}(n+1), t+\frac{\tau}{N}n|I\right) = \prod_{\mu=1}^{M}\left(1-\omega_\mu(I)\frac{\tau}{N}+\mathcal{O}\left(N^{-2}\right)\right) \tag{4.2.8}$$

The logic behind this is a bit long, by in summary, the r.h.s. of eq. (4.2.8) states that the system does not change by either of the M process, which are expanded to first order in N. These probabilities are the expanded to first order in N^{-1}. Expanding the product, one gets that

$$P_0\left(t+\frac{\tau}{N}(n+1), t+\frac{\tau}{N}n|I,t\right) = 1-\left(\sum_{\mu=1}^{M}\omega_\mu(I)\right)\frac{\tau}{N}+\mathcal{O}\left(N^{-2}\right) = 1-W(I)\frac{\tau}{N}+\mathcal{O}\left(N^{-2}\right) \tag{4.2.9}$$

Here $W=\sum_{\mu=1}^{M}\omega_\mu(I)$ is the sum of the rates given the system is in the state I. It is assumed here that $W\neq 0$. If $W=0$ the system would be static, which would break probability conservation of $P(\mu,\tau|I,t)$. Given that at some point the system reaches a state where $W=0$, the simulation is stopped and no further calculations of the PDF is necessary, thereby evading the problem all together. This is discussed in more detailed when the algorithm is described in details, sec. 4.2.3.

Inserting eq. 4.2.9 into eq. (4.2.7), the probability of the system not changing in the interval $]t;t+\Delta\tau]$ takes the form of

$$P_0(\tau+t,t|I,t) = \prod_{n=0}^{N-1}\left[1-W(I)\frac{\tau}{N}+\mathcal{O}\left(N^{-2}\right)\right] = \left(1-W(I)\frac{\tau}{N}\right)^N+\mathcal{O}\left(N^{-1}\right)\to e^{-W(I)\tau} \tag{4.2.10}$$

for $N\to\infty$. The PDF, $\mathcal{P}(\tau,\mu|I,t)$, will therefore decay exponentially.

$$\mathcal{P}(\tau,\mu|I,t) = w_\mu e^{-W\tau}, \tag{4.2.11}$$

This probability density function satisfies the probability conservation described in eq. (4.2.2)

$$1=\sum_{\mu=1}^{M}\int_0^\infty \mathcal{P}(\tau,\mu|I,t)d\tau = \left(\sum_{\mu=1}^{M}\omega_\mu(I)\right)\left(\int_0^\infty e^{-W(I)\tau}d\tau\right) = W(I)\frac{1}{W(I)} = 1\checkmark. \tag{4.2.12}$$

4.2.2 The direct method

The direct method is described in more detail in Gillespie's paper[27]. The basis idea here is that the probability density function $\mathcal{P}(\mu,\tau|I,t)$ can be split into the product

$$\mathcal{P}(\mu,\tau|I,t) = \mathcal{P}_1(\tau|I,t)P_2(\mu|\tau,t,I) \tag{4.2.13}$$

Here $\mathcal{P}_1(\tau|I)$ is the PDF corresponding to the next process happens in the time interval $]t;t+\tau]$ while $P_2(\mu|I,\tau,t)$ is the probability that the process performed is the μ'ht process, given that a process occurs in the time interval. From eq. (4.2.13), then summing over μ yields

$$\mathcal{P}_1(\tau|I,t) = \sum_\mu \mathcal{P}(\mu,\tau|I,t) \quad \text{and} \quad P_2(\mu|\tau,t,I) = \frac{\mathcal{P}(\mu,\tau|I,t)}{\sum_\nu \mathcal{P}(\nu,\tau|I,t)} \tag{4.2.14}$$

To show this, it is used that $\sum_{\mu=1}^{M}P_2(\mu|\tau,t,I)=1$. This is because the system must change using on of the M processes given that the system changes.

Inserting eq. (4.2.11) into eq. (4.2.14), one gets

$$\mathcal{P}_1(\tau|I,t) = W(I)e^{-W(I)\tau} \quad \text{and} \quad P_2(\mu|\tau,t,I) = \frac{\omega_\mu(I)}{W(I)} \tag{4.2.15}$$

From the first condition of eq. (4.2.15), a random time interval can be picked. One does this by using that the probability of picking a time interval Δt greater than some time interval τ is

$$P(\Delta t > \tau|I,t) = \int_\tau^\infty \mathcal{P}(\tau'|I,t)d\tau' = -\frac{1}{W(I)}\left[W(I)e^{-W(I)\tau'}\right]_\tau^\infty = e^{-W(I)\tau} \tag{4.2.16}$$

Generating a random number r from a uniform distribution $[0,1]$, one can get a random time interval from the PDF $\mathcal{P}_1$ via

$$\Delta t = -\frac{1}{W(I)}\ln r \in \mathbb{R}_+ \tag{4.2.17}$$

A random produces can then be picked by, again, generating a random number r_2 from a uniform distribution $[0,1[$. From this, a random $\mu \in \{1,\cdots,N\}$ can be picked following the probability distribution P_2 by finding the smallest μ such that

$$\sum_{\nu=1}^{\mu} w_\nu > W r_2 \tag{4.2.18}$$

One can easily see why this is by imagining "lining up" the M processes on the real number line with a length proportional to $P_2(\mu|I,\tau,t)$. The probability of throwing a dart randomly at the real number line, equivalent to picking r_2, and hitting the the ν'th process will then be equal to $P(\nu|I,\tau,t)$. The "dart" will therefore pick the process ν with if

$$\sum_{\mu=1}^{\nu-1}\frac{w_\mu}{W} \leq r_2 < \sum_{\mu=1}^{\nu}\frac{w_\mu}{W} \Leftrightarrow \sum_{\mu=1}^{\nu-1} w_\mu \leq r_2 W < \sum_{\mu=1}^{\nu} w_\mu \tag{4.2.19}$$

Here $w_0 = 0$ and $w_{M+1} = 1$.

4.2.3 The algorithm

Given a way of generating the pair (μ,τ), the outline of the Gillespie algorithm can be described. Applied to the KIM, the algorithm goes as following:

1. **Initial the system.** The first step is to initialize the system in a given configuration $\{\sigma\}$. Additionally, the simulation time is initialized as well $t = 0$.

2. **Calculate rates.** Given the current configuration, the set of rates $\{\omega_\mu(\{\sigma\})\}$ can be calculated. Summing over all rates, the total rate $W(\{\sigma\})$ is evaluated too. If the total rate is zero, the simulation stops since the system is static and all dynamics are dead.

3. **Increment time.** Since $W \neq 0$, the simulation time can be incremented by picking a random number r_1 from a uniform distribution $]0;1[$, which is used in $\tau = -W^{-1}\ln r_1$. The time is then incremented $t \to t + \tau$

4. **Pick a process.** To pick which process the current state is altered by, one generated another random number r_2 from a uniform distribution $[0;1[$. The smallest μ satisfying $\sum_{\nu=1}^{\mu} w_\nu > W r_2$ is then chosen and the μ'th process are performed on the current configuration. The system is now in a new configuration and has its time variable incremented.

5. **New loop.** If the number of maximum iterations has been reached, the simulation is not allowed any more moves and the simulation is stopped. This is to prevent the code to run forever, if for all configurations then $W(\{\sigma\}) \neq 0$. If the maximum iterations hasn't been reached, the algorithm jumps back to step **2.**

As said in the start of the chapter, this algorithm is implemented in Cython, which are described now.

4.3 Overall structure of the code

The code that simulates the KIM is implemented in Cython as an extension class. This is a kind of object, which in computer science, is a data structure defined by three properties[29]:

- **Identity**: An identity that distinguishes it from the other. In Cython, this is simply the memory location where the object is stored.
- **Value**: Objects can store data in variables knows as attributes.
- **Type**: This specifies the behaviour of the object, which is accessible using a collection of methods saved in it. In Cython, the methods of an object must always take the objects itself as an input. The standard notation for this is to use the keyword: self. An objects methods can then use an alter the attributes of the object.

These three things makes an objects what it is. It is possible to create multiple instances of a given object, meaning that a lot of simulation can be created and stored in memory at the same time. Each instance their own set of attributes and methods, which can be accessed and altered independently of each other.

To simulate the KIM, a Cython extension class named Gillespie_cy is created. One does this by starting the code block describing the object by cdef class Gillepsie_cy: followed by a doc-string.

```
cdef class Gillespie_cy:
        """ Doc string """
```

The doc-string does not actively serve any purpose, except for describing the code. It is always a good practice do this! After the doc-string, the attributes of the extension call are statically typed using the cdef keyword. These attributes are listed in table 4.3.1. Since Gillespie_cy is a Cython extension type, all attributes of it must be statically types. Even those who are Python objects. Afterwards the methods are defined. There are no limitation on which methods can be used, meaning def, cdef, and cpdef functions are all allowed. [4] Note that only def and cpdef methods can be called from outside the object. Gillespie_cy has a lot of method, which will not all be covered in this chapter. The important ones will thou and is done in next sections. The full list of all methods can be found in appendix C.4 with a small description of what they do.

4.3.1 Initialization of a Gillespie_cy instance

When an instance of the Gillespie_cy object is creates, Cython calls a series of special methods. This is initiated by calling Gillespie_cy with a given set of inputs:

$$\text{Gillespie\_cy(J,h,init,N,temp,Nmax,delta,run\_sim).} \tag{4.3.1}$$

There are eight input in total where only five of them are required, being (J,h,init,N,temp). The type and value limitations of the inputs are:

[4] The difference between the three types of functions can be found in the Cython documentation[28].

List of attributes		
Variable name	Data type	Description
N	int	Number of sites of KIM
Nmax	int	Maximum number of iterations of simulation
ended_at	int	Number of iteration before system stopped. (-1 if system did not before static before Nmax iterations)
delta	double	local variable in Glauber rates $\delta \in [-1, 1]$
beta	double	inverse temperature (-1 if zero temperature)
J	double[:N]	Nearest neighbour couplings
h	double[:N]	Longitudinal fields
time	double[:Nmax+1]	Array of saved times
mag_even	double[:Nmax+1]	Instantaneous magnetization of even sub-lattice
mag_odd	double[:Nmax+1]	Instantaneous magnetization of even odd-lattice
energy	double[:Nmax+1]	Instantaneous energy
hist	int[:Nmax]	history of moves
initial_state	int[:N]	Initial states of simulation
end_state	int[:N]	end states of simulation
ran	bint	boolean variable to check is simulation has been ran

Figure 4.3.1: Table of attributes of the Gillespie. First column are the third names, the second column are their data types, and the last column describes that data is stored here.

- J: A general Python object that described the nearest neighbour interaction. Given different types and values of J, different space-dependent nearest neighbour couplings are defined. The exact correspondence between input and output is described in appendix C.1.
- h: A general Python object that described the longitudinal field. Given different types and values of h, different space-dependent fields are defined. The exact correspondence between input and output is described in appendix C.1.
- init: A general Python object that described the initial configuration of the KIM. Given different types and values of init, different initial configurations are defined. The exact correspondence between input and output is described in appendix C.1.
- N: An integer describing the number of sites in the system.
- temp: A python float or a C double describing the temperature of the system. temp = -1 is interpreted as an infinite temperature.
- Nmax: An integer described the number of iteration the algorithm can perform before it is stopped. As a default value, it is set to be $100N$.
- delta: Glauber parameter δ as a python float or a C double. Must be in the interval $[-1, 1]$. Default value is zero.
- run_sim: A boolean variable that tell the object to run the simulation when the instance is created. Default value is true.

When the creation of an instance is initiated, all attributes and methods are allocated in Memory. A special method __cinit__ is then called, which takes the same inputs as described above. In here, attributes that are C data types are set/allocated. The instance is not yet a proper Python object, so one should be careful about attributes that are Python object. To set there, the special method

__init__ is called. Here the rest of the attributes are set and, at the end of the method, the instance should be ready to simulate the KIM. If run_sim = True, then the simulation is ran at the end of __init__ method. It does this be calling the run_sim_cy method, where the Gillespie Algorithm is performed on the system. That is until the system enter a static state, making it impossible for the algorithm to process further, or the maximum number of iterations allowed are reached. The simulation results, such as the history of the energy, magnetization, and simulation history, is then saved. These result can then be outputted to the user either by the get_attribute_py method, which simply converts all attributes to Python objects and outputs them as a dictionary, or by the plotting method then plots the simulation history.

In the next sections, some of the important methods are described in detail. On this should be noted thou. All the methods of an object will automatically take the instance itself as an input. Always!. This is so that the methods have access to its attributes and other methods. It is standard to name the instance itself for self, and is done so here too.

4.3.2 __cinit__

The special method is a Python function and is called immediately after the instance is allocated in memory. As said before, the inputs of Gillespie_cy are past directly into here together with the instance itself.

The method then saved the number of sites N into its corresponding attribute self.N[5] The maximum number of iterations self.N_max, and the Glauber parameter δ are then set, while the self.beta attribute is calculated from the temp input. If temp is non-zero, then self.beta is set to the reciprocal value of the input temperature 1/temp. If the input temperature is infinite, represented by a -1, then self.beta $= 0$, while if the input temperature is zero, then self.beta is infinite, again represented by -1.

At last the self.J, self.h, self.time, self.mag_even, self.mag_odd, and self.energy attributes are allocated as memoryviews[6] of C doubles. The same is done for the self.history, self.initial_state, and self.end_state attributes except that they are allocated as int memoryviews.

Before proceeding to __init__, the last attributes two attributes are set. These being the self.ran and self.ended_at attributes, which are set to False and -1 respectively, since the simulation hasn't ran yet.

At this point, if not errors has been raised yet, the program continues to __init__.

4.3.3 __init__

This special method is a Python function which takes the same inputs as the __cinit__ method did. At this point, the instance is a fully defined Python object, which means that attributes can be manipulated using Python function.

The goal of this method is to prepare the instance and make it ready to simulate the dynamics of the KIM. It does so by first defining the nearest neighbour coupling self.J, the longitudinal field self.h, and the initial configuration self.initial_state. This is done using the self.get_J_att, the self.get_h_att, and the self.get_init_att respectively. These methods takes J, h, and init as input and alters their corresponding attributes using the rules states in appendix C.2 and C.3. After these are set, the time array self.time has its first element set to 0.

After defining the physical parameters and the initial configuration, the initial conditions of the system are set and calculated. First, the even and odd magnetization of the initial configuration are calculated using the self.magnetization method, the result of which are saved in the self.mag_even and self.mag_odd variables, first element. Afterwards, the energy of initial configuration is calculated by

[5] The object.something notation is the way one access attributes and methods of a given object in the Python languages.
[6] A Cython data-types used to store arrays. See documentation for more information[31]

emulating the equation

$$E(\{\sigma\}) = \sum_{i=1}^{N} J_i \sigma_i \sigma_{i+1} + h_i \sigma_i \tag{4.3.2}$$

with a while loop. The result is stored in the first elements of the energy attribute self.energy.

At the end of the method, if the run_sim input is True, the simulation is started by calling the self.run_sim_cy method. If run_sim = False, the method returns and the simulation is not ran.

4.3.4 run_sim_cy

This method is an inline C-function with the goal of simulating the behaviour of the KIM.

```
cdef inline void run_sim_cy(self):
  cdef:
    int loop_counter = 0, m

    double r, W, sum_var, P

    # Allocate memory for arrays
    int[:] config = np.empty([self.N,]dtype = int)
    double[:] rates = np.empty([self.N,]dtype = np.double)

  # Copy the elements of the initial state over to the config
  # array
  config[:] = self.initial_state

  # Run simulation loop
  while loop_counter < Nmax:
      # Calculate the rate of the current configuration
      # and save the results in the rates array
      self.glauber_rates(config,rates)

      # Calculate the sum of all rates
      W = 0
      m = 0
      while m < (self.N - 1):
        W += rates[m]
        n += 1
      # Code goes here after the loop over m.

      # If sum of rates are zero, then the system is static and
      # the system does not evolve anymore.
      if W == 0:
          # If true, break out of the while loop running the
          # simulation.
          break

      # Generate a random number in interval ]0,1[ and save it in P
      P = random_number_in_exclude_exclude(0,1)
```

```
    # Generate a random number in interval [0,W[ and save it in r
    r = random_number_in_exclude_include(0,W)

    # Generate the time it takes for the system to transition,
    # increment the time and save the new time in the
    # in the corresponding element of time_array
    self.time_array[n + 1] = self.time_array[n] - log(P)/W

    # Find the smallest "m" such that so that sum of the first
    # "m + 1" rates is greater than "r".
    m = 0
    sum_var = 0.0

    while m < (N - 1):
      # Increment sum variable by the "m"'th rate
      sum_var += rates[m]
      m += 1

      if sum_var > r:
        # The current m satisfies the condition.
        # Stop searching
        break;

      # The current m did not satisfy the contition.
      # Continue searching
      m += 1

    # After the while loop oveer "m", the code goes here.

    # Save which process was performed in the self.hist
    # attribute
    self.hist[loop_counter] = m

    # Perform the m'th process by flipping the m'th spin
    config[m] *= -1

    # Calculate magnetization of new system and save the
    # results in the self.mag_even and self.mag_odd
    # attributes
    self.magnetization(config)

    # Calculate the energy of the current configuration
    # and save the results in the self.energy attribute.
    self.calc_energy_diff(config,m)

    # Increment loop counter
    loop_counter += 1

# After the simulation while loop, the code goes here.
```

```
    # Set the ran flag as well as how many itterations
    # the simulation ran
    self.ran = True
    self.ended_at = loop_counter

    # Save the last configuration in the self.ended_at
    # attribute
    self.ended_at = config
```

Note that this is not a carbon copy of the real code, but should be seen as a demonstration of its structure.

4.3.5 Building the file

In this chapter, the non-equilibrium behaviour of the classical Ising model is ran for different parameters using the Gillespie_cy cython extension class described in the previous chapters. One does this by working in Python, that imports the Gillespie_cy method by first cythonize it[32]. This by creating a Python setup file on the form

```
from setuptools import setup
from Cython.Build import cythonize

setup(
    ext_modules = cythonize("Gillespie_cy_2.pyx")
)
```

which builds the Cython file when

```
$ python setup.py build_ext --inplace
```

in a command line. The Gillespie_cy object can then be imported and used in Python code. This can then be implemented in other Python codes which is used a lot to simulate the results presented in the next chapter.

Chapter 5

Simulating the KIM

In this chapter, the Gillespie_cy object is used to simulate the non-equilibrium dynamics of the Kinetic Ising model, for different parameter settings. This is done by simulating the same set of parameters a given number times, often between a hundred and a thousand times. The data is then analysed using statistics to interpret the dynamics of the KIM. Starting with zero temperature, the system can be simulated for different fields and initial configurations. For each single simulation, properties such as magnetization, history, and simulation time can be measured, which can be summarized is histograms. As also stated in chapter 3, at zero temperature, the statistical averages of the spin projections will decay exponentially into a given configuration. The states of which could be controlled by single local field on the first site. This prediction also defined the limitations of the analytical work.

As mentioned in chapter 3 when the heat bath has a temperature of zero, the heat bath is frozen and cannot give energy the the spins. At any point in time, the energy of the spins can therefore not increase, but can either decrease or be kept unchanged. The result of this is that the system of spins will "move" closer and closer to a ground state configuration. For different values of the longitudinal field h, the system's long-term behaviour differs greatly. For some values, the system decays into one of the zero-field AFM ground states were it becomes static. For small non-zero field strengths, the system decays into a disordered state, and for large field strengths, the system decays into a zero-field FM ground state. In this first section of the chapter, the system is simulated for AFM coupling, zero temperature, an $\delta = 0$. The value of h is changed gradually to explore the system in different fields. Since the temperature is zero, the explicit value of the field does not matter, only whether or not it is strong enough to rearrange the energetic order of the energy level. Due to an unknown bug in the program, only simulations with $\delta = 0$ are considered. The bug makes it so the energy can sometimes increase even for $T = 0$. Since this is forbidden, one must conclude that the program simulated the $\delta \neq 0$ dynamics incorrectly. This will hopefully be fix in later patches of the code.

The overall behaviour of the system is determined by creating different initial states and running multiple simulations on them. The measured quantities are based on averages over different initial states and over different runs. More details about the specific data is explain in the sections below.

5.1 AFM - Zero temperature - zero longitudinal field

Starting simple, if the longitudinal field is zero, the only term in the energy function is the nearest neighbour coupling. The system will therefore have its $\mathbb{Z}_2$ symmetry preserved, which results in both ground states having the same energy. When averaging over all initial configurations, one would therefore except that the frequency of decaying into one of the AFM ground states should be equal to that of the other.

At $T = h = \delta = 0$ the Glauber rates can be evaluated so that the allowed moves can be determined. Because the creation of a pair of domain wall and the creation of a single edge wall has a positive

energy cost, the Glauber rates

$$\omega_{\mathrm{PC}} = \omega_{\mathrm{EC}} = 0. \tag{5.1.1}$$

This is because the Fermi function takes the form of a step function

$$n_F\left(\frac{\Delta E}{T}\right) = \begin{cases} 1 & \text{for} \quad \Delta E < 0 \\ 0.5 & \text{for} \quad \Delta E > 0 \\ 0 & \text{for} \quad \Delta E = 0 \end{cases} \quad \text{for} \quad T \to 0^+ \tag{5.1.2}$$

On the other hand, since the system releases energy when either two domain wall are annihilated or a wall is annihilated on an edge, then

$$\omega_{\mathrm{PA}} = \omega_{\mathrm{EA}} = \tau^{-1}. \tag{5.1.3}$$

At last, since domain wall can be moved for free in terms of energy, then $\Delta E = 0$ for domain wall motion and

$$\omega_{\mathrm{M}} = 0.5\tau^{-1}. \tag{5.1.4}$$

Remember that wall have an equal probability of moving to the left and the right given that the wall is in the bulk of the material. Because of this, each wall will move as a random walker on a one-dimensional line, which can annihilate with other walkers. The number of domain wall are therefore forced to decrease over time, since at some point each domain wall will either collide with another or hit an edge. Each time this happens, there is a probability of the wall(s) gets annihilated. The wall(s) also has(have) a probability of moving, which may extend their life time for a bit. Keeping that in mind, the walls cannot continue to be lucked and their life must eventually come to an end.

5.1.1 Behaviour of the zero-field KIM

This can be observed in fig. 5.1.1a and 5.1.1e where two randomly generated initial states are simulated for $T = h = \delta = 0$ with $J > 1$ and $N = 30$. Because the initial states are generated randomly, a lot of domain walls are present in the beginning of the simulation. In the plots, domain walls will sit between two nearest neighbouring sites of the same colour, because $J > 0$. As time goes on, the walls are annihilated either by pair annihilation or edge annihilation. This is reflected in the energy history of the simulation, depicted in fig. 5.1.1b and 5.1.1e. The energy drops quickly in the start and slows down later on, but is always decreasing. Note the number of time steps used on the x-axis on the fig. 5.1.1a and d, while the simulation time is used in fig. 5.1.1b and e. Due to the nature of the Gillespie algorithm, the simulation time between each time step is randomly chosen. There is therefore not a direct map between the x-axis of the two kinds of plots.

As time goes on, fewer and fewer walls remains which slows the rate annihilated event. In the end only one or two domain walls remain. In the first case, the last wall moves as a random walk until it hits one of the edges. Here it has a 2/3 probability of annihilating and a 1/3 probability of moving away from the wall. Even if the wall is lucky and manages to move away, it has a 50/50 change of moving back to the wall again. It can therefore happen that a wall can bounce on the edge until it is annihilated. Even if it manages to escape one wall, it can at maximum move over to the other wall where it has the same options. As for all the other walls, the life of the last wall must come to an end as well. One observes this in fig. 5.1.1a, where the last wall is annihilated in the end. Most of the same things can be said if two walls remains. Either both walls are annihilated on edges, or they annihilate each other as seen in fig. 5.1.1d. When no walls are left, the system is in one of the zero-field AFM ground state configuration, where it becomes static and the simulation is ended. Tracing the even and odd magnetizations of both system, fig 5.1.1c and 5.1.1f, one observes that they end with $(m_{\mathrm{even}}, m_{\mathrm{odd}}) \in \{(1,-1),(-1,1)\}$.

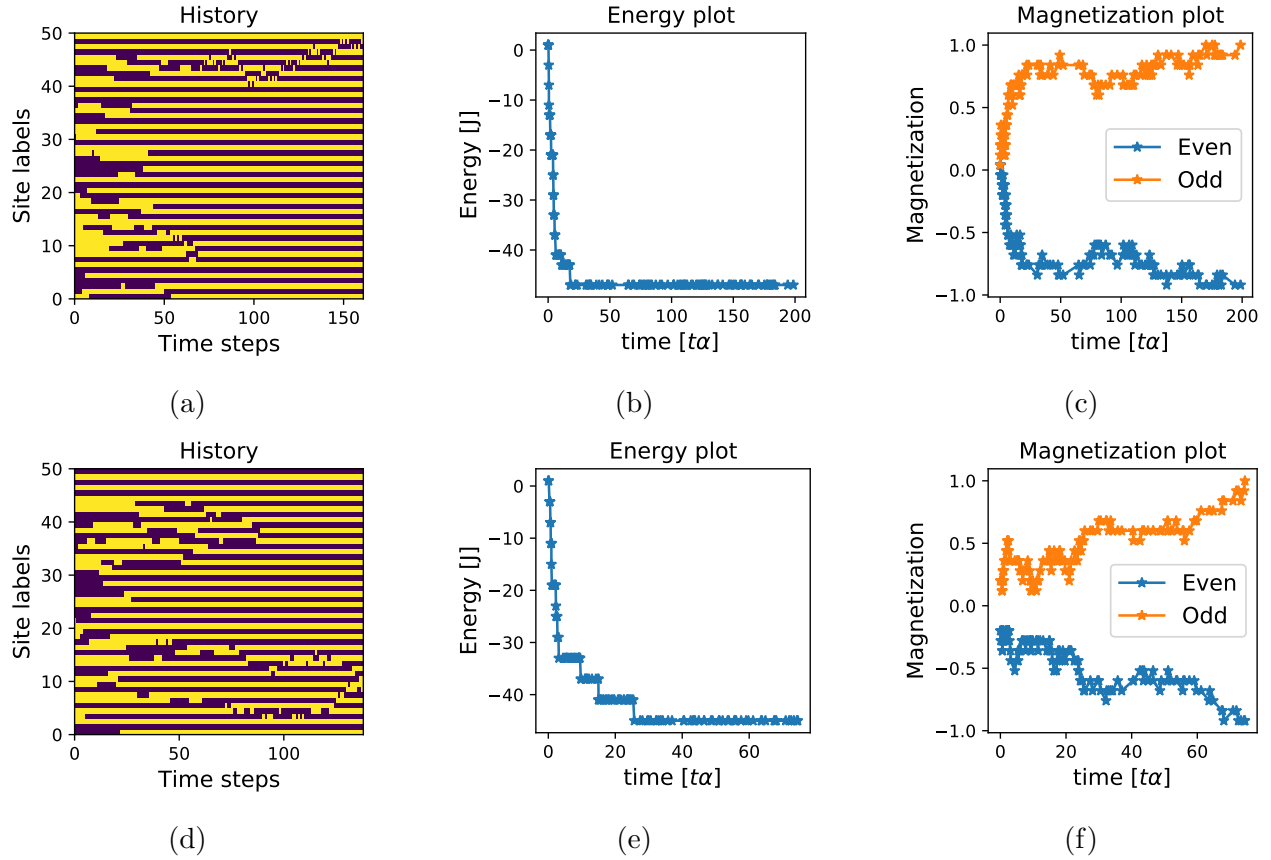

Figure 5.1.1: History and magnetization of single Gillespie_cy simulation with $(T, h, \delta) = (0, 0, 0)$ given an arbitrary ground state. Each row shows data from the same simulation. In **a)** and **d)**, the histories of the simulations are depicted. Here, the dark sites represents spin down states while the light sites represents spin up states. In b) and **e)**, the energy history are depicted. In **c)** and **f)** the history of the even and odd magnetization are shown. Note that the x-axis depicts the number of steps performed for **a)** and **d)** while for the rest, the simulation time in units of the characteristic Glauber rate α, are used.

5.1.2 Measuring simulation time

Given how a general initial state behaves for $h = 0$, one can ask how long it takes for such system to relax into a ground state. To answer this question for a given initial state, the have simulation can be ran multiple times. For each run, the simulation time is saved. The measured data can then be summarized in a histogram using ten bins as shown in fig 5.1.2. For each bin, the uncertainty in frequency are based on the fact that counts follow a Poison distribution[33]. The uncertainty in number of simulation in a given bin n_i is then equal to $\sqrt{n_i}$. The uncertainty in frequency of each bin with $n_i \neq 0$ is then

$$\delta f_i = \frac{\delta n_i}{n_{\text{total}}} = \frac{\sqrt{n_i}}{n_{\text{total}}} = \sqrt{\frac{f_i}{n_{\text{total}}}} \tag{5.1.5}$$

Here n_{total} is the total number of simulations performed. Also, the uncertainty in time is simply set to half of the bin widths. From the histogram, it seem that the frequencies decay exponentially. To test this hypothesis, the data can be fitted to an exponential decay $y = Ae^{-\lambda t}$. One way of doing this is to scale the bin heights logarithmically and fitting it to a linear model since $\ln y = \ln A - \lambda t$. When

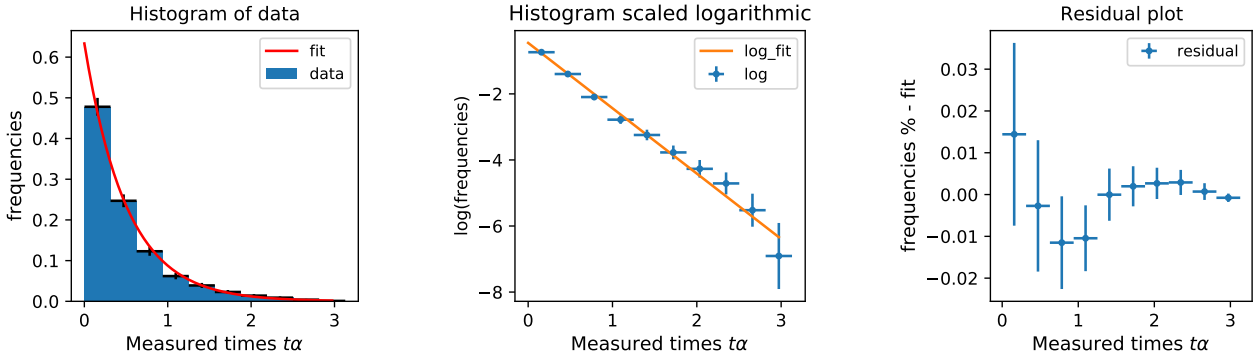

(a) (b) (c)

Figure 5.1.2: Fit of simulation times from 10,000 simulations of the KIM with a randomly generated initial state with a 50/50 distribution of spin up and spin down states. The simulations are performed for $N = 30$ sites, $h = T = \delta = 0$ and AFM nearest neighbour couplings $J = 1$.

doing this, the uncertainties in frequencies will for $f_i \neq 0$ scale to

$$\delta \ln(f_i) = \frac{\partial \ln f_i}{\partial f_i} \delta f_i = \frac{\delta f_i}{f_i} = \frac{1}{\sqrt{f_i n_{\text{total}}}} = \frac{1}{\sqrt{n_i}}. \tag{5.1.6}$$

Using the numpy.polynomial.polynomial.Polynomial.fit method[1], one generates the fit depicted in fig. 5.1.2b. Note that because the logarithmically errors are inversely proportional to the square root of the count, bins with more data points are weighted higher in the fit than bins with less data points. The fit look good in logarithmic space following the data closely. When converting from the real data, in fig 5.1.2a, the fit is translated as well. The new fit still follows the data, with the difference between data and theory shown in fig 5.1.2c. The largest disagreement between data and fit is for the first bin and decreases when $t\alpha$ gets larger. For the first bins, which are weighed the most in the fit, the relative error is only around 10%, which are within the errors of the data points. The hypothesis can therefore be accepted for now.

From the measured fit parameters, one can measure both a decay rate λ and a normalization constant A for a given initial configuration[2].

5.1.3 Correlation between A and λ

Given an initial state $\{\sigma\}$ as before. If one was to simulate it many many time, then the frequency $f(I_n)$ of measuring a simulation with simulation time in the interval $I_n \subset \mathbb{R}_+$ should approach the probability $P(I_n|\{\sigma\})$ of such an even. As measured before, if a bin size of Δt is chosen, then the probability of measuring a simulation with time $t \in [\Delta tn, \Delta t(n+1)[$ should be

$$P([\Delta tn, \Delta t(n+1)[|\{\sigma\}) = Ae^{-\lambda \Delta t\left(n+\frac{1}{2}\right)}, \tag{5.1.7}$$

using the results from the previous subsection. Summing over these probabilities, the result should be one since the simulation times must be a real, positive number. Therefore

$$1 = \sum_{n=0}^{\infty} P([\Delta tn, \Delta t(n+1)[|\{\sigma\}) = Ae^{-\lambda \Delta t/2} \sum_{n=0}^{\infty} e^{-\lambda \Delta tn} = \frac{Ae^{-\lambda \Delta t/2}}{1 - e^{-\lambda \Delta t}} = \frac{A}{2\sinh\left(\frac{\lambda \Delta t}{2}\right)}. \tag{5.1.8}$$

[1] For more details about the method, read [34]. And yes, the number of polynomials are correct!
[2] Well in principle it is $\ln A$ that is measured, but it hardly matters.

A and λ must therefore be correlated via the relation $A = 2\sinh\left(\frac{\lambda\Delta t}{2}\right)$. In the third equality of eq. 5.1.8, the geometric series is used. This is allowed since $\lambda\Delta t > 0$ which implies $|e^{-\lambda\Delta t}| < 1$, which implies convergence of the geometric series. This statement is tested in the next section where different initial configurations are generated and simulated. As a final note, the probability density function associated with the simulation is then

$$\mathcal{P}(t;\lambda,\{\sigma\}) = \lambda e^{-\lambda t} \tag{5.1.9}$$

so that

$$\int_0^\infty \mathcal{P}(t;\lambda)dt = 1 \quad \text{and} \quad \int_{I_n} \mathcal{P}(t;\lambda)dt = \int_{\Delta tn}^{\Delta t_{n+1}} \lambda e^{-\lambda t'}dt' = 2\sinh\left(\frac{\lambda\Delta t}{2}\right)e^{-\lambda t_n} \tag{5.1.10}$$

From this, the average decay time can be evaluated as

$$\langle t\rangle = \int_0^\infty t\mathcal{P}(t;\lambda)dt = \int_0^\infty \frac{t}{\lambda}e^{-\lambda t}dt = \lambda^{-1}. \tag{5.1.11}$$

The average decay time are therefore reciprocal to the decay rate λ. This fact will be used throughout this section.

5.1.4 λ's dependence on initial states percentage

To determine how λ and A depends on the initial state, one can generate a large amount of different initial states and perform the previously described analysis on each state. For a given percentage %, being a measure of the fraction of spin down states in the initial configuration, the 100 initial states can be generated for $N = 30$, which can be simulated 1,000 times each. From these simulations a hundred pairs (A, λ) which can be analysed. In fig. 5.1.3a, initial states with 70 % of its spins pointing down. The decay time measurement λ^{-1} can then be summarized in a histogram, which shows that the initial state distributes symmetrically around 300α and does not seem to depend on the number of domain walls in the initial system. This is in agreement with the fact that the simulation time is dominated by the motion of the last domain wall. To show that probabilities adds to one, the (A, λ) are plotted again each other over all the generated states. One can therefore define the decay time $\lambda^{-1}(\%)$, as a function of %, being the decay time averaged over initial states with the same percentage of spin down states %.

To find how λ^{-1}'s depends on %, a 100 initial states are randomly generated for each % where each state is simulated 1,000 times, as before. From the thousand measurements, the measured simulation times are fitted to a fit, as done earlier. This gives a hundred decay rates pr. percentage, which are averaged over, which are shown in the first plot of fig. 5.1.3b. The error bars are here set to be the standard deviation of the hundred measurements for each %. In the second plot of 5.1.3b, the measured decay rates of each initial states is plotted against the number of domain walls in that configuration. From these two plots, one can conclude that the average simulation time does not depend on the percentage of down spins in the initial state nor does it depend on the number of domain walls.

Averaging over %, the average decay time of the KIM for $N = 30$ sites with AFM nearest neighbour coupling and no longitudinal field, are

$$\tau_{\text{decay}} = (302 \pm 7)\tau \tag{5.1.12}$$

5.1.5 λ's dependence on system size

If the size dependence of λ and τ_{decay} is to be analysed, one needs to simulate the KIM for many different sizes. Since the decay rate in general does not depend on the initial configuration, one can estimate $\tau_{\text{decay}}(N)$ without the need of scanning through all possibilities of % for each system size.

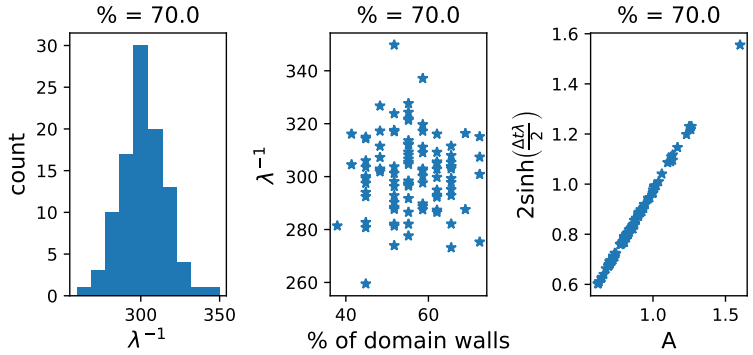

(a)

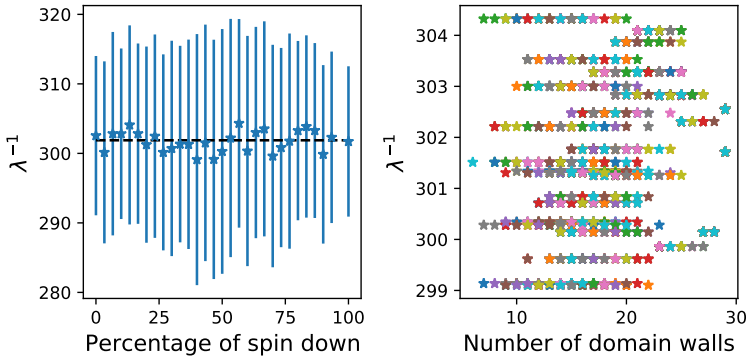

(b)

Figure 5.1.3: Simulation depicting how λ^{-1} depends on the initial configuration. In **(a)**, a given percentage, here 70%, is picked. 100 randomly generated initial states for which the decay time λ^{-1} is measured using 1,000 simulations. A histogram of λ^{-1} is shown on the left, and λ^{-1} is plotted against the number of domain walls. On the right, the fit parameters (A, λ) are plotted against each other where λ is scaled corresponding $2\sinh(\Delta t\lambda/2)$, which shows a linear dependence. In **(b)**, each data point is an average over the decay time of 100 randomly generated initial states with a given % of spin down, each simulated 1,000 times. The average decay time over % is $\langle\lambda^{-1}\rangle = (302 \pm 7)\tau$

One can simply pick a few percentages, such as $\% \in \{0, \frac{1}{9}, \cdots, \frac{8}{9}, 1\}$ and make due with generating ten initial states pr. percentage for each system size N. This gives a 100 measurements of λ, exactly like in the previous subsection, but with only a tenth of the generated initial states. Averaged over these measurement, one gets the data shown in figure fig. 5.1.4. From the logarithmic plot, one observed that

$$\ln \tau_{\text{decay}} = Exp \cdot \log(N) + \log(a) \Leftrightarrow \tau_{\text{decay}} = aN^{Exp} \tag{5.1.13}$$

with a and Exp measured to be

$$Exp = 2.05188 \pm 0.00006 \quad \text{and} \quad a = (0.27881 \pm 0.00016)\tau \tag{5.1.14}$$

5.1.6 Summary

In summary, for $h = T = \delta = 0$, the probability density associated with measuring the simulation time of KIM follows

$$\mathcal{P}(t; \lambda) = \lambda e^{-\lambda t}. \tag{5.1.15}$$

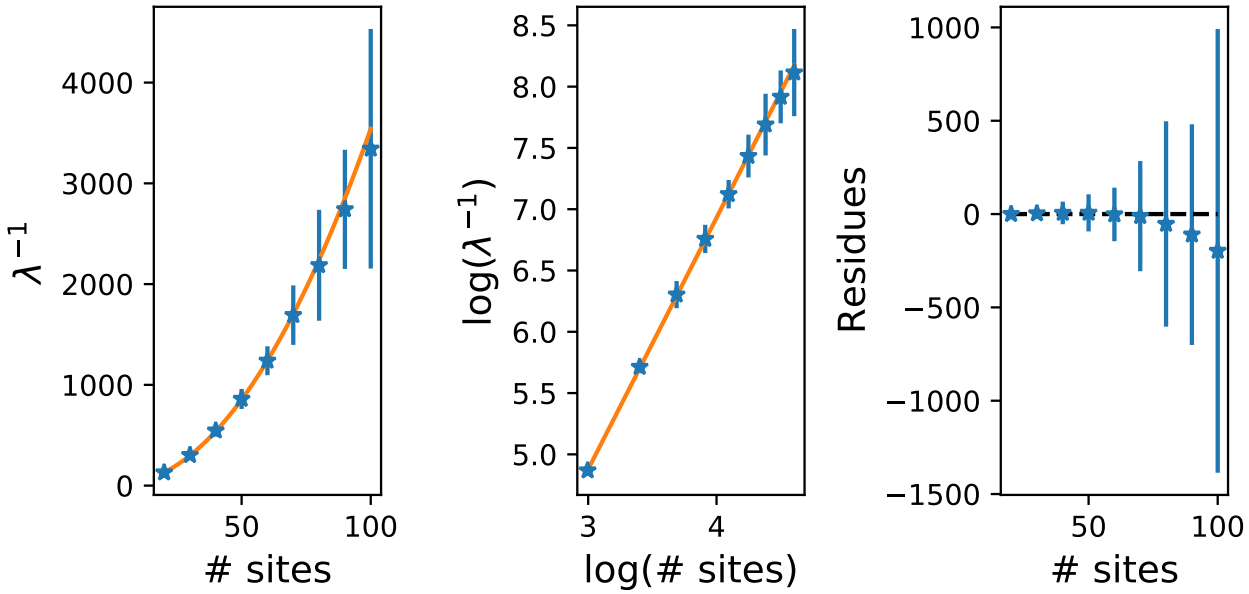

Figure 5.1.4: Data from scanning over the system size fitting to a power law. The left window shows the average decay time are plotted for different system sizes with error bars being equal to the standard deviation of the sampled data. This is done by randomly generating 10 initial states with for 10 different percentages %, so 100 states in total, which each are simulated 1,000 times each. In the middle window, the same data is plotted in logarithmically scaled axis. Errors are here estimated using error propagation. In the last window, the difference between fit and data is presented.

Here λ^{-1} is average simulation time and is, in general, independent of the initial state. It does depend on the system size thou via a power law with exponent Exp and front factor a measured to be

$$Exp = 2.05188 \pm 0.00006 \quad \text{and} \quad a = (0.27881 \pm 0.00016)\tau \tag{5.1.16}$$

This result agrees with the equilibrium calculation performed in chapter 2. Compared to the kinetic Ising model, the assumption that the system decays into a randomly chosen zero-field AFM ground state for $h = 0$ is correct as well.

5.2 AFM - Zero temperature - Non-zero field

5.2.1 Small non-zero longitudinal field

If a longitudinal field is turned on, the Z_2 symmetry is broken. From the analytical calculation in chapter 2, the overall statistical average of the magnetization should be zero. This is because the nearest neighbour coupling between spin are still dominating for $0 < |h| < J$. One would therefore expect the system would still decay into a zero-field AFM ground state. This does actually no happen here. Instead, the system will end op in a disordered where it becomes states. An example of this is shown in fig. 5.2.1. One can explain this phenomenon by looking at the rates.

Because of the non-zero longitudinal, the allowed domain wall moves must be labelled with a sign $\pm$ corresponding to its equivalent spin-flip process. This is described in the end of section 2.1. In this context given the following processes

$$\uparrow\downarrow\downarrow \rightarrow \uparrow\uparrow\downarrow \quad \text{costs} \quad \Delta E = 2h \quad \text{to perform. In domain wall picture} \quad \circ\bullet \rightarrow \bullet\circ \tag{5.2.1}$$

$$\downarrow\uparrow\uparrow \rightarrow \downarrow\downarrow\uparrow \quad \text{costs} \quad \Delta E = -2h \quad \text{to perform. In domain wall picture} \quad \circ\bullet \rightarrow \bullet\circ \tag{5.2.2}$$

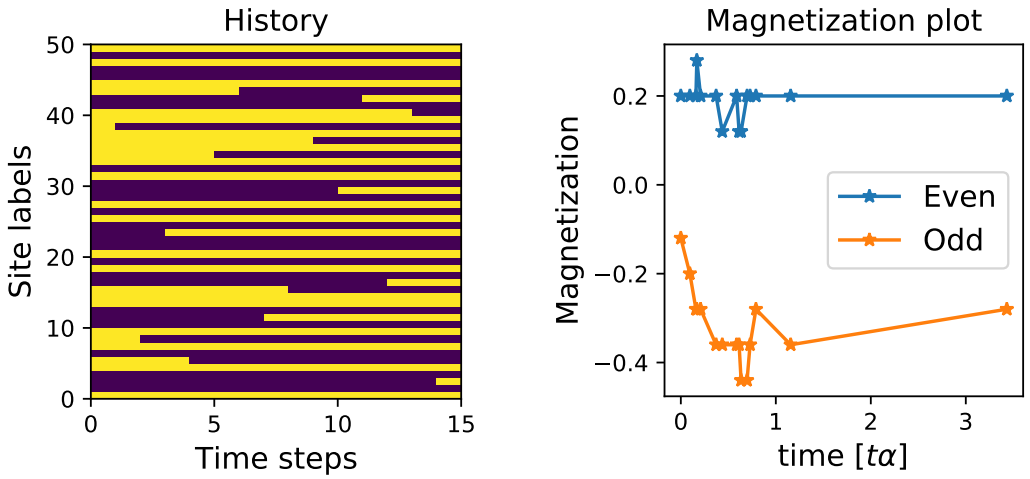

(a) (b)

Figure 5.2.1: Simulation of KIM for small fields satisfying $0 < |h| < J$ for AFM coupling $J > 0$ and $h = T = 0$. The randomly generated initial states with 30 sites decays into a disordered configurations.

Even thou the two processes look identical in the domain wall picture, the energy cost differs by a sign. One therefore defined the process in eq. (5.2.1) and eq. (5.2.2). Evaluating these rates for homogeneous fields and nearest neighbour couplings, one gets an asymmetry in the domain wall motion

$$\omega^{\pm}_{\mathrm{PC}} = \omega^{\pm}_{\mathrm{EC}} = 0, \qquad \omega^{\pm}_{\mathrm{PA}} = \omega^{\pm}_{\mathrm{EA}} = \tau^{-1}, \quad \text{and} \quad \omega^{\pm}_{\mathrm{M}} = \begin{cases} \tau^{-1} & \text{for} \quad + \\ 0 & \text{for} \quad - \end{cases} \tag{5.2.3}$$

For these calculations it is assumed that $h > 0$. If one wishes to know the equivalent dynamics for $h < 0$, one can simply flip all spin, then run the calculations, and then flip all spins back again. The same is true for the rest of this chapter.

As for $h = 0$, the processes of creating domain walls are not allowed so the have a rate of 0. Also domain wall annihilations are allowed and happens on the time scale of τ. The system differs from $h = 0$ by the asymmetry between domain wall motion. A wall can be moved if is results in a spin to be flipped from $\uparrow$ to $\downarrow$, while if it results in $\downarrow$ to $\uparrow$ is forbidden. This results in some configurations having domain wall setting in the bulk of the system which cannot be annihilated. As an example, if one considers a single, lonely domain wall in the bulk of the system, as depicted in fig. 5.2.2a. Two spin configurations can correspond to such domain wall configuration. In one case, the wall cannot move, because to move in either direction, the system must perform a $+$ domain wall move. In the second case, the wall can move in either direction because the moves required are both of $-$ kind, but after a single move, the wall requires moves of $+$ kind to move in either direction. Lonely domain walls will therefore get stuck in the bulk of the system, which results in disorder. If two walls are placed next to each other, so they are nearest neighbours, then in one case, the only move allowed is pair annihilation, which results in the domain between the wall collapsing, fig 5.2.2b. In the other case, pair annihilation are also allowed, but both walls are also allowed to move away from each other. Following the diagram in fig 5.2.2b, and using the theory on how the Gillespie algorithm picks these processes, there will be a probability of $2/3$ of the domain collapsing. The other possibility is that the domain is widened and two wall are stuck in the bulk. The last option results in a disordered configuration.

If domain walls are separated further, or more domain walls are introduced, the diagram required to describe the possible dynamics becomes quite large and complicated. They will therefore not be described here. In conclusion, the AFM KIM can in a small longitudinal field happen to decay into a disordered ground state.

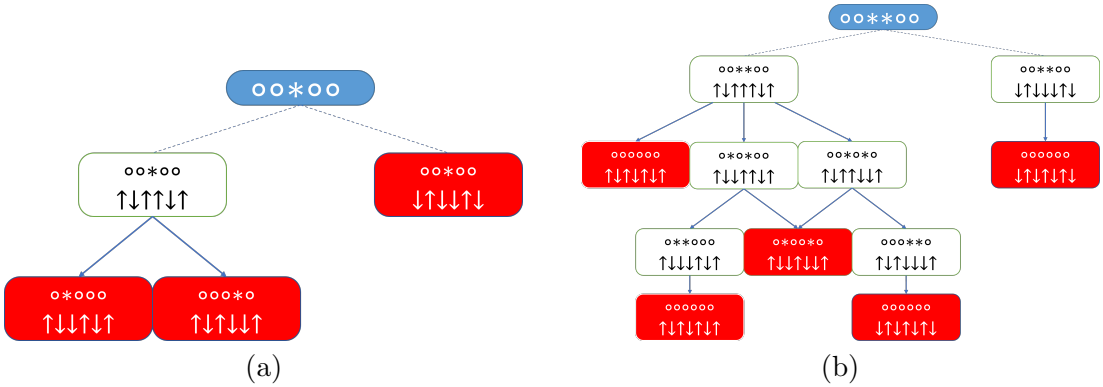

Figure 5.2.2: Diagrams showing how domain walls will move for an AFM KIM in a longitudinal field $0 < h < J$. In **(a)**, the moves a single domain wall can perform are shown. This will always lead to the wall getting stuck in the bulk. In **(b)** the moves two nearest neighbour domain wall can perform. These moves will sometimes lead to the walls getting stuck in the bulk. In both sub figures, the static configurations are marked by red.

5.2.2 When the field matches the nearest neighbour coupling - edge flip line

For longitudinal fields whose strength matches the nearest neighbour coupling, $h = J$, something special happens at the edges. Since each edge spin only has a single nearest neighbour, the energy difference when flipping an edge spin is now zero for some configurations. Compared to $0 < J < h$, then

$$w^-_{\mathrm{EC}} = w^+_{\mathrm{EA}} = \frac{1}{2\tau}. \tag{5.2.4}$$

The rest of the rates are similar for $h = J$ and $0 < h < J$. This means that the bulk of the system still ends up being stuck in a disordered state. The difference from $0 < h < J$ is that now that if a spin down happens to be next to one of the edge spin, the edge spin can flip freely. The dynamics of some simulation will therefore never stop as shown in fig. 5.2.3a. Here, only one of the edge spins are flipping constantly, but simulations can occur were neither or both of the edge spins flips.

5.2.3 Medium longitudinal field: $J < h < 2J$

Not much new can be said in the section since systems with $J < h < 2J$ acts very much like systems with $0 < h < 2J$. One exception is present thou. The rates of the edge related processes are now

$$w^+_{\mathrm{EC}} = w^+_{\mathrm{EA}} = 0 \quad \text{and} \quad w^-_{\mathrm{EC}} = w^-_{\mathrm{EA}} = \frac{1}{2\tau}. \tag{5.2.5}$$

This means that edge spins will always end up being opposite to the field. This can be seen in fig. 5.2.3b.

5.2.4 Critical field: $h_c = 2J$

The statistical average calculations of the magnetization of the system at $T = 0$, sec. 2.2, predicts a phase transition at $h = 2J$, where the system goes from having $m = 0$ to $m = -h$. One should therefore expect that the simulation to shown some kind of critical behaviour. And indeed it does. Setting $h = 2h$, some of the pair creation rates will become non-zero. In summary

$$\omega^+_{\mathrm{PC}} = \omega^+_{\mathrm{EC}} = \omega^+_{\mathrm{EA}} = \omega^+_{\mathrm{M}} = 0, \quad \text{and} \quad \omega^+_{\mathrm{PA}} = \frac{1}{2\tau} \tag{5.2.6}$$

$$\omega^-_{\mathrm{EC}} = \omega^-_{\mathrm{PA}} = \omega^-_{\mathrm{EA}} = \omega^-_{\mathrm{M}} = \tau^{-1}, \quad \text{and} \quad \omega^-_{\mathrm{PC}} = \frac{1}{2\tau} \tag{5.2.7}$$

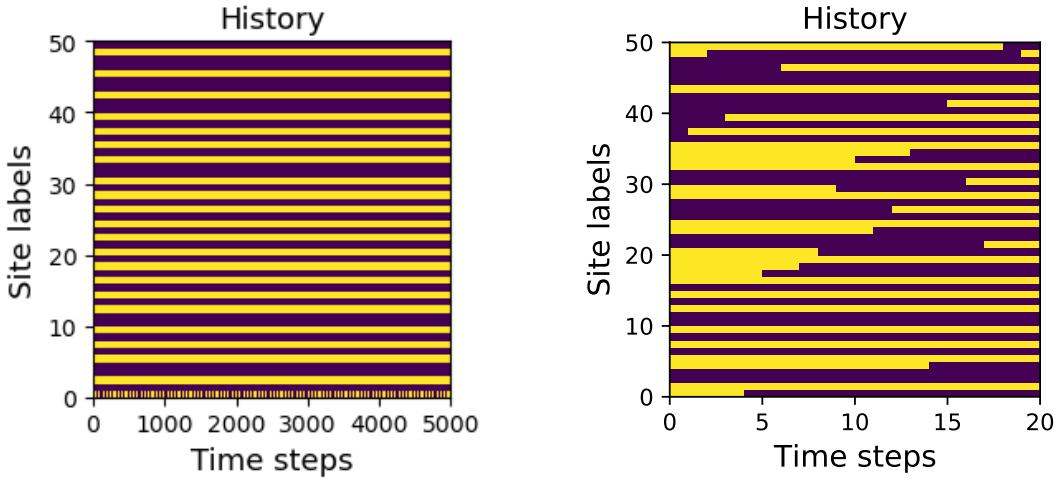

(a) $h = J$ (b) $J < h < 2J$

Figure 5.2.3: Simulations of an AFM KIM for **(a)** $h = J$ and for **(b)** $J < h < 2J$. In both cases, the bulk of the system gets stuck in a disordered state with the exception the edge spin flipping constantly in **(a)**.

The heat bath can therefore create certain domain wall, which introduces disorder to the system. The system will therefore never settle down and the simulation never becomes static. The disorder of the system also becomes enormously high because of the many domain wall pairs constantly being created and annihilated. In figure 5.2.4a, this disorder is shown.

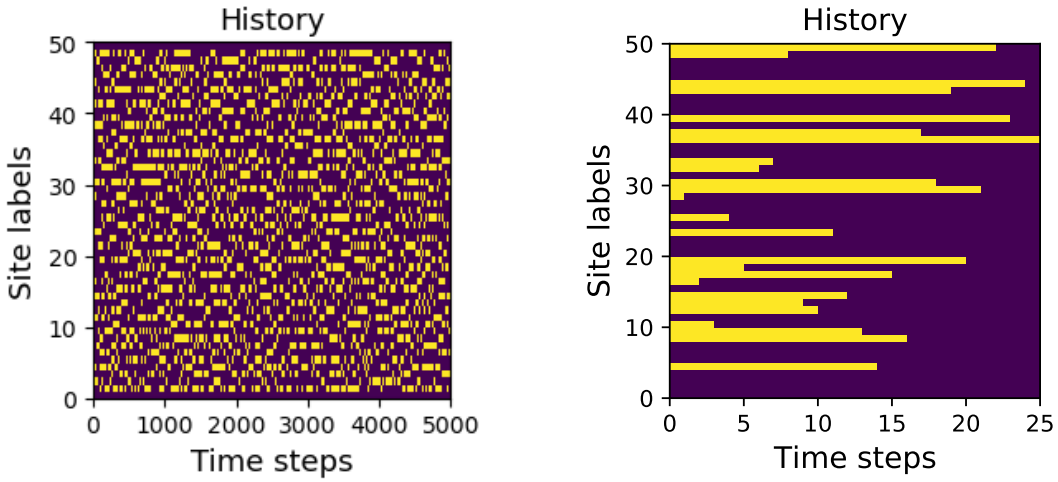

(a) (b)

Figure 5.2.4: Simulations of an AFM KIM for **(a)** $h = 2J$ and for **(b)** $h > 2J$. In **(a)**, domain wall pairs are created and annihilated at the same rate, which implies a very disordered simulation. In **(b)**, the field dominated the energy scales which results in the system decaying into a zero-field AFM ground state.

5.2.5 Super-critical phase

Exceeding the critical field value, so that $h > 2J$, the field becomes the dominating term in the energy. All rates of $+$ kind will therefore reduce to zero, while all the rates of $-$ kind evaluates to τ^{-1}. The system can therefore create pairs of domain walls which cannot be annihilated. This implies that when $t \gg \tau$ the system will be in a state saturated by domain wall excitations of $\downarrow\downarrow\downarrow$ kind. In spin space, this configuration is the state were all spins points opposite to the longitudinal field, fig. 5.2.4b. The system therefore decays in a zero-field FM ground states.

5.2.6 Discussion of results

Compared with the equilibrium calculation of chapter 2, the results presented here are different. Chapter 2 predicted that for $T = 0$ the system would either decay into one of the zero-field AFM ground state for $T \ll |h| < 2J$. If the system size was even, the ground state was picked randomly while for odd system sizes, one of the states was preferred. Here on the other hand, the system does not decay into any of the ground states. One could explain this disagreement by the fact the equilibrium calculations does not take the initial configuration into account. Since the field is not strong enough to change the energetically order of the energy level, then one would except that the even and odd magnetization could take any sign when averaging over all initial configuration. If true, the average magnetizations could agree with the equilibrium dynamics. More data is needed to say this for sure thou.

Chapter 6

Open 1D transverse field Ising model

In the last four chapters, the quantum dynamics of the original system, described in chapter 1, was completely ignored. This lead to the study about classical thermal dynamics which introduced the Kinetic Ising model. In reality, it is not necessary the case that the quantum dynamics can be ignored. It is therefore wise to analyse these dynamics also. If there is a difference in the dynamics of the classical and quantum system, experiments can be performed to determine if the QDCA can be considered as a classical object or not. The question of whether there is a difference between the two will not be answered in the chapter nor will the statistical properties be explored fully. The goal of this chapter is instead to take the first steps in the direction and solve the eigenstate problem for the Hamiltonian in eq. (1.4.14) for certain conditions.

6.1 Introduction

Returning to the introduction, the basis states of the electron on the quantum dots could be maps to the 1D, OBC, nearest neighbour, quantum Ising model, in a magnetic field $\vec{h}(x)$

$$\mathcal{H} = \sum_{i=1}^{N-1} J_i \sigma_i^x \sigma_{i+1}^x + \sum_{i=1}^{N} \left(h_i^z \sigma_i^z + h_i \sigma_i^x \right). \tag{6.1.1}$$

Note that this Hamiltonian different to the one written in chapter 1 by a $\frac{\pi}{2}$ rotation around the y-axis. The reason for this will becomes clear later when the eigenstates are to be evaluated. One can always rotate back if one want to compare the two. Term first term in eq. (6.1.1) is similar to the nearest neighbour term in the classical, nearest neighbour, Ising model's energy function. They are indeed very similar and both forces spins to align/anti align depending on the sign of J. The convention of $J > 0$ being an AFM coupling is also used in this chapter. Similar to the classical case, the interaction part of the Hamiltonian is also $\mathbb{Z}_2$ symmetric with respect to the transformation

$$R = \prod_{\ell=1}^{N} (-i\sigma_i^z) \tag{6.1.2}$$

that flips the sign of a all σ_i^x operators. This implies that for $\vec{h} = \vec{0}$, all energy levels are at least two-fold degenerate. This changes with the field interaction is including, which breaks this symmetry for non-zero longitudinal field h_i^x. The reason that no y-component of the field are considered is because it can generally be ignored. To shown this, one considers the rotation $R_x(\vec{\theta})$ around the x-axis, defined

by

$$R_x(\vec{\theta}) = e^{-i\sum_{j=1}^{N}\frac{\theta_j}{2}\sigma_j^x} = \prod_{j=1}^{N}\left[\cos\left(\frac{\theta_j}{2}\right)\mathbb{I} - i\sin\left(\frac{\theta_j}{2}\right)\sigma_j^x\right] \quad \text{with} \tag{6.1.3}$$

$$\theta_i = \begin{cases} \mp\tan^{-1}\left(\frac{h_i^y}{h_i^z}\right) & \text{for} \quad h_i^z \neq 0 \\ \mp\frac{\pi}{2} & \text{for} \quad h_i^z = 0 \end{cases}. \tag{6.1.4}$$

Applying the to the interaction term does not alter it since R_x commutes with σ_i^x nor does it alter the interaction with the longitudinal field. It does change the rest of the field thou, by mapping

$$\sum_{i=1}^{N} h_i^y\sigma_i^y + h_i^z\sigma_i^z = \pm\sum_{i=1}^{N}\sqrt{(h_i^y)^2 + (h_i^z)^2}\sigma_i^z \tag{6.1.5}$$

The longitudinal field, h_i^x acts as a Zeemann term and splits the degeneracy coming from the $\mathbb{Z}_2$ symmetry. If this is the only active term in the field interaction, then σ_i^x commutates with the Hamiltonian and they share eigenstates. The spectrum therefore overlaps the classical, nearest neighbour Ising model in a longitudinal field. The transverse field h_i^z mixes the basis since $[\mathcal{H}, \sigma_i^x] \propto h_i^z$ which implies $\mathcal{H}$ and σ_i^x cannot share basis states. In this chapter, $\mathcal{H}$ is diagonalized for $h_i^z = 0$. The reason why the longitudinal field must be excluded will be clear later. The model remaining is knows as the transfer field quantum Ising model (TFQIM).

6.2 Analytical solution for zero-longitudinal fields

6.2.1 Jordan-Wigner transformation

When diagonalizing the TFQIM, the first thing to do, is to perform a Jordan-Wigner transformation[35, 36, 37]. This transformation maps the Hilbert space of a system of N spin-1/2 particles into the Fock space of N spin-less fermions. More specifically, the spin-down state is mapped to an occupied site, while the spin-up state is mapped to an empty site, fig. 6.2.1. In this way, the product of spin ladder operators $\sigma_i^+\sigma_i^-$ is mapped to the product of fermion operators, $c_i c_i^\dagger$. Here c_i and $c_i^\dagger$ are the creation/annihilation operators of a spin-less fermion sitting on the i'th site. One could therefore make the naïve guess that one should map the spin-ladder operators to the fermion creation/annihilation operators directly via $\sigma_i^+ \to c_i$ and $\sigma_i^- \to c_i^\dagger$. This is unfortunately the wrong way to do it, since the commutator relations for the spin operators cannot be satisfies simultaneously with the fermion anti-commutator relations.[1] Therefore, the map must be more sophisticated. One such map is the non-local Jordan-Wigner transformation:

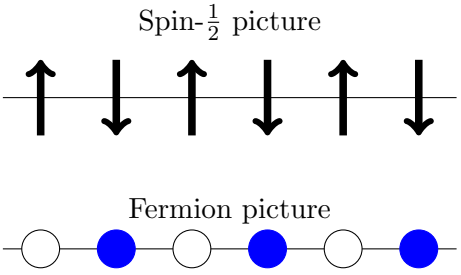

Figure 6.2.1: Representation of the Jordan-Wigner transformation. The picture shows a configuration of a spin-$\frac{1}{2}$ system with 6 sites. This gets mapped to the spin-less fermion state represented by the lower picture. Here an empty circle represents an empty site while a blue circle represents an occupied site.

$$\sigma_i^+ \leftrightarrow \prod_{j=1}^{i-1}(-1)^{c_j^\dagger c_j}c_i. \quad \text{and} \quad \sigma_i^- \leftrightarrow \prod_{j=1}^{i-1}(-1)^{c_j^\dagger c_j}c_i^\dagger. \tag{6.2.1}$$

[1] As an example $[\sigma_i^+, \sigma_j^-] = 0$ for $i \neq j$ while $[c_i, c_j^\dagger] = c_i c_j^\dagger - c_j^\dagger c_i = 2c_i c_j^\dagger \neq 0$ for $i \neq j$. From the naïve map, these commutators should map to each other, which they clearly don't.

From this map, it can be shown that $\sigma_i^+\sigma_i^- \to c_i c_i^\dagger$, while

$$\sigma_i^+\sigma_j^- \to c_i \prod_{\ell=\min(i,j)}^{\max(i,j)-1} (-1)^{c_\ell^\dagger c_\ell} c_j^\dagger \tag{6.2.2}$$

Products of spin operators on different sites will therefore map to products of fermion operators with a sign depending on the number of fermions between the two sites. Using relation (6.2.1), all the other spin operators can be mapped to their corresponding fermion operators. From commutator relation $[\sigma_i^+, \sigma_j^-] = \delta_{ij}\sigma_i^z$, the anti-commutator relation $\{c_i, c_i^\dagger\} = \mathbb{I}$, and the fact that $[A, B] = \{A, B\} - 2BA$, one gets

$$\sigma_i^z = [\sigma_i^+, \sigma_i^-] = \{\sigma_i^+, \sigma_i^-\} - 2\sigma_i^-\sigma_i^+ \leftrightarrow \{c_i, c_i^\dagger\} - 2c_i^\dagger c_i = \mathbb{I} - 2c_i^\dagger c_i. \tag{6.2.3}$$

Here, the distinction between the identity operator acting on spin Hilbert space and the identity operator acting on the Fock space are not made because they are always mapped to each other. The correct use of identity operator is given by context. From eq. (6.2.3), the inverse Jordan-Wigner transformation can be realized as

$$c_j \leftrightarrow \left(\prod_{\ell=1}^{j-1} \sigma_\ell^z\right) \sigma_j^+ \quad \text{and} \quad c_j^\dagger \leftrightarrow \left(\prod_{\ell=1}^{j-1} \sigma_\ell^z\right) \sigma_j^-. \tag{6.2.4}$$

With eq. (6.2.1) and eq. (6.2.4), one can jump back and forwards between spin and fermion picture.

The remaining Pauli operators

When mapping σ_i^x and σ_i^y to Fock space, the parity of the sub chain consisting of the sites j with $j < i$, becomes important. Writing σ_i^x and σ_i^y as a linear combination of ladder operators, eq. (6.2.1) can be used to gets show that

$$\sigma_j^x = \sigma_j^+ + \sigma_j^- \leftrightarrow \left(c_j^\dagger + c_j\right) \prod_{\ell=1}^{j-1} (-1)^{c_\ell^\dagger c_\ell} \quad \text{and} \quad \sigma_j^y = -i(\sigma_j^+ - \sigma_j^-) \leftrightarrow -i\left(c_j^\dagger - c_j\right) \prod_{\ell=1}^{j-1} (-1)^{c_\ell^\dagger c_\ell} \tag{6.2.5}$$

As will be clear later in this chapter, it can be advantageous to thing of these products as in terms of the Majorana operators

$$\gamma_i^+ = c_i^\dagger + c_i \quad \text{and} \quad \gamma_i^- = i(c_i^\dagger - c_i) \tag{6.2.6}$$

These operator anti-commute with each other and squares to identity

$$\{\gamma_i^s, \gamma_j^{s'}\} = 2\delta_{ij}\delta^{ss'} \qquad (\gamma_i^+)^2 = (\gamma_i^-)^2 = \mathbb{I}. \tag{6.2.7}$$

Since $\gamma_i^+\gamma_i^- = i(c_i^\dagger + c_i)(c_i^\dagger - c_i) = i(-1)^{c_i^\dagger c_i}$, then the parity $\prod_{j=1}^{i-1}(-1)^{c_i^\dagger c_i} = \prod_{j=1}^{i-1}(-i\gamma_i^+\gamma_i^-)$, which implies

$$\sigma_j^x \leftrightarrow \gamma_j^+ \left(\prod_{\ell=1}^{j-1} -i\gamma_j^+\gamma_j^-\right) \quad \text{and} \quad \sigma_j^y \leftrightarrow \gamma_j^- \left(\prod_{\ell=1}^{j-1} -i\gamma_j^+\gamma_j^-\right) \tag{6.2.8}$$

Since all Pauli operators are now mapped to the Fork space of spin-less fermions, the Hamiltonian of the TFQIM can be mapped as well. In doing so, the nearest neighbour interaction term will take the form of

$$\sigma_j^x\sigma_{j+1}^x \leftrightarrow \left(\prod_{\ell=1}^{j-1} -i\gamma_\ell^+\gamma_\ell^-\right) \gamma_j^+ \left(\prod_{\ell=1}^{j} -i\gamma_\ell^+\gamma_\ell^-\right) \gamma_{j+1}^+ = -i\left(\prod_{\ell=1}^{j-1} \left(-i\gamma_\ell^+\gamma_\ell^-\right)^2\right) (\gamma_j^+)^2\gamma_j^-\gamma_{j+1}^+ \tag{6.2.9}$$

$$= -i\gamma_j^-\gamma_{j+1}^+ = c_j^\dagger c_{j+1} + c_{j+1}^\dagger c_j + c_j^\dagger c_{j+1}^\dagger + c_{j+1}c_j \tag{6.2.10}$$

In the first equality, the the anti-commutator relation $\{\gamma_i^s, \gamma_j^{s'}\} = 2\delta_{ij}\delta_{ss'}$ is used where $s, s' \in \{+, -\}$. In the second equality, the fact that $(-i\gamma_i^+\gamma_i^-)^2 = (\gamma_j^+)^2 = (\gamma_j^-)^2 = \mathbb{I}$ is used. The TFQIM Hamiltonian will therefore take form

$$\mathcal{H} = \sum_{i=1}^{N-1} J_i(c_i^\dagger c_i + c_{i+1x}^\dagger c_{i+1}^\dagger + \text{h.c.}) - \sum_{i=1}^{N} h_i^x(c_i + c_i^\dagger)\left(\prod_{\ell=1}^{i-1}(1 - 2c_\ell^\dagger c_\ell)\right) + h_i^z(\mathbb{I} - 2c_i^\dagger c_i). \tag{6.2.11}$$

in Fock space. For zero longitudinal field and uniform nearest neighbour coupling and transverse field, this Hamiltonian is equivalent to a Kitaev chain [38, 39] with superconducting gap $\Delta = -J$, hopping amplitude[2] $w = -J$, and chemical potential $\mu = 2h$. One should therefore expect zero modes[3] in the spectrum the system for certain values of (J, h)[39]. With a non-zero longitudinal field, eq. (6.2.11) becomes incredibly hard to diagonalize, even for homogeneous fields. This is because the longitudinal-field term includes up to N-point interaction terms all happening at the same order of magnitude. This means that non of them can be considered as a perturbation w.r.t. the interaction J and transverse field h^z. To make any attempts to diagonalize eq. (6.2.11), the longitudinal field must first be set to zero. The Ising Hamiltonian will therefore reduce to

$$\mathcal{H} = \sum_{i=1}^{N-1} J_i\left(c_i^\dagger c_{i+1} + c_i^\dagger c_{i+1}^\dagger + \text{h.c.}\right) - \sum_{i=1}^{N} 2h_i c_i^\dagger c_i + \left(\sum_{i=1}^{N} h_i\right)\mathbb{I} \tag{6.2.12}$$

with $h_i = h_i^z$. Solving the eigenvalue problem for this Hamiltonian is much simpler since only quadratic terms are left. The way to approach the problem here are very dependent on the boundaries. To do this, one cannot simply Fourier expand the fermion operator as done when working with PBC[36]. This is because Fourier expansion of c_i, $c_i^\dagger$, and J_i does not cooperate well with the sum $\sum_{i=1}^{N-1}$. If the Fourier transformation of the annihilation operator is $\hat{c}_k := \frac{1}{\sqrt{N}}\sum_{j=1}^{N} c_j e^{-i\frac{2\pi k}{N}j}$ with $k \in \{1, \cdots, N\}$, then the Hamiltonian can be written as

$$\begin{aligned}\mathcal{H} =& \frac{1}{\sqrt{N}}\sum_{k,q}^{N}\left(\hat{J}_q\left(e^{i\frac{2\pi k}{N}} + e^{-i\frac{2\pi(k+q)}{N}}\right) - 2\hat{h}_q\right)\hat{c}_k^\dagger\hat{c}_{k+q} \\ &+ \frac{1}{\sqrt{N}}\sum_{k,k'=1}^{N}\left(\hat{J}_{k+k'}^*\frac{e^{i\frac{2\pi k'}{N}} - e^{i\frac{2\pi k}{N}}}{2}\hat{c}_k^\dagger c_{k'}^\dagger + \hat{J}_{k+k'}\frac{e^{-i\frac{2\pi k}{N}} - e^{-i\frac{2\pi k'}{N}}}{2}\hat{c}_k\hat{c}_{k'}\right)\end{aligned} \tag{6.2.13}$$

with $\tilde{J}_k := \frac{1}{\sqrt{N}}\sum_{j=1}^{N} J_j e^{-i\frac{2\pi k}{N}j}$. Even for homogeneous nearest neighbour coupling and transverse field, the Hamiltonian takes the form of

$$\mathcal{H}_{\text{homo}}^{\text{OBC}} = \mathcal{H}_{\text{homo}}^{\text{PBC}} + \mathcal{H}_{\text{homo}}^{\text{Edge}} \tag{6.2.14}$$

$$\mathcal{H}_{\text{homo}}^{\text{PBC}} = J\sum_{k=1}^{N}\left\{2\left[\frac{N}{N-1}\cos\left(\frac{2\pi k}{N}\right) - g\right]c_k^\dagger c_k - i\frac{N}{N-1}\sin\left(\frac{2\pi k}{N}\right)\left(c_k^\dagger c_{-k}^\dagger - c_{-k}c_k\right) + g\right\} \tag{6.2.15}$$

$$\mathcal{H}_{\text{homo}}^{\text{Edge}} = -\frac{J}{N}\sum_{k\neq k'}(e^{i\frac{2\pi k}{N}} + e^{i\frac{2\pi k'}{N}})c_k^\dagger c_{k'} + c_k^\dagger c_{k'}^\dagger\frac{e^{i\frac{2\pi k'}{N}} - e^{i\frac{2\pi k}{N}}}{2} + c_k c_{k'}\frac{e^{-i\frac{2\pi k}{N}} - e^{-i\frac{2\pi k'}{N}}}{2} \tag{6.2.16}$$

This first term, eq. (6.2.15), describes a TFQIM with PBC and can be diagonalized by a Bogoliubov transformation[36]. This results in a set of fermions labelled by k whose spectrum are given by

$$\epsilon_k = 2|J|\frac{N-1}{N}\sqrt{1 + \left(\frac{Ng}{N+1}\right)^2 - \frac{2gN}{N-1}\cos\left(\frac{2\pi k}{N}\right)} \tag{6.2.17}$$

[2] In ref. [39] the superconducting gap is equal to J. The rest of the constant agree.

[3] For finite chains, these zero modes will not be exactly zero. Instead these states will have exponentially small energy compared to the characteristic energy scales, being J and h. [39]

which in the thermodynamics limit, $N \to \infty$, takes the form $2\sqrt{J^2+h^2-2Jh\cos(\theta_k)}$ where $\theta_k \in]0, 2\pi]$. The boundary term of the same as J meaning that it cannot be seen as a perturbation. One must therefore use other techniques to diagonalize eq. (6.2.12).

6.2.2 Real space Bogoliubov transformation

A better way to diagonalizing the open boundary condition TFQIM, (6.2.12), is to perform a real space Bogoliubov transformation [40, 41]. This is done by introducing fermion creation and annihilation operators, denoted η_k and $\eta_k^\dagger$ as linear combinations of c_j and $c_j^\dagger$.

$$\eta_k^\dagger = \sum_{i=1}^{N} \alpha_{ki} c_i^\dagger + \beta_{ki} c_i \quad \text{and} \quad \eta_k = \sum_{i=1}^{N} \alpha_{ki} c_i + \beta_{ki} c_i^\dagger. \tag{6.2.18}$$

The coefficients α_{ki} and β_{ki} are chosen so that η_k and $\eta_k^\dagger$ diagonalizes $\mathcal{H}$.

$$\mathcal{H} = \sum_{k=1}^{N} \epsilon_k \left(\eta_k^\dagger \eta_k - \frac{1}{2} \right). \tag{6.2.19}$$

Here, the $-1/2$ term in eq. (6.2.19) is introduced to ensure a zero trace of $\mathcal{H}$. This is because $\mathrm{tr}[\sigma_i^\alpha] = 0$ which implies $\mathrm{tr}[\mathcal{H}] = 0$ in the original form of TFQIM eq. (6.1.1). Using the method described in appendix A and B of reference [41], one rewrites the zero-longitudinal field TFQIM Hamiltonian, eq. (6.2.12). in terms of normal terms and anomalous term.

$$H = \sum_{i,j=1}^{N} \left[c_i^\dagger A_{ij} c_j + \frac{B_{ij}}{2} (c_i^\dagger c_j^\dagger - c_i c_j) \right] + \left(\sum_{i=1}^{N} h_i \right) \mathbb{I}. \tag{6.2.20}$$

Here $\mathbf{A}$ and $\mathbf{B}$ are real $N \times N$ matrices where $\mathbf{A}$ is symmetric and $\mathbf{B}$ is anti-symmetric. The exact form of $\mathbf{A}$ and $\mathbf{B}$ are

$$A_{ij} = -2h_i\delta_{ij} + J_i\delta_{i+1,j} + J_j\delta_{i,j+1} \quad \text{and} \quad B_{ij} = J_i\delta_{i+1,j} - J_j\delta_{i,j+1}. \tag{6.2.21}$$

This way of writing the Hamiltonian is useful because it allows one to relate the matrices $\mathbf{A}$ and $\mathbf{B}$ with the coefficients α_{ki} and β_{ki}. By using the commutation relation $[\eta_k, \mathcal{H}] = \epsilon_k \eta_k$, it can be shown that the vectors $(\vec{\phi}_k)_i = \alpha_{ki} + \beta_{ki}$ and $(\vec{\psi}_k)_i = \alpha_{ki} - \beta_{ki}$ are related by

$$(\mathbf{A}+\mathbf{B})\vec{\phi}_k = \epsilon_k \vec{\psi}_k \quad \text{and} \quad (\mathbf{A}-\mathbf{B})\vec{\psi}_k = \epsilon_k \vec{\phi}_k. \tag{6.2.22}$$

Multiplying the first equation in (6.2.22) by $(\mathbf{A}-\mathbf{B})$ and the second equation by $(\mathbf{A}+\mathbf{B})$, one observes that $\vec{\phi}_k$ and $\vec{\phi}$ are eigenvectors of matrices defined from $\mathbf{A}$ and $\mathbf{B}$.

$$\mathbf{M}_1\vec{\phi}_k := (\mathbf{A}-\mathbf{B})(\mathbf{A}+\mathbf{B})\vec{\phi}_k = (\mathbf{A}-\mathbf{B})\epsilon_k\vec{\psi}_k = \epsilon_k^2\vec{\phi}_k \tag{6.2.23}$$

$$\mathbf{M}_2\vec{\psi}_k := (\mathbf{A}+\mathbf{B})(\mathbf{A}-\mathbf{B})\vec{\psi}_k = (\mathbf{A}+\mathbf{B})\epsilon_k\vec{\phi}_k = \epsilon_k^2\vec{\psi}_k \tag{6.2.24}$$

The coefficients α_{ki} and β_{ki} can therefore be determined by solving the eigenvalue problem eq. (6.2.24). This gives both the vectors $\vec{\psi}_k$ as well as the spectrum ϵ_k. For non-zero ϵ_k, the corresponding $\vec{\phi}_k$ vectors can be determined from eq. (6.2.22). For $\epsilon_k = 0$, the corresponding $\vec{\phi}$ vector can be determines by solving eq. (6.2.23). From this procedure, the coefficients α_{ki} and β_{ki} are determined as well as the

spectrum of the Hamiltonian. For general nearest neighbour coupling, J_i and field h_i one can write

$$4\begin{pmatrix} h_1^2+J_N^2 & -J_1h_1 & 0 & \cdots & 0 \\ -J_1h_1 & J_1^2+h_2^2 & -J_2h_2 & \ddots & \vdots \\ 0 & \ddots & \ddots & \ddots & 0 \\ \vdots & \ddots & -J_{N-2}h_{N-2} & J_{N-1}^2+h_{N-1}^2 & -J_{N-1}h_{N-1} \\ 0 & \cdots & 0 & -J_{N-1}h_{N-1} & J_{N-1}^2+h_N^2 \end{pmatrix}\vec{\phi}_k = \lambda_k\vec{\phi}_k \tag{6.2.25}$$

$$4\begin{pmatrix} J_1^2+h_1^2 & -J_1h_2 & 0 & \cdots & 0 \\ -J_1h_2 & J_2^2+h_2^2 & -J_2h_3 & \ddots & \vdots \\ 0 & \ddots & \ddots & \ddots & 0 \\ \vdots & \ddots & -J_{N-2}h_{N-1} & J_{N-1}^2+h_{N-1}^2 & -J_{N-1}h_N \\ 0 & \cdots & 0 & -J_{N-1}h_N & J_N^2+h_N^2 \end{pmatrix}\vec{\psi}_k = \lambda_k\vec{\psi}_k \tag{6.2.26}$$

with $\lambda_k = \epsilon_k^2$. For OBC $J_N = 0$. This result also holds for both time dependent J_i and h_i which results in time-dependent coefficients $\alpha_{ki}(t)$ and $\beta_{ki}(t)$ as well as time dependent energies $\epsilon_k(t)$. This will not be discussed further in this thesis thou. For homogeneous parameters, the complexity of the eigenvalue problems eq. (6.2.23) and (6.2.24) can be reduced even further.

6.2.3 Semi-analytical solution for homogeneous J and h

From the vector-matrix product in eq. (6.2.26), it can be concluded that for $\vec{\psi}_k$ to be an eigenvector of $\mathbf{M}_1$, its elements must satisfy the following recursion relation.

$$(a-\lambda)\psi_{k1} - b\psi_{k2} = 0 \tag{6.2.27a}$$

$$-b\psi_{k,i-1} + (a-\lambda_k)\psi_{ki} - b\psi_{k,i+1} = 0 \quad \text{for} \quad 1 < i < N \tag{6.2.27b}$$

$$-b\psi_{k,N-1} + (a'-\lambda_k)\psi_{kN} = 0 \tag{6.2.27c}$$

Here $a = 4(J^2+h^2)$, $a' = 4h^2$, and $b = 4Jh$. Eq. (6.2.27b) is a second-order, linear, and homogeneous difference equation with boundary conditions given by eq. (6.2.27a) and (6.2.27c). A general non-zero solution to such system can be written $\psi_{kj} = Cr_{k,+}^j + Dr_{k,-}^j$, where $r_{k,\pm}$ are the solutions to the quadratic equation[25]

$$-b + (a-\lambda_k)r_{k,\pm} - br_{k,\pm}^2 = 0. \tag{6.2.28}$$

For $b \neq 0$, these solution are given explicit as

$$r_{k,\pm} = \frac{a-\lambda_k}{2b} \pm \sqrt{\left(\frac{a-\lambda_k}{2b}\right)^2 - 1} \tag{6.2.29}$$

which are reciprocal to each other since $r_{k,+}r_{k,-} = 1$.

The two solutions are equal

If the two solutions happens to equal, $r_{k,+} = r_{k,-} = r^*$, the form of ψ_{kj} are modified to $\psi_{kj} = (C+jD)r^j$[25]. For this to be true, the square root in eq. (6.2.29) must be zero, which implies $\lambda_k = 4(J \pm h)^2$. Therefore $r_k^* = \mp 1$ and $\psi_{kj} = (C+jD)(-1)^j$. From the boundary conditions, it can be shown that $C = 0$ and that $D \neq 0$ if and only if $h = \pm\frac{N}{N+1}J$. It can therefore be concluded that

$$\psi_{kj} = \mathrm{sgn}(g)^j \frac{\sqrt{6}j}{\sqrt{N(N+1)(2N+1)}} \tag{6.2.30}$$

is an eigenvector of $\mathbf{M}_1$ with eigenvalue $\epsilon^* = \frac{2|J|}{N+1}$ if and only if $|g| = \frac{N}{N+1}$. One therefore defined the critical order parameter $g_c = \frac{N}{N+1}$. For large N, the energy of this state vanishes and becomes a zero in the thermodynamic limit.

The two solution are different

For $r_{k,+} \neq r_{k,-}$, the eigenvectors takes the form[25] of $\psi_{kj} = Cr_{k,+}^j + Dr_{k,-}^j$. Here D/C and λ_k can be determined by the boundary conditions while C acts as a normalization constant. Inserting the general form of $\vec{\psi}_k$ into the first boundary condition, eq. (6.2.27a), one gets

$$0 = C\left[(a-\lambda_k) - br_{k,+}\right] r_{k,+} + D\left[(a-\lambda_k) - br_{k,-}\right] r_{k,-} \tag{6.2.31}$$

Since $(a-\lambda_k) - br_{k,\pm} = br_{k,\mp}$ and $r_{k,+}r_{k,-} = 1$, then eq. (6.2.31) is true if and only if $C = -D$. The value of $r_{k,+}$, and therefore the value of λ_k, can then be determined from the second boundary condition, eq. (6.2.27c). Inserting $\psi_{kj} = C(r_{k,+}^j - r_{k,-}^j)$ into the eq. (6.2.27c), it is possible to shown that the set $\{r_{k,+}, r_{k,-}\}$ are complex roots of a $2(N+1)$-degree polynomial

$$P(z) = g(z^{2(N+1)} - 1) + (1 - z^{2N})z = 0. \tag{6.2.32}$$

$P(z)$ has two trivial roots, namely $z = \pm 1$. For $g \neq g_c$, both of these roots corresponds to the zero vector $\vec{0}$ which is not considered a eigenvector. If $|g| = g_c$, then $z = \mathrm{sgn}(g)$ corresponds to the eigenvector eq. (6.2.30) while $z = -\mathrm{sgn}(g)$ corresponds to the zero vector.[4]. Since $z = \pm 1$ are irrelevant for this discussion, they are divided out of $P(z)$ leaving a N-degree polynomial

$$Q(z) = \frac{P(z)}{z^2-1} = g\sum_{n=0}^{N} z^{2n} - \sum_{n=0}^{N-1} z^{2n+1} = gz^{2N} + (g-z)\sum_{n=0}^{N-1} z^{2n} \tag{6.2.33}$$

which roots are to be found. Evaluating the roots of Q numerically, one get that for supercritical

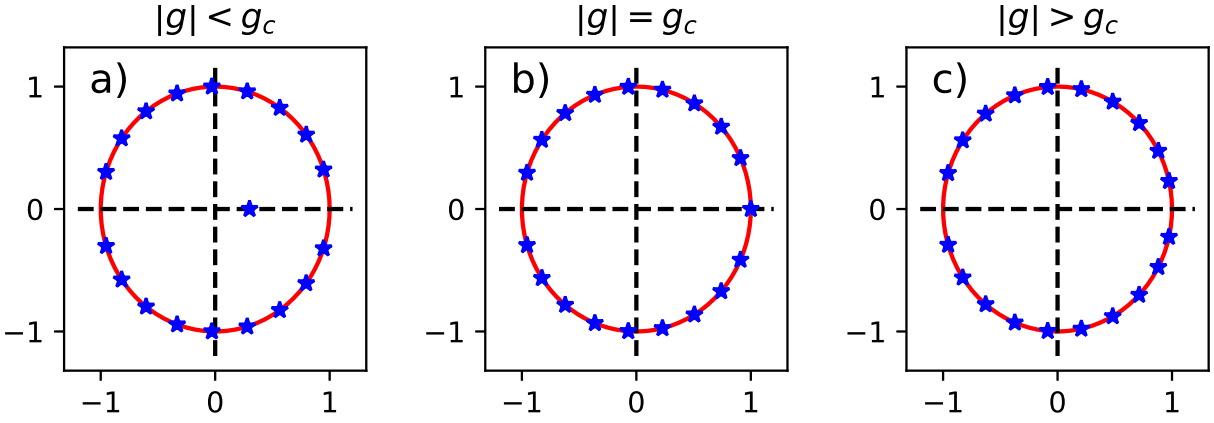

Figure 6.2.2: Roots of the complex polynomial $Q(z)$ for different values of $|g|$. In **a)**, $|g| < \frac{N}{N+1}$, for **b)**, $|g| = \frac{N}{N+1}$ and for **c)** $|g| > \frac{N}{N+1}$. All plot are created for $N = 10$.

fields, $|g| > g_c$, all the complex roots of $Q(z)$ lay on the unit circle in the complex plane, 6.2.2c). For subcritical fields, $|g| < g_c$, $2(N-1)$ of the roots lay on the unit circle while two lay on the real number line, fig. 6.2.2a). These real roots will also be reciprocal since $Q(z) = z^{2N}Q(z^{-1})$. One of being in the interval $[-1, 1]$, while the being outside. For critical fields $|g| = g_c$, the real roots is $z = \pm 1$, fig.

[4]One could also argue that these roots cannot be treated here since $|r_{k,+}| = 1$ which does against the assumption $r_{k,+} \neq r_{k,-}$. Both ways yield the same result: Exclude $z = \pm 1$ from the current discussion!

6.2.2b), which corresponding to eigenvector eq. (6.2.30). This is another example of the difference in the behaviour of the systems in the different regimes.

The roots on the unit circle can all be written in terms of an angles θ_k being the argument of the root. For $r_{k,+} = e^{i\theta_k}$ to be a root of $Q(z)$, then θ_k must satisfy

$$T(\theta_k) = g\sin[(N+1)\theta_k] - \sin(N\theta_k) = 0 \text{ for } \theta_k \in [0, 2\pi]\backslash\{0, \pi\} \tag{6.2.34}$$

The roots of $T(\theta)$ are neither equidistant nor can be expressed analytically for $g \neq 0$. One thing can be said thou. Since $r_{k,+}r_{k,-} = 1$, then $\arg(r_{k,+}) = -\arg(r_{k,-})$, which implies $r_{k,\pm} = r^{\pm i\theta_k}$. The roots on the upper half of the complex unit circle are therefore identified with $r_{k,+}$, while the roots on the lower half are identified with $r_{k,-}$. This is also reflected in $T(\theta)$ since it is an odd function. Therefore if θ_k is a root of T, then $-\theta_k$ is also a root of T. Since the roots cannot be found analytically, they must be evaluated numerically. When done so, any eigenvector $\vec{\psi}_k$ associated with there k'th root of $T(\theta)$, can be expressed as

$$\psi_{kj} = \frac{\sin(j\theta_k)}{\sqrt{\sum_{n=1}^{N}\sin^2(n\theta_k)}} \tag{6.2.35}$$

with corresponding eigenvalues

$$\lambda_k = 4\left(J^2 + h^2 - 2Jh\cos(\theta_k)\right) \tag{6.2.36}$$

Since $\lambda_k > 4J^2(1-|g|)^2$, the spectrum of these states are gapped for $|g| \neq 1$ with gap size $\Delta(g) = 2|J|\big|1-|g|\big|$. For $|g| = 1$ then $\Delta(g) = 0$ but since $\theta_k \in \{0, \pi\}$ are not associated with any eigenvectors, then the spectrum is still gapped. This smaller gap is of order $\mathcal{O}\left(N^{-1}\right)$ which vanishes in the thermodynamic limit. For supercritical fields, $|g| > g_c$, all the roots of $Q(z)$ sits on the complex unit circle, see fig. 6.3.1a).

For $|g| \to g_c$ from above, the energy gap decreases and one of the complex roots move closer to the real number line, fig. 6.3.1b). This results in its corresponding eigenvalue approaching $\epsilon^* = 2|J|/(N+1)$ from above. At the critical point field $|g| = g_c$, the the eigenvector eq. (6.2.30) becomes an eigenvector of $\mathbf{M}_2$ with eigenenergy ϵ^*.

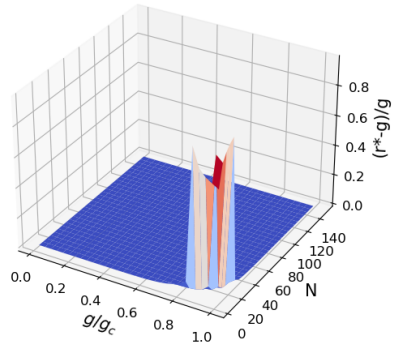

Figure 6.2.3: Real root of $Q(z)$ compared with g for different values of N and g/g_c. Here $N \in \{10, 20, \cdots, 300\}$ and $g/g_c \in [0.1, 1]$.

For subcritical fields, $0 < |g| < g_c$, the polynomial Q will have two real roots, $\tilde{r}$ and $\tilde{r}^{-1}$. The exact value of these roots cannot be found analytically and must therefore be evaluated numerically, if needed[5]. It can be shown that in most cases, these roots are approximately g and g^{-1}, fig. 6.2.3. In the figure, the percentage error of the initial guess g compared to the real root is close to zero. This error becomes large when N is small and $g \approx g_c$. This is because $Q(g) = g^{2N+1} \ll 1$ for $N \gg 1$ and $g < g_c$.

For the large root $\tilde{r}^{-1}$ even thou the functional value at the initial Guess $Q(g^{-1}) = g$ cannot be considered to be small for general $|g| \in]0; g_c[$ it is still close to the real root. This is due to $Q(z)$ having the property that if $\tilde{x} \neq 0$ is a root of Q then $\tilde{x}^{-1}$ is also a root of Q since

$$P\left(\tilde{x}^{-1}\right) = g\left(\tilde{x}^{-2(N+1)} - 1\right) + (\tilde{x}^{-2N} - 1)\tilde{x}^{-1} \tag{6.2.37}$$

$$= -\frac{g\left(\tilde{x}^{2(N+1)} - 1\right) + (\tilde{x}^{2N} - 1)\tilde{x}}{\tilde{x}^{2(N+1)}} \tag{6.2.38}$$

$$= -\frac{P(x)}{\tilde{x}^{2(N+1)}} \tag{6.2.39}$$

[5] You know where to look

Therefore

$$Q(\tilde{r}^{-1}) = \frac{P(\tilde{r}^{-1})}{\tilde{r}^{-2}-1} = \frac{-\tilde{r}^{-2(N+1)}P(\tilde{r})}{\tilde{r}^{-2}-1} = \frac{-\tilde{r}^{-2(N+1)}P(\tilde{r})}{\tilde{r}^{-2}(1-\tilde{r}^{2})} = \frac{Q(\tilde{r})}{\tilde{r}^{2N}} \tag{6.2.40}$$

Since $Q(\tilde{r}) = 0$ then $Q(\tilde{r}^{-1}) = 0$. From this result, the eigenvalue $\tilde{\lambda}$ can be written evaluated

$$\tilde{\lambda} = \sqrt{J^2 + h^2 - Jh\left[\tilde{r} + \tilde{r}^{-1}\right]} = \sqrt{g\delta}\sqrt{1-g^2} + \mathcal{O}\left(\delta^{5/2}\right) \tag{6.2.41}$$

Here $\delta = \tilde{r} - g$ is the difference between the real root of Q and the initial guess g. The corresponding eigenvector will therefore take the form of

$$\psi_{Nn} = \frac{|g|^{-n} - |g|^{n}}{\sqrt{\sum_{m=1}^{N}(g^{-m} - g^{m})^2}} + \mathcal{O}(\delta) \tag{6.2.42}$$

The last vector here is defined in a way so it's elements are positively. For completeness, if $h = 0$, the off-diagonal terms in both $\mathbf{M}_1$ and $\mathbf{M}_2$, and their eigenvectors are the unit vectors $\{\hat{e}_1, \cdots, \hat{e}_N\}$ with eigenvalues $\{0, J\}$. Actually any vector, whose N component is zero, is an eigenvector of $\mathbf{M}_2$. The same is true for $\mathbf{M}_1$ excepts for its first component. There is therefore a some freedom in how the α_{ki} and β_{ki} coefficients can choose. A natural choice of vectors is to pick them so they are consistent with the limits $\lim_{g\to 0}\vec{\phi}_i$ and $\lim_{g\to 0}\vec{\psi}_i$.

Spin-wave basis

Since the limiting behaviour of the function $T(\theta)$ are

$$\lim_{g\to 0^+} T(\theta) = -\sin(N\theta) \tag{6.2.43}$$

then the Bogoliubov angles will approach

$$\theta_k = \frac{\pi k}{N} \quad \text{as} \quad g \to 0 \quad \text{for} \quad k \in \{1, \cdots, N-1\}. \tag{6.2.44}$$

Therefore, the first $N-1$ eigenvectors can be picked so

$$\psi_{kn} = \sqrt{\frac{2}{N}}\sin\left(\frac{\pi k}{N}n\right) \quad \text{with eigenvalues} \quad \epsilon_k = 2J \tag{6.2.45}$$

Here, $\sqrt{\frac{2}{N}}$ is the normalization constant. Note that $\psi_{kN} = 0$ here. $Q(x)$ cannot be used to get the last vector since it's real root is zero. The reciprocal does therefore not exist and eq. (6.2.42) cannot be used. Other methods are therefore needed. Since the $\vec{\phi}_k$ vectors are orthogonal to each other, appendix D.1, then the last eigenvector must be orthogonal to all the others which implies

$$\psi_{Nn} = \delta_{N,n} \quad \text{with eigenvalue} \quad \epsilon_N = 0 \tag{6.2.46}$$

The ϕ vectors

Given the set of eigenvectors $\{\psi_k\}$, the eigenvectors of the matrix $\mathbf{M}_1$ can be evaluated. This is done using the second condition of eq. (6.2.22). If the eigenvalues ϵ_k is non-zero, then one can express $\vec{\phi}_k$ in terms of $\vec{\phi}_k$ via

$$\vec{\phi}_k = \frac{1}{\epsilon_k}(\mathbf{A} - \mathbf{B})\vec{\psi}. \tag{6.2.47}$$

Written explicit, eq. (6.2.47) simplifies to

$$\phi_{kn} = \begin{cases} -\frac{h_n}{\epsilon_k/2}\psi_{kn} & \text{for} \quad n = 1 \\ \frac{J_{n-1}\psi_{kn-1} - h_n\psi_{kn}}{\epsilon_k/2} & \text{for} \quad n \neq 1 \end{cases} \tag{6.2.48}$$

If $\epsilon_k = 0$, this method does not work since eq. 6.2.48 diverges. One therefore has to use other method. Since one a maximum of of vector are an eigenvalue of zero, namely the ϕ_N vector, only one vector does not suit eq. (6.2.48). One can then use that the eigenvectors are orthonormal to each other, appendix D.1, to generate the last vector using Gram-smith orthogonalization[42].

Summary of the results

To summarize, the eigenvectors of the matrices $\mathbf{M}_1$ and $\mathbf{M}_2$ takes the form of

$$\psi_{kn} = \begin{cases} \delta_{N,n} & \text{for} \quad g = 0 \text{ and } k = N \\ \sqrt{\frac{2}{N}}\sin\left(\frac{\pi k}{N}n\right) & \text{for} \quad g = 0 \text{ and } k \neq N \\ \frac{|\tilde{r}|^{-n} - |\tilde{r}|^{n}}{\sqrt{\sum_{n=1}^{N}(\tilde{r}^n - \tilde{r}^{-n})^2}} & \text{for} \quad |g| < g_c \text{ and } k = N \\ \mathrm{sgn}(g)^n \frac{\sqrt{6}n}{\sqrt{N(N+1)(N+2)}} & \text{for} \quad |g| = g_c \text{ and } k = N \\ \frac{\sin(n\theta_k)}{\sqrt{\sum_{i=1}^{N}\sin^2(n\theta_k)}} & \text{else} \end{cases} \tag{6.2.49}$$

and

$$\phi_{kn} = \begin{cases} \frac{-h\psi_{k1}}{\epsilon_k/2} & \text{for} \quad n = 1 \text{ and } \epsilon_k \neq 0 \\ \frac{J_{n-1}\psi_{kn-1} - h_n\psi_{kn}}{\epsilon_k/2} & \text{for} \quad n \neq 1 \text{ and } \epsilon_k \neq 0 \\ \text{Use orthogonalization} & \text{for} \quad \epsilon_k = 0 \end{cases} \tag{6.2.50}$$

with eigenvectors

$$\epsilon_k = \begin{cases} 0 & \text{for} \quad g = 0 \text{ and } k \neq N \\ 2J & \text{for} \quad g = 0 \text{ and } k \neq N \\ 2\sqrt{J^2 + h^2 - Jh[\tilde{r} + \tilde{r}^{-1}]} & \text{for} \quad |g| < g_c \text{ and } k = N \\ \frac{2|J|}{N+1} & \text{for} \quad |g| = g_c \text{ and } k = N \\ 2\sqrt{J^2 + h^2 - 2Jh\cos\theta_k} & \text{for} \quad |g| > g_c \end{cases} \tag{6.2.51}$$

As a conclusion to this section it is worth mentioning that the orthogonal properties of the vectors $\{\phi_k\}$ and $\{\psi_k\}$ can be used to prove that the inverse Bogoliubov transformation are given by

$$c_i^\dagger = \sum_k \alpha_{ki}\eta_k^\dagger + \beta_{ki}\eta_k \quad \text{and} \quad c_i = \sum_k \alpha_{ki}\eta_k + \beta_{ki}\eta_k^\dagger \tag{6.2.52}$$

This is shown in appendix D.2.

6.3 Energy bands

Sign of ϵ_k

Since the energies ϵ_k are calculated from a square root of the eigenvalues of $\mathbf{M}_1$ and $\mathbf{M}_2$, the question of which sign to choose comes up naturally. It can be shown that the sign of ϵ_k does not matter since the transformation $\epsilon_k \to -\epsilon_k$ leaves the Hamiltonian invariant. This is because a sign change of ϵ_k

results in a sign change of ϕ_{ki} which leads to α_{ki} becoming β_{ki} and β_{ki} becoming α_{ki}. Therefore, due to eq. (6.2.52), the creation and annihilation operator changing places. In summary

$$\epsilon_k \to -\epsilon_k \Rightarrow \phi_{ki} \to -\phi_{ki} \Rightarrow \alpha_{ki} \leftrightarrow \beta_{ki} \Rightarrow \eta_k^\dagger \leftrightarrow \eta_k \tag{6.3.1}$$

The Hamiltonian therefore undergoes the transformation

$$\mathcal{H} \to \sum_k -\epsilon_k \left(\eta_k \eta_k^\dagger - \frac{1}{2}\right) = \sum_k -\epsilon_k \left(1 - \eta_k^\dagger \eta_k - \frac{1}{2}\right) = \sum_k \epsilon_k \left(\eta_k^\dagger \eta_k - \frac{1}{2}\right) = \mathcal{H} \tag{6.3.2}$$

One can therefore pick the sign of ϵ_k to always be positive so that the vacuum state $|\emptyset_\eta\rangle$, satisfying

$$\forall k \in \{1, \cdots, N\} \ \eta_k |\emptyset_\eta\rangle = 0, \tag{6.3.3}$$

is a ground state of the Hamiltonian. Excited states can then be created by using creation operators $\eta_k^\dagger$ on the vacuum state, thereby building a tower

$$|k_1, \cdots, k_n\rangle = \eta_{k_1}^\dagger \cdots \eta_{k_n}^\dagger |\emptyset_\eta\rangle \tag{6.3.4}$$

with the highest excited state being $\eta_{k_N}^\dagger \cdots \eta_{k_1}^\dagger |\emptyset_\eta\rangle$.

Limiting behaviour

As a sanity check, the limiting behaviour of the eigenvectors $\vec{\psi}_k$ and $\vec{\phi}_k$ can be checked. For small fields

To first order in g with first order energy being $E_{\text{GS}} = -(N-1)|J|$. Since

$$\epsilon_k = \pm 2|J|\sqrt{1 + g^2 - 2g\cos(\theta_k)} \approx \pm 2|J| + \mathcal{O}\left(g^2\right) \tag{6.3.5}$$

then

$$E_{\text{GS}} = -\frac{1}{2}\sum_{k=2}^{N} \epsilon_k = -|J|(\#_+ - \#_-) \tag{6.3.6}$$

with $\#_\pm$ being the number of positive and negative signs respectively. This can only be true if all energies ϵ_k are positive. The same can be said for the opposite limit, $g \gg g_c$, where the ground state are the

$$|GS\rangle = \begin{cases} \bigotimes_{i=1}^N |\downarrow_x\rangle & \text{for} \quad h > 0 \\ \bigotimes_{i=1}^N |\uparrow_x\rangle & \text{for} \quad h < 0 \end{cases} \tag{6.3.7}$$

The energy of this state is, to first order in g^{-1} equal to $-N|h|$. Expanding ϵ_k to first order in g^{-1}, one gets

$$\epsilon_k = \pm 2|h| + \mathcal{O}\left(g^{-2}\right) \tag{6.3.8}$$

Again, the ground state energy is therefore given by

$$E_{\text{GS}} = -\frac{1}{2}\sum_{k=1}^{N} \epsilon_k = -|h|(\#_+ - \#_-) \tag{6.3.9}$$

Again, this can only be satisfied if and only if all the sign are positive. The energy cost of exciting the k'th Bogoliubov fermion are therefore $\epsilon_k/2 \geq 0$ and the energy gain for creating a k hole is $-\epsilon_k/2 \leq 0$. The particle/hole spectrum of the Bogoliubov fermion can therefore be plotting in terms of their angle in the complex plane θ_k. This is done in fig. 6.3.1. Here the gap is clearly visible and the present of

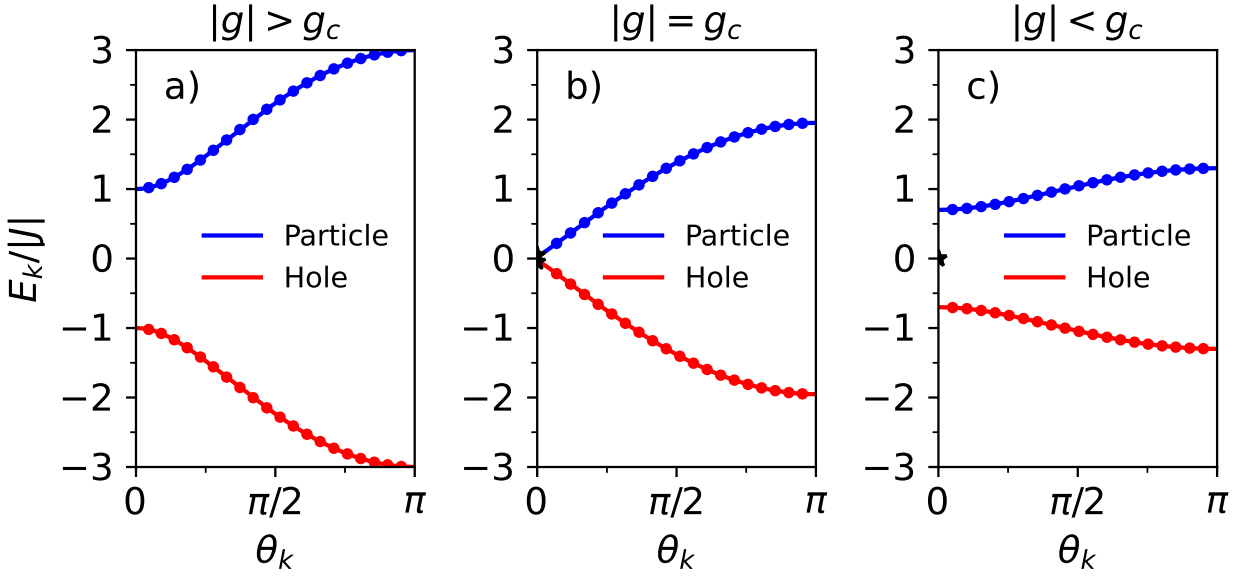

Figure 6.3.1: Spectrum of the system for different values of g for particles and holes. **a)** For $|g| > g_c$, the spectrum is gapped with $\Delta(g) = \big|1-|g|\big|$ and approximates the function $E(k) = \pm\sqrt{J^2+h^2-2Jh\cos\theta}$. The gap gets small for $g \to g_c$.**b)** At critical field $|g| = g_c$ a zero mode appears at $\theta = 0$ in the thermodynamic limit. **c)** For $|g| < g_c$, the gap Δ widens but the spectrum still have a zero mode. Plots are generated for $N = 20$, exchange coupling $J = 1$ and fields $h = 0.3$, $h = \frac{20}{21}$, and $h = 1.3$.

low-energy mode As observed in fig. 6.3.1b) and c), the energy required to create the $k = N$ fermion is very small compared to the rest of the spectrum. This is due to the Z_2 symmetry present in the low field regime. The $k = N$ Bogoliubov fermion can therefore be excited with a small energy cost for sub-critical field, implying an (almost) two-fold degeneracy for all energy levels. This symmetry breaks when the field h becomes dominating. The low-energy state will, at $g = g_c$ begin increasing in energy and the energy gap widens. The Hamiltonian can be seen as a system of free fermions with momentum k and dispersion relation $E_\pm(k)$. The vacuum state, $|\mathbf{0}_B\rangle$ where no quasi-particles are present, must therefore satisfy $\forall k \in \mathbb{I}\ \eta_k|\mathbf{0}_B\rangle = 0$ and have energy

$$E_0 = -\frac{1}{2}\sum_{k=1}^{N} E(k) \tag{6.3.10}$$

The higher excited states of the TFQIM can then be reached by acting on the vacuum state with one or more creation operators $\eta_k^\dagger$. The excited states can be labelled by the vector $\mathbf{k} \in \{0,1\}^N$ which is defined as

$$|\mathbf{k}\rangle = \left(\prod_{k\in I_\mathbf{k}} \eta_k^\dagger\right)|\mathbf{0}_B\rangle \tag{6.3.11}$$

where $\mathcal{N}_\mathbf{k} = \{k \in \mathcal{N} | \mathbf{k}_k = 1\}$ is the set of indices k such that the k's element of $\mathbf{k}$ is 1. Note that the product is ordered such that the operators $\eta_k^\dagger$ with smallest k is furthest to the right. Inverting relation (6.2.18), one can express the fermion creation/annihilation operators in terms of $\eta_k/\eta_k^\dagger$

$$c_i^\dagger = \sum_k \alpha_{ki}\eta_k^\dagger + \beta_{ki}\eta_k \quad \text{and} \quad c_i = \sum_k \alpha_{ki}\eta_k + \beta_{ki}\eta_k^\dagger \tag{6.3.12}$$

which is proven in appendix D.2. For $|g| \geq \frac{N}{N+1}$, the ground state is non-degenerate, while for $|g| < \frac{N}{N+1}$, the ground state is degenerate and the ground state manifold is $\left\{|\mathbf{0}_B\rangle, \eta_1^\dagger|\mathbf{0}_B\rangle\right\}$. In the limits of $h \gg J$, the energy levels approximates $E_\pm(k) = \pm h$, which implies a ground state energy of $E_0 = -hN$. This is expected since all spins point in the same direction in opposite direction of the field h. If the energy $h \ll J$, the single particle spectrum is reduced to $E_\pm(k) = \pm(1 - \delta_{kk'})J$, which implies ground state energy $E_0 = -(N-1)J$ which is in agreement with the ground state energies of $J\sum_{n=1}^{N-1}\sigma_i^x\sigma_{i+1}^x$.

Chapter 7

Summary and outlook

7.1 Summary of results

In chapter 1 it was shown that a (2,N) - quantum dot cellular automaton can be mapped to an open boundary condition, anti ferromagnetic, quantum Ising model in a magnetic field. If the Coulomb interaction between electrons can be considered to rapidly decay, only nearest neighbour spins will interact, and the QDCA will map to a nearest neighbour quantum Ising model, which has Hamiltonian

$$\mathcal{H} = \sum_{i=1}^{N-1} J_i \sigma_i^z \sigma_{i+1}^z + \sum_{i=1}^{N} h_i^z \sigma_i^z + h_i^x \sigma_i^x \tag{7.1.1}$$

In chapter 2, it is assumed that the quantum dynamics of the system can be ignored and the quantum Ising model reduces to the classical Ising model. Each spin can therefore only be in either a spin up state or a spin down state, which makes transverse field in the Hamiltonian vanish. It does so because it will always be perpendicular to the spin projections. The classical Ising model is then analysed for both ferromagnetic and anti ferromagnetic couplings. Here, the system was coupled to a heat bath of temperature T. The equilibrium properties could then be calculated, which predicted that the system would follow the phase diagram in figure 2.2.3. For AFM coupling, the equilibrium calculations predicted that the system should decay into a zero-field AFM ground state configuration for $T \ll |h| < 2J$. Depending on the number of sites in the system, the system has a 50/50 chance of going into either zero-field ground state configurations, or will pick the same one every time.

Since the calculations performed in chapter 2 does not describe how any given initial configuration acts, the theory non-equilibrium classical Ising model dynamics is described was chapter 3. Here the Kinetic Ising model was introduced which is simply a classical Ising model coupled to one or more heat baths. This was done through the master equation where detailed balance was assumed. Throughout the chapter, Glauber dynamics was the only type of dynamics to be considered in calculations. The dynamics works by flipping single spins in the Ising model, and occurs at time scales depending on the energy difference they would cause if applied to the system.

From explicit calculation of the magnetization vector $\mathbf{m}$, whose elements are the statistical average of the spins projections, it was shown that for $T = 0$

$$\mathbf{m}(t) \to \begin{cases} C_{\text{AFM}} \left(-1, 1, -1, 1 \cdots\right)^T & \text{for} \quad J > 0 \\ C_{\text{FM}} \left(1, \cdots, 1\right)^T & \text{for} \quad J > 0 \end{cases} \quad \text{for} \quad t \to \infty \tag{7.1.2}$$

where C_{AFM} and C_{FM} are constant that depends on the initial configuration of the system. The exact meaning of these constant was not clear from the theory presented in chapter 3. The best guess was that the system picks a random ground states which is decays into. This was bases on the fact that the sign m_i alternated with i for $J > 0$ while the sign does not change with i for $J < 0$. This is also what was predicted in chapter 2. From chapter 3, it was also shown that the decay could be controlled by

a single local field at the first site. For local field strength $|h| < 2J$, then for $T = 0$, nothing changes compared to $h = 0$. On the other hand, if $|h| > 2|J|$, the system decays into a zero-field FM ground state, which first site is opposite to the field.

In chapter 5, the non-equilibrium dynamics of the KIM was simulated for $T = 0$. This is done using the Gillespie algorithm, which was described in chapter 4. Here it was shown that for AFM couplings and zero field, the system indeed did decay into a zero-field AFM ground state. For a given initial configuration is was shown that the time it takes for the system to decay into its final state is distributed via the probability density function

$$\mathcal{P}(t;\lambda) = \lambda e^{-t\lambda}. \tag{7.1.3}$$

The decay rate λ is in general not dependent on the initial state, but depends on the size of system. It does so via a power law

$$\lambda(N) = aN^{Exp} \quad \text{with} \quad \begin{cases} Exp & = 2.05188 \pm 0.00006 \\ a & = (0.27881 \pm 0.00016)\tau \end{cases} \tag{7.1.4}$$

with τ being the time scale of Glauber rates.

When turning a longitudinal field on, then for small field $0 < |h| < J$, it was shown in chapter 5 that the system decays into a disordered state with domain walls in the bulk. The same was shown to be true for $J \leq |h| < 2J$ with the exception that for $|h| = J$, the edge spin of the final state will sometimes have the ability to flip without any energy cost. If this is the case, the edge spin(s) will flip with a rate of $0.5\tau^{-1}$. If the field has a magnitude similar to $2J$, then is was shown that domain walls can be created spontaneously in the bulk. This result in a long-term behaviour of the KIM where domain walls are created and annihilated constantly and the system never settles into a ground state. If the first is increased further, so $|h| > 2J$, the system was shown to decay into a zero-field FM ground state.

7.2 Outlook

The tone of this section might be a bit different in the section since it describes ways of improving the code and what I, personally, thing would be interesting to use this thesis for. It is maybe not a precise and scientific as the rest of the thesis, but is more like a discussion of what to do next. This section can be skipped if you don't care about the code.

7.2.1 The code

The code performs quit well in general. It is fast, has a somewhat easy way to aces to its attributes, and creates plot fine. Except for the $\delta \neq 0$ bug, the code seems to simulate the KIM with Glauber rates correctly. There are a few thing that can be improve thou:

Inclusion of Kawasaki dynamics In its current for, the Gillespie_cy object cannot simulate Kawasaki dynamics. This is a problem because it does not give the fully picture of the dynamics of KIM. As its current form, I cannot simply stitch Kawasaki dynamics onto the current object. To include it, I would need to rework the algorithm from scratch. It shouldn't be that hard to do, but it takes time, which I didn't have under my thesis.

The of pre-calculated lookup tables code When performing the Gillespie algorithm, the spin-flip rates are recalculated each iterations. This is excepted since the rates depends on the configurations and therefore should change when the configuration is updated, but is not the

most efficient way. The code can be improved by using a pre-calculated lookup table instead. Since the Gillespie rates only really depends on three spins each, since

$$\omega_i(\{\sigma\}) = \tilde{\omega}(i, \sigma_{i-1}, \sigma_i, \sigma_{i+1}) = \tau^{-1} n_F \left(-2\sigma_i \frac{J_{i-1}\sigma_{i-1} + J_i\sigma_{i+1} + h_i}{T} \right) (1 - \delta\sigma_{i+1}\sigma_{i-1}), \quad (7.2.1)$$

there are in reality only eight different values the i'th rate can evaluate to. One can therefore create a $N \times 2 \times 2 \times 2$ lookup table which stored these values. When the Glauber rates are needed, one simply lookup in the table and fetches the values needed. The code therefore only has to calculate the lookup table once, which saves a lot of function calls. this should speed up the code dramatically since, at maximum, the Fermi function n_F is called $8N$ times for Glauber rates only. This mean that the Gillespie algorithm only needs to run eight iterations to match the number of times it calls the Fermi function. Since a typical simulation is ran around a few hundred times pr. simulation, and I usually reuse the same instance to thousand simulations, the typical number of n_F calls are at minimum a few hundred thousands times N. Much more than $8N$.

The need of a good __getattr__ method In the current code, it the user needs to know the value of a given attribute, the need to use the get_attribute_py method, which converts ALL the attributes to a Python equivalent and returns ALL the attributes to the user as a dictionary. This is incredible inefficient if the user only needs to know a the value of a single attribute. This method is especially unnecessary since a special function, called __getattr__ already exists for Python objects. Designing the __getattr__ method to work properly can save a lot of time, if done correctly, especially if combined with some of the suggestion below.

Messy code The code is very messy. There are several reasons why

Unnessecary cythonization In the get_J_att, get_h_att, and get_initial_att methods, a lot of lines of code are put into generating the J, h, and initial_state attributes. Much of the code here is actually pure python, or could be ran faster using functions from the numpy module. The code could therefore be written simpler, faster, and shorter if converted to pure Python. At the same time, many of the rules for generating J and h are equivalent. One could therefore use the get_h_att method to generate self.J with periodic boundary condition, which then can be taken care of in get_J_att. This avoids the need of repeating code, which also makes the code easier to debug and patch later.

Too many inputs The Gillespie object has a lot of inputs due to many parameters needed to describe the KIM with Glauber rates. This number will only increase if Kawasaki dynamics is to be added later. One solution to the large amount of input could be fixed with the use of python dictionaries and **kwargs input. I will not go into more details about it here, but this solution could decrease the number of mandatory input without reducing the control of the user.

Too many attributes The same problem is present for the number of attributes of Gillespie_cy. This could also be reduced by using dictionaries which can decrease the number of attributes without restricting the behaviour of the simulations.

Too many brances Some of the if/else statements have way too many braces, especially in the get_J_att, get_h_att, and get_initial_att methods. These can be reduces greatly without changing the code very much, reducing the number of braces and making the code more structured.

Comments about comments In its current form of the code, a lot of redundant comment are present, which makes the code unnecessarily crowded. Commenting you code is always good so that people, and even yourself at a later point, can read and understand your code. But

it can be too much. There are a lot of examples in the code where I comment lines which are self explanatory if one know Pythons syntax.

All these problem can only be explain by one factor, being a my lack of experience with and knowledge of the Python and Cython languages. A basically began this project with almost zero knowledge of of the two and have taught myself on the fly. The code described in this thesis isn't even my first draft. The first version was so horribly slow than a single simulation could take seconds!. Now it takes around 0.1 ms. With more experience, I hope to improve the code in the future to make the code even better!

Chapter 8

Conclusion

By analysing the interactions between electrons in the quantum dots of the (2,N) - quantum-dot cellular automaton, it can be concluded that when prepared correctly, it can be mapped to the quantum Ising model. Ignoring the quantum dynamics of this model, the system is described as a classical Ising model.

From equilibrium calculations, it is concluded that the classical Ising model does not have any phase transitions for positive temperatures. For anti ferromagnetic couplings and small temperatures, the classical Isng model will have a small overall magnetization for longitudinal field strengths smaller than twice the nearest neighbour coupling. If does so because it localized around either both zero-field AFM ground state configurations or only one of them. This depends on if the number of sites in the system are odd or even. If the field is increase further than that, the system magnetizes opposite to the field. It does so by localizing around one of the zero-field FM ground state configuration.

The non-equilibrium dynamics of the classical Ising model are described using the Gillespie algorithm. The rates uses here, are the rates of the Master equation, which are evaluated using detailed balance. From simulations of the KIM's dynamics for anti ferromagnetic coupling constants and zero temperature, using a program written in Cython, it is concluded that for zero field, any initial configuration decays into a randomly chosen zero-field AFM ground state.

From running multiple simulations of many different initial configurations, it is concluded that the average time does not depend on the initial configuration. It can also be concluded that the the average time depends on the size of the system via a power law with an exponent of 2.05188 ± 0.00006.

In the analysis of the Quantum Ising model, it can be concluded that there exists a zero mode when the transverse field is smaller than the nearest neighbour coupling constant. If the field in increased past the value, the zero mode vanishes.

Appendix A

Classical Appendix

In this appendix, some of the mathematical theorem used in chapter 2 is proven.

A.1 A composition of two infinite differentiable functions is also infinite differentiable

In the main text, at the ending of section 2.2, it is claimed that any composition of two infinite differentiable functions is also infinite differentiable. This is not completely true to the authors knowledge, but it is good enough for the calculations in the main text. To see the limitations of this claim, one attempts to prove it and see where it goes wrong. To prove the claim, it is first necessary to exactly define what an infinitely differentiable function is.

Definition of k differentiable: A real function $f : \Omega \to \mathbb{R}$ that maps an open subset $\Omega \subseteq \mathbb{R}^d$ to the real numbers, the f is k differentiable if and only if

$$\forall k \in \mathbb{N} \quad \forall i \in \{1, \cdots, d\}^k \qquad \frac{\partial^k f}{\partial x_{i_1} \cdots \partial x_{i_N}} \quad \text{exists and is continuous on } \Omega \tag{A.1.1}$$

The class of all k differentiable functions on Ω are denoted $C^k(\Omega)$[26]. For f to be infinite differentiable on Ω, the for all $k \in \mathbb{N}$, then $f \in C^k(\Omega)$. The class of infinite differentiable functions on Ω are denoted $C^\infty(\Omega)$.

Before proving the statement, one must first consider a few lemma's.

Product lemma: Let $f, g \in C^\infty(\Omega)$ be infinite differentiable functions on an open interval $\Omega \subset \mathbb{R}^d$, then if $h = f \cdot g$ is the product of the two function, then $h \in C^\infty(\Omega)$.

Proof of product lemma: This statement is proven by induction. For $k = 1$, then

$$\forall i \in \{1, \cdots, d\} \frac{\partial h}{\partial x_i} = \frac{\partial f}{\partial x_i} g + f \frac{\partial g}{\partial x_i} \tag{A.1.2}$$

Since $f, g \in C^1(\Omega)$, then f, g, $\partial_i f$ and $\partial_i g$ are all continuous. Therefore both $(\partial_i f)g$ and $f(\partial_i g)$ are continuous, which makes $\partial_i h$ continuous as well. The lemma is therefore true for $k = 1$.

Defining the higher order partial differential coefficient $D^{(k)}_{\mathbf{i}}$ as

$$D^{(k)}_{\mathbf{i}} = \frac{\partial^{(k)}}{\partial x_{i_1} \cdots \partial x_{i_k}} \tag{A.1.3}$$

where $\mathbf{i} \in \{1, \cdots, d\}^k$, then for all $\mathbf{i} \in \{1, \cdots, d\}^{k+1}, \mathbf{j} \in \{1, \cdots, d\}^{k+1}, \ell \in \{1, \cdots, d\}$

$$D_{\mathbf{i}}^{(k+1)} h = D_{\mathbf{j}}^{(k)} \frac{\partial}{\partial x_\ell} h = D_{\mathbf{j}}^{(k)} \left[(\partial_{x_\ell} f)\, g + g\, (\partial_{x_\ell} f) \right] = D_{\mathbf{j}}^{(k)} \left[(\partial_{x_\ell} f)\, g \right] + D_{\mathbf{j}}^{(k)} \left[g\, (\partial_{x_\ell} f) \right]. \tag{A.1.4}$$

Since $f, g \in C^\infty(\Omega)$, then f, g, $\partial_{x_\ell} f$, and $\partial_{x_\ell} g$ are all infinite differentiable functions. Assuming the lemma to be true for k, then

$$D_{\mathbf{j}}^{(k)} \left[(\partial_{x_\ell} f)\, g \right] \text{ and } D_{\mathbf{j}}^{(k)} \left[(\partial_{x_\ell} f)\, g \right] \text{ both exists and are continuous on } \Omega. \tag{A.1.5}$$

This implies $D_{\mathbf{i}}^{(k+1)} h$ exists and is continuous, which proves the lemma. □

Theorem of composition: Let $g : \Omega \to I$ be an infinite differentiable function on $\Omega \subset \mathbb{R}$ with $I \subset \mathbb{R}$, and let f be an infinite differentiable function that can be expanded around every point in I using a Taylor expansion with a non-zero radius of convergence R, then $h = f \circ g \in C^\infty(\Omega)$.

Proof: Since g is continuous then

$$\forall \mathbf{a} \in \Omega\ \exists \delta > 0\ \forall \mathbf{v} \in \Omega\ |\mathbf{v} - \mathbf{a}| < \delta \Rightarrow |g(\mathbf{v}) - g(\mathbf{a})| < R \tag{A.1.6}$$

This implies that

$$h(\mathbf{v}) = h(\mathbf{a}) + \sum_{n=1}^{\infty} \frac{1}{n!} f^{(n)} \left(g(\mathbf{a}) \right) \left(g(\mathbf{v}) - g(\mathbf{a}) \right)^n \tag{A.1.7}$$

is true and converges correctly. Because $g \in C^\infty(\Omega)$ then from the product lemma, $(g(\mathbf{v}) - g(\mathbf{a}))^n \in C^\infty(\Omega)$ which implies $h \in C^\infty(\Omega)$. □.

Compared to the main text, an extra requirement of the real function having a non-zero radius of convergence was needed. This is no problem for the main text since $\cosh x$, $\sinh x$ e^x infinite radius of converges for all $x \in \mathbb{R}$, while $\ln x$ and $\sqrt{x}$ have a non-zero radius of convergence for $x \in \mathbb{R}_+$. a

A.2 Proof fo entropy theorem

Given is a statistical ensemble of a system. If x denotes a possible configuration of the system, then $p(x)$ denotes the probability of the system being in x. A system is then said to localize in a given state y if the probability p has the limiting behaviour:

$$p(x) \to \begin{cases} 1 & \text{if} \quad x = y \\ 0 & \text{if} \quad x \neq y \end{cases} \tag{A.2.1}$$

for some limit. The theorem, which is to be proven here, then states that the entropy

$$S = -\sum_x p(x) \ln p(x). \tag{A.2.2}$$

approaches zero if and only if the system localized. Said differently

$$\textit{Localization} \Leftrightarrow S = 0 \tag{A.2.3}$$

The prove goes as follows.

Proof To prove the theorem, one first proves that $\textit{Localization} \Rightarrow S = 0$ and then prove that $S = 0 \Rightarrow \textit{Localization}$.

First implication The first implication is simple to prove. Since $x \ln x \to 0^-$ for $x \to 0^+$, then the part of the entropy S corresponding to configurations $x \neq y$ will vanish. The only term left of the entropy are therefore

$$S = -p(y) \ln p(y), \tag{A.2.4}$$

which also vanishes since $\ln 1 = 0$. One therefore concludes that $Localization \Rightarrow S = 0$. □

Second implication The second implication can be proved by contradiction. Assuming that the system does not localized, then there most exist at least two configuration must have non-vanishing probabilities. Labelling one of these configurations as y, then one can define

$$p(y) = 1 - \sum_{x \neq y} p(x) > 0 \tag{A.2.5}$$

Since $p \ln p > 0$ for $p \in]0; 1[$, then the entropy takes the form of

$$S = -\sum_x p(x) \ln p(x) = -\sum_{x \neq y} p(x) \ln p(x) - \left(1 - \sum_{x \neq y} p(x)\right) \ln \left(1 - \sum_{x \neq y} p(x)\right) > 0 \tag{A.2.6}$$

A non-localized ensemble with therefore have a non-zero entropy which is equivalent to $S = 0 \Rightarrow Localization$. □
To conclude the proof, since $Localization \Rightarrow S = 0$ and $S = 0 \Rightarrow Localization$, then the bi implication is true. □

Appendix B

Kinetic Ising model appendix

B.1 Derivation of master equation from first principles

Given a state space $\mathcal{S}$, being the set of all possible states that a given system can be in, then one can define the predicate $s(t)$ to be

$$s(t) = \begin{cases} \text{True} & \text{if the system is in state } s \in \mathcal{S} \text{ at time } t \in \mathbb{R} \\ \text{Flase} & \text{else} \end{cases}. \tag{B.1.1}$$

The probability of the predicate $s(t)$ being true, given the a priori knowledge I can then be written as $P(s(t)|I)$. Given the knowledge of the probability distribution at a given time $t \in \mathbb{R}$, it is possible to determine the probability distribution at a later time $t + \Delta t$ for $\Delta t > 0$. To do this, one write the following tautology

$$\text{True} = \bigvee_{s \in S} s(t) \tag{B.1.2}$$

since the system must be on of the states in $\mathcal{S}$ at any given time $t \in \mathbb{R}$. One can therefore write that

$$s(t + \Delta t) = s(t + \Delta) \wedge \left(\bigvee_{s' \in S} s'(t) \right) = \bigvee_{s' \in S} \big(s(t + \Delta t) \wedge s'(t) \big) \tag{B.1.3}$$

In the last equality, the distributive property of AND and OR operations are used. Using this, the probability distribution at time $t + \Delta t$ can be expanded as

$$P(s(t + \Delta)|I) = P\left(\bigvee_{s \in S} \left(s(t + \Delta t) \wedge s(t) \right) \middle| I \right) = \sum_{s' \in S} P(s(t + \Delta t) \wedge s'(t)|I) \tag{B.1.4}$$

Here, the addition rule of probabilities are used together with the fact that $s(t) \wedge s'(t)$ is false for $s \neq s'$. For each term in eq. (B.1.4), the probability that $s(t + \Delta t)$ and $s(t)$ is true simultaneously can be expended using the multiplication rule of probabilities. The result in

$$P\left(s(t + \Delta) \wedge s'(t)|I \right) = P(s' \to s|\Delta t, I) P(s'(t)|I), \tag{B.1.5}$$

where $P(s' \to s|\Delta t, I)$ is the probability that the system transitions into a state s' within a time interval Δt given that $s(t)$ is true. It is assumed here, the the probability $P(s' \to s|\Delta t, I)$ is not explicit time depended, but only depends on the length of the time interval Δt. This bring that probability of $s(t + \Delta t)$ to be true on the form

$$P(s(t + \Delta t)|I) = \sum_{s' \in S} P(s' \to s|\Delta t, I) P(s'(t)|I). \tag{B.1.6}$$

Now, one of these terms can be expanded further. Because of probability conservation, the probability of the system not transitioning in the time interval Δt must equal

$$P(s \to s|I, \Delta t) = 1 - \sum_{s' \in S\setminus\{s\}} P(s \to s'|I, \Delta t) \tag{B.1.7}$$

This is because that if the system not that say in state s, it must have transitioned to another state $s' \neq s$. One can therefore write

$$P(s(t+\Delta t)|I) = \sum_{s' \in S\setminus\{s\}} P(s' \to s|\Delta t, I)P(s'(t)|I) + \left(1 - \sum_{s' \in S\setminus\{s\}} P(s \to s'|I, \Delta t)\right) P(s(t)|I) \tag{B.1.8}$$

$$= P(s(t)|I) + \sum_{s' \in S\setminus\{s\}} \left[P(s' \to s|\Delta t, I)P(s'(t)|I) - P(s \to s'|\Delta t, I)P(s(t)|I)\right] \tag{B.1.9}$$

The last step before making time continuous is to expand the $P(s' \to s|\Delta t, I)$ probabilities. Assuming Δt is so small that the system only has time to interact with one heat bath, then the process $s \to s'$ must be due to interaction with one and only one of the heat baths. One can therefore write

$$P(s' \to s|\Delta t, I) = \sum_{\alpha=1}^{M} P_\alpha(s' \to s|I, \Delta t), \tag{B.1.10}$$

with $P_\alpha(s' \to s|I, \Delta t)$ being the probability that the system transitioned from s' to s in the time interval Δt via interaction with the α'th heat bath. The discrete time master equation can then be written as

$$P(s(t+\Delta t)|I) - P(s(t)|I) = \sum_{\alpha=1}^{M} \sum_{s' \in S\setminus\{s\}} \left[P(s' \to s|\Delta t, I)P(s'(t)|I) - P(s \to s'|\Delta t, I)P(s(t)|I)\right] \tag{B.1.11}$$

In the limit of small time intervals $\Delta t \to 0^+$, one can define time derivative $\dot{P}(s|I, t)$ and decay rates $\omega_\alpha(s \to s'|I)$ as

$$\dot{P}(s|I, t) = \lim_{\Delta t \to 0^+} \frac{P(s(t+\Delta t)|I) - P(s(t)|I)}{\Delta} \quad \text{and} \quad \omega_\alpha(s \to s'|I) = \lim_{\Delta t \to 0^+} \frac{\omega_\alpha(s \to s'|I)}{\Delta t} \tag{B.1.12}$$

The limit yields the Master equation

$$\dot{P}(s|I, t) = \sum_{\alpha=1}^{M} \sum_{s' \in S\setminus\{s\}} \left[\omega_\alpha(s' \to s|\Delta t, I)P(s'(t)|I) - \omega_\alpha(s \to s'|\Delta t, I)P(s(t)|I)\right] \tag{B.1.13}$$

B.2 Calculation of limiting behaviour

To calculate the limiting behaviour of the classical Ising model in a local field $h_i = h\delta_{i,1}$ with critical value, it is necessary to calculate the vector

$$\lim_{t \to \infty} \mathbf{m}(t) = \mathcal{A}^{-1}\mathbf{g} \tag{B.2.1}$$

Here $\mathcal{A}^{-1}$ is the inverse of the time derivative matrix

$$\mathcal{A} = \begin{pmatrix} 1 & \frac{1}{2} & 0 & 0 & 0 & 0 \\ \frac{1}{2} & 1 & \frac{1}{2} & 0 & 0 & 0 \\ 0 & \frac{1}{2} & 1 & \frac{1}{2} & 0 & 0 \\ 0 & 0 & \frac{1}{2} & 1 & \frac{1}{2} & 0 \\ 0 & 0 & 0 & \frac{1}{2} & 1 & \frac{1}{2} \\ 0 & 0 & 0 & 0 & 1 & 1 \end{pmatrix} \tag{B.2.2}$$

and $(\mathbf{g})_i = -\delta_{1,i}/2$. Since $\mathbf{g}$ only has one non-zero element, namely the first elements, only the $(\mathcal{A}^{-1})_{n1}$ elements are needed. One can calculate these elements using the following property of any general, invertible matrix

$$\mathcal{A}^{-1} = \frac{1}{\det \mathcal{A}} \mathrm{adj}(\mathcal{A}) \tag{B.2.3}$$

with $\mathrm{adj}(\mathcal{A})$ being the adjoint of $\mathcal{A}$. This theorem is described in theorem 7.13 of Robert Messer's Linear Algebra[42]. The adjoint of $\mathcal{A}$ is defines as the matrix with elements

$$(\mathrm{adj}(\mathcal{A}))_{ij} = (-1)^{i+j} \det \mathcal{A}_{(j,i)} \tag{B.2.4}$$

where $\mathcal{A}_{(j,i)}$ is the sub-matrix of $\mathcal{A}$ where the j'th row and the i'th column has been removed. Writing some of these sub-matrices out explicit

$$\mathcal{A}_{(1,1)} = \mathcal{A}^{(N-1)}, \qquad \mathcal{A}_{(1,2)} = \begin{pmatrix} \frac{1}{2} & * \\ \mathbf{0}_{1N} & \mathcal{A}^{N-2} \end{pmatrix} \qquad \mathcal{A}_{(1,3)} = \begin{pmatrix} \frac{1}{2} & 1 & * \\ 0 & \frac{1}{2} & \\ \mathbf{0}_{2N} & & \mathcal{A}^{(N-3)} \end{pmatrix} \tag{B.2.5}$$

$$\mathcal{A}_{(1,N-1)} = \begin{pmatrix} \frac{1}{2} & 1 & \frac{1}{2} & 0 & \cdots & 0 & 0 \\ 0 & \ddots & \ddots & \ddots & \ddots & \vdots & \vdots \\ \vdots & \ddots & \ddots & \ddots & \ddots & 0 & \vdots \\ \vdots & & \ddots & \ddots & 1 & \frac{1}{2} & \vdots \\ \vdots & & & \ddots & \frac{1}{2} & 1 & 0 \\ 0 & \cdots & \cdots & \cdots & 0 & \frac{1}{2} & \frac{1}{2} \\ 0 & \cdots & \cdots & \cdots & 0 & 0 & 1 \end{pmatrix} \qquad \mathcal{A}_{(1,N)} = \begin{pmatrix} \frac{1}{2} & 1 & \frac{1}{2} & 0 & \cdots & 0 \\ 0 & \ddots & \ddots & \ddots & \ddots & \vdots \\ \vdots & \ddots & \ddots & \ddots & \ddots & 0 \\ \vdots & & \ddots & \ddots & \ddots & \frac{1}{2} \\ \vdots & & & \ddots & \frac{1}{2} & 1 \\ 0 & \cdots & \cdots & \cdots & 0 & 1 \end{pmatrix} \tag{B.2.6}$$

One observes that for $1 < i < N-1$ the sub-matrix $\mathcal{A}_{(1,i)}$ decomposes into the block matrix

$$\mathcal{A}_{(1,i)} = \begin{pmatrix} B^{(i-1)} & * \\ \mathbf{0} & \mathcal{A}^{(N-i)} \end{pmatrix} \tag{B.2.7}$$

Here B is a triangle matrix whose diagonal elements are all $\frac{1}{2}$, $\mathcal{A}^{(N-i)}$ is a $N - i \geq 2$ dimensional version of $\mathcal{A}$, and $*$ is a matrix whose elements are not important for the current discussion. For $i = 1$, then $\mathcal{A}_{(1,1)} = \mathcal{A}^{N-1}$. For $i = N-1$ and $i = N$, then $\mathcal{A}_{(1,i)}$ is a triangle matrix with diagonal elements being either $\frac{1}{2}$ or 1. The first column of the adjoint matrix will then take the form of

$$\mathrm{adj}(\mathcal{A})_{i1} = \begin{cases} \det \mathcal{A}^{(N-1)} & \text{for} \quad i = 1 \\ (-1)^{1+i} \det B^{(i-1)} \det \mathcal{A}^{(N-i)} & \text{for} \quad 1 < i < N-1 \\ (-1)^{i+1} \left(\frac{1}{2}\right)^{N-1} & \text{for} \quad i \in \{N-1, N\} \end{cases} \tag{B.2.8}$$

Since the determinant of a triangle matrix is the product of its diagonal elements then, because the diagonal elements of $B^{(M)}$ are all $\frac{1}{2}$, one gets that

$$\det B^{(M)} = \frac{1}{2^M} \tag{B.2.9}$$

which implies that

$$\mathrm{adj}(\mathcal{A})_{i1} = \begin{cases} \det \mathcal{A}^{(N-1)} & \text{for} \quad i = 1 \\ (-1)^{1+i} \frac{1}{2^{i-1}} \det \mathcal{A}^{(N-i)} & \text{for} \quad 1 < i < N-1 \\ (-1)^{1+i} \frac{1}{2^{i-1}} & \text{for} \quad i \in \{N-1, N\} \end{cases} \tag{B.2.10}$$

To get the determinant of the $\mathcal{A}^{(M)}$ matrices, one defines the set $\{f_M\}$ as

$$f_M = (-\tau)^M \det \mathcal{A}^{(M)} \tag{B.2.11}$$

for $M \geq 2$. These numbers satisfies the following recursive relation

$$f_M = f_{M-1} - \frac{1}{4} f_{M-2} \tag{B.2.12}$$

which can be shown using Laplacian expansion of f_M. This difference equation can be solved using the method described in Tom Lindstrøm's Kalkulus[25], which gives solution

$$f_M = \frac{A + MB}{2^M} \tag{B.2.13}$$

since

$$f_2 = \det \begin{pmatrix} 1 & \frac{1}{2} \\ 1 & 1 \end{pmatrix} = \frac{1}{2} \quad \text{and} \quad f_3 = \det \begin{pmatrix} 1 & \frac{1}{2} & 0 \\ \frac{1}{2} & 1 & \frac{1}{2} \\ 0 & 1 & 1 \end{pmatrix} = \frac{1}{4} \tag{B.2.14}$$

then

$$\frac{A+3B}{8} = \frac{1}{4} \quad \text{and} \quad \frac{A+2B}{4} = \frac{1}{2} \Leftrightarrow (A = 2 \text{ and } B = 0) \tag{B.2.15}$$

Therefore

$$f_M = \frac{1}{2^{M-1}} \Rightarrow \det \mathcal{A}^{(M)} = \frac{1}{2^{M-1}} \tag{B.2.16}$$

The first column of the adjoint matrix is therefore

$$\mathrm{adj}(\mathcal{A})_{i1} = (-1)^{i+1} \frac{1}{2^{N-2}} \tag{B.2.17}$$

for all $i \in \{1, \cdots, N\}$. The first column of the inverse matrix is therefore

$$\left(\mathcal{A}^{-1}\right)_{i1} = \frac{1}{\det \mathcal{A}^{(N)}} (-1)^{i+1} \frac{1}{2^{N-2}} = 2(-1)^{i+1} \tag{B.2.18}$$

The long-term behaviour of $\mathbf{m}$ will therefore be

$$\left(\lim_{t\to\infty} \mathbf{m}(t)\right)_i = \left(\mathcal{A}^{-1}\mathbf{g}\right)_i = -\frac{1}{2}\left(\mathcal{A}^{-1}\right)_{i1} = (-1)^i \tag{B.2.19}$$

which was what was needed to be calculated.

Appendix C

Classical Numerics appendix

C.1 Overview of input variables

In this section, the input to the Gillespie_cy Cython extension class is presented as well as which values they accept. In total, the simulation object takes nine inputs being:

- J - Python object that described the nearest neighbour coupling between spins.
- h - Python object that described the longitudinal field over the system.
- init - Python object that described the initial state configuration.
- N - The number of spins in the system as an Python int or a C int
- Temp - The temperature of the system as a Python float or a C double. Infinite temperature is represented as then Temp = -1.
- Nmax - The maximum number of times the main loop is ran before the simulation is stopped. Has $100N$ as a default value.
- delta - The Glauber parameter δ represented as a Python float or a C double. Has zero as its default value.
- run_sim - Boolean flag to tell the simulation if it should run the simulation when a given instance of the Gillespie_cy object is created. True is its default value.
- PBC - A boolean flag that is true if the system has periodic boundary conditions. PBC is false on default.

For different types and values of the three general Python objects, being J, h, and init, different arrays are created representing the physical parameters given from the inputs. This is done using the get_J_att, get_h_att, and get_initial_att methods which translates certain inputs into attribute of the Gillespie_cy object. These methods are described here.

C.2 get_J_att and get_h_att

Even thou the J and h attributes represents very different physical parameters, they are still very similar in terms of variables. Both are arrays with equal length being the number of sites, N whose elements are all C doubles. The inputs J and h can therefore also take similar values and types. The only exception to this is that the h input can take an extra input compared to the J input. This will be noted thou. The input are:

List of inputs		
Type	Value	Description
int/float	any real number	Generate a homogeneous array with elements being the input value.
list/numpy.ndarray	elements can take any value	The elements of the input is copied to attribute. If the input object is too short, the rest of the elements in the attribute is set to zero. If the list is too long, the extra elements are ignored.
string	random	Pick the elements in the array from the uniform distribution [-1,1].
	random - (x,y)	Pick the elements in the array from a normal distribution with mean x and standard deviation y.
	local - (n,x)	The array has all its elements set to zero except the n'th site which is set to x. (h exclusive.)

C.3 get_initial_att

To get the initial configuration of the simulation, one uses the get_initial_att method is used. This is given the init variable as an input which.

List of inputs		
Type	Value	Description
int/float	[0,1]	Create an initial state with a given fraction of spin being spin down. (Rounded down)
list/numpy.ndarray	elements are either -1 or 1	The elements of the input is copied to attribute. If the input object is too short, the rest of the elements in the attribute is set to zero. If the list is too long, the extra elements are ignored.
string	AFMp	Array are on the form [1,-1,1,-1,$\cdots$]
	AFMm	Array are on the form [-1,1,-1,1,$\cdots$]
	FMp	All elements are 1
	FMm	All elements are -1
	DW - single - AFM - (x,n)	The initial state is an AFM ground state with the first site having the value x but with a domain wall introduced at site n
	DW - single - FM - (x,n)	The initial state is an FM ground state with the first site having the value x but with a domain wall introduced at site n

C.4 List of Gillespie_cy's methods

List of attributes				
Method	Type	Input	Output	Description
__cinit__	Python	object J, object h, object initial, int N, float temp, int Nmax, float delta, bint run_sim	-	run_sim optional and True by default. Initializes attributes and allocates memory for memoryview variables.
__init__	Python	object J, object h, object initial, int N, float temp, int Nmax, float delta, bint run_sim	-	Generates self.J, self.h, and self.initial_state. Also, even/odd magnetization and energy of initial state is calculated.
run_sim_cy	void	-	-	Run the Gillespie algorithm for a maximum of "Nmax" iterations
glauber_rates	void	int[:] config, double[:] rates	-	Calculate the Glauber rates given a configuration. Results saved in self.rates
overlaps	void	int[:] config	double mag, double ol	Calculate the magnetization and overlap with the AFM ground state "-+-+ ..." for the configuration "config"
get_J_att	Python	object J	-	Generate the nearest neighbour couplings J_i according to sec. C.1
get_h_att	Python	object h	-	Generate the longitudinal field h_i according to sec. C.1
get_initial_att	Python	object initial	-	Generate the initial configuration according to sec. C.1
run_sim	Python			
get_attributes_py	Python			

Appendix D

Theorems of used in Open 1D transverse field Ising model

D.1 Othornormality of ϕ and ψ

In chapter 6.2.3 the eigenvectors of the matrices $\mathbf{M}_1$ and $\mathbf{M}_2$ are claimed to form two orthonormal sets. This is proven here by using the symmetric and antisymmetric properties of $\mathbf{A}$ and $\mathbf{B}$ respectively. Since $\mathbf{A}$ is symmetric, $\mathbf{A}^T = \mathbf{A}$, and $\mathbf{B}$ is skew-symmetric,$\mathbf{B}^T = -\mathbf{B}$, then the matrices $\mathbf{M}_1$ and $\mathbf{M}_2$ are symmetric.

$$\mathbf{M}_1^T = ((\mathbf{A}-\mathbf{B})(\mathbf{A}+\mathbf{B}))^T = (\mathbf{A}+\mathbf{B})^T(\mathbf{A}-\mathbf{B})^T = (\mathbf{A}-\mathbf{B})(\mathbf{A}+\mathbf{B}) = \mathbf{M}_1 \tag{D.1.1}$$

$$\mathbf{M}_2^T = ((\mathbf{A}+\mathbf{B})(\mathbf{A}-\mathbf{B}))^T = (\mathbf{A}-\mathbf{B})^T(\mathbf{A}+\mathbf{B})^T = (\mathbf{A}+\mathbf{B})(\mathbf{A}-\mathbf{B}) = \mathbf{M}_2. \tag{D.1.2}$$

Since the vectors $\{\phi_k\}$ are eigenvectors of $\mathbf{M}_1$ and all have different eigenvalues, one can prove that they are indeed orthogonal to each other. This is done using the inner product $\phi_k^T\mathbf{M}_1\phi_{k'}$. One can evaluate this product in two way. Either with respect to $\vec{\phi}_k$ or with respect to $\vec{\phi}_{k'}$.

$$\lambda_{k'}\phi_k^T\phi_{k'} = \phi_k^T\mathbf{M}_1\phi_{k'} = (\phi_{k'}^T\mathbf{M}_1^T\psi_k)^T = (\phi_{k'}^T\mathbf{M}_1\psi_k)^T = \lambda_k(\phi_{k'}^T\psi_k)^T = \lambda_k\phi_k^T\psi_{k'} \tag{D.1.3}$$

$$\lambda_{k'}\psi_k^T\psi_{k'} = \psi_k^T\mathbf{M}_2\psi_{k'} = (\psi_{k'}^T\mathbf{M}_2^T\psi_k)^T = (\psi_{k'}^T\mathbf{M}_2\psi_k)^T = \lambda_k(\psi_{k'}^T\psi_k)^T = \lambda_k\psi_k^T\psi_{k'}. \tag{D.1.4}$$

Subtracting the l.h.s. from the r.h.s., one gets the follow

$$0 = (\lambda_k - \lambda_{k'})\phi_k^T\phi_{k'} \Leftrightarrow \lambda_k = \lambda_{k'} \text{ or } \phi_k^T\phi_{k'} = 0 \tag{D.1.5}$$

$$0 = (\lambda_k - \lambda_{k'})\psi_k^T\psi_{k'} \Leftrightarrow \lambda_k = \lambda_{k'} \text{ or } \psi_k^T\psi_{k'} = 0 \tag{D.1.6}$$

Since $\lambda_k = \lambda_{k'}$ if and only if $k = k'$ for $g \neq 0$, then $\phi_k^T\phi_{k'} = \psi_k^T\psi_{k'} = 0$ and for $k \neq k'$. Since the vectors are also normalized, the two sets of eigenvectors $\{\psi_k\}$ and $\{\phi_k\}$ both form orthonormal sets.

D.2 Inverse Bogoliubov transformation

In the main text it is claimed that

$$c_i^\dagger = \sum_k \alpha_{ki}\eta_k^\dagger + \beta_{ki}\eta_k \quad \text{and} \quad c_i = \sum_k \alpha_{ki}\eta_k + \beta_{ki}\eta_k^\dagger \tag{D.2.1}$$

forms the inverse Bogoliubov transformation. This can be proven by inserting eq. (6.2.18) into eq. (D.2.1). This results in

$$\sum_k \alpha_{ki}\eta_k^\dagger + \beta_{ki}\eta_k = \sum_{k,j} (\alpha_{ki}\alpha_{kj} + \beta_{ki}\beta_{kj})\, c_j^\dagger + (\alpha_{ki}\beta_{kj} + \beta_{ki}\alpha_{kj})\, c_j \tag{D.2.2}$$

$$\sum_k \alpha_{ki}\eta_k + \beta_{ki}\eta_k^\dagger = \sum_{k,j} (\alpha_{ki}\alpha_{kj} + \beta_{ki}\beta_{kj})\, c_j + (\alpha_{ki}\beta_{kj} + \beta_{ki}\alpha_{kj})\, c_j^\dagger \tag{D.2.3}$$

Expanding the parenthesis in terms of $\vec{\phi}_k$ and $\vec{\psi}_k$, one gets

$$\alpha_{ki}\alpha_{kj} + \beta_{ki}\beta_{kj} = \frac{1}{2}\left(\phi_{ki}\phi_{kj} + \psi_{ki}\psi_{kj}\right) \quad \text{and} \quad \alpha_{ki}\beta_{kj} + \beta_{ki}\alpha_{kj} = \frac{1}{2}\left(\phi_{ki}\phi_{kj} - \psi_{ki}\psi_{kj}\right) \tag{D.2.4}$$

since $\alpha_{ki} = \frac{1}{2}(\phi_{ki} + \psi_{ki})$ and $\beta ki = \frac{1}{2}(\phi_{ki} - \psi_{ki})$. From the orthonormality of $\{\psi_k\}$ and $\{\phi_k\}$, proven in appendix. D.1, it is possible to prove that $\sum_k \phi_{ki}\phi_{kj} = \sum_k \psi_{ki}\psi_{kj} = \delta_{ij}$. The proof goes as following: First one defines the matrices $J_{ij} = \sum_k \phi_{ki}\phi_{kj}$ and $K_{ij} = \sum_k \psi_{ki}\psi_{kj}$. Second, one observes that for a general vector $\mathbf{v}$ which can be written in the eigenvectors

$$\mathbf{v} = \sum_{k=1}^{N} a_k\vec{\phi}_k = \sum_{k=1}^{N} b_k\vec{\psi}_k \tag{D.2.5}$$

Applying the matrices $\mathbf{J}$ and $\mathbf{K}$ one the vector $\mathbf{v}$ which results in

$$(\mathbf{Jv})_i = \sum_j J_{ij}v_j = \sum_{k,k'} \phi_{k'i}a_{k'} \sum_j \phi_{k'j}\phi_{kj} = \sum_{k,k'} \phi_{k'i}a_{k'}\delta_{kk'} = \sum_k a_k\phi_{ki} = v_i \tag{D.2.6}$$

$$(\mathbf{Kv})_i = \sum_j K_{ij}v_j = \sum_{k,k'} \psi_{k'i}b_{k'} \sum_j \psi_{k'j}\psi_{kj} = \sum_{k,k'} \psi_{k'i}b_{k'}\delta_{kk'} = \sum_k b_k\psi_{ki} = v_i \tag{D.2.7}$$

In the first equality, $\mathbf{v}$ is expanded in terms of the two sets of eigenvector. In the second equality, $\mathbf{J}$ and $\mathbf{K}$ are expanding in terms of the eigenvectors. In the third equality, the the orthonormal properties are used. J and K are therefore the identity matrix since both matrices transforms all vectors to themselves. Therefore $J_{ij} = K_{ij} = \delta_{ij}$. Using this, eq. (D.2.4) reduces to

$$\sum_k \left(\alpha_{ki}\alpha_{kj} + \beta_{ki}\beta_{kj}\right) = \delta_{ij} \quad \text{and} \quad \sum_k \left(\alpha_{ki}\beta_{kj} + \beta_{ki}\alpha_{kj}\right) = 0 \tag{D.2.8}$$

which implies

$$\sum_k \alpha_{ki}\eta_k^\dagger + \beta_{ki}\eta_k = \sum_j \delta_{ij}c_j^\dagger + 0c_j = c_j^\dagger \tag{D.2.9}$$

$$\sum_k \alpha_{ki}\eta_k + \beta_{ki}\eta_k^\dagger = \sum_j \delta_{ij}c_j + 0c_j^\dagger = c_j \tag{D.2.10}$$

One can therefore conclude that eq. (D.2.1) must be true.

Bibliography

[1] Terry Farrelly. A review of Quantum Cellular Automata. *Quantum*, 4:368, Nov 2020.

[2] Karoline Wiesner. Quantum Cellular Automata. In *Encyclopedia of Complexity and Systems Science*, pages 7154–7164. Springer, New York, NY, New York, NY, USA, 2009.

[3] Gregory S. Engel, Tessa R. Calhoun, Elizabeth L. Read, Tae-Kyu Ahn, Tomáš Mančal, Yuan-Chung Cheng, Robert E. Blankenship, and Graham R. Fleming. Evidence for wavelike energy transfer through quantum coherence in photosynthetic systems. *Nature*, 446(7137):782–786, Apr 2007.

[4] C. M. Chandrashekar. Discrete-Time Quantum Walk - Dynamics and Applications. *arXiv*, Jan 2010.

[5] Joel E. Moore. The birth of topological insulators. *Nature*, 464(7286):194–198, Mar 2010.

[6] Masoud Mohseni, Patrick Rebentrost, Seth Lloyd, and Alán Aspuru-Guzik. Environment-Assisted Quantum Walks in Photosynthetic Energy Transfer. *arXiv*, May 2008.

[7] P. Douglas Tougaw and Craig S. Lent. Logical devices implemented using quantum cellular automata. *J. Appl. Phys.*, 75(3):1818–1825, Feb 1994.

[8] John Timler and Craig S. Lent. Power gain and dissipation in quantum-dot cellular automata. *J. Appl. Phys.*, 91(2):823–831, Jan 2002.

[9] Stephen Wolfram. Statistical mechanics of cellular automata. *Rev. Mod. Phys.*, 55(3):601–644, Jul 1983.

[10] Softology. Multiple Neighborhoods Cellular Automata, Mar 2018. [Online; accessed 12. May 2021].

[11] Softology. 3D Cellular Automata, Dec 2017. [Online; accessed 12. May 2021].

[12] Softology. 4D Cellular Automata, Dec 2017. [Online; accessed 12. May 2021].

[13] D. G. Green, A. P. N. House, and S. M. House. Simulating spatial patterns in forest ecosystems. *Math. Comput. Simul.*, 27(2):191–198, Apr 1985.

[14] D. G. Green. Cellular automata models in biology. *Math. Comput. Model.*, 13(6):69–74, Jan 1990.

[15] John E. Hopcroft and Jeffrey D. Ullman. *Formal languages and their relation to automata.* Addison-Wesley Longman Publishing Co., Inc., Jan 1969.

[16] Eric W. Weisstein. Elementary Cellular Automaton. *Wolfram Research, Inc.*, Apr 2002.

[17] P. Douglas Tougaw and Craig S. Lent. Dynamic behavior of quantum cellular automata. *J. Appl. Phys.*, 80(8):4722–4736, Oct 1996.

[18] Stephen G. Brush. History of the Lenz-Ising Model. *Rev. Mod. Phys.*, 39(4):883, Oct 1967.

[19] Ernst Ising. Beitrag zur Theorie des Ferromagnetismus. *Z. Phys.*, 31(1):253–258, Feb 1925.

[20] Stefan Bornholdt. Expectation bubbles in a spin model of markets: Intermittency from frustration across scales. *arXiv*, May 2001.

[21] Zoltán Rácz. *Kinetic Ising models with competing dynamics: mappings, correlations, steady states, and phase transitions*. Cambridge University Press, 1997.

[22] Stephen J. Cornell. 1D kinetic Ising models at low temperatures—critical dynamics, domain growth, and freezing. In *Nonequilibrium Statistical Mechanics in One Dimension*, pages 111–140. Cambridge University Press, Cambridge, England, UK, Feb 1997.

[23] Roy J. Glauber. Time-Dependent Statistics of the Ising Model. *J. Math. Phys.*, 4(2):294–307, Feb 1963.

[24] Kyozi Kawasaki. Diffusion Constants near the Critical Point for Time-Dependent Ising Models. I. *Phys. Rev.*, 145(1):224–230, May 1966.

[25] Tom Lindstrøm. *Kalkulus*. 4 edition.

[26] Tage Gutmann Madsen Søren Eliers, Ernst Hansen. *Indledende Matematisk Analyse*. Institut for matematiske fag, 8 edition, 2016.

[27] A general method for numerically simulating the stochastic time evolution of coupled chemical reactions, Dec 1976. [Online; accessed 25. May 2021].

[28] Cython - an overview — Cython 3.0a7 documentation, Jun 2021. [Online; accessed 19. Jun. 2021].

[29] Kurt W. Smith. *Cython*. O'Reilly Media inc., 1005 Gravenstein Highway North, Sebastopol, CA 95472, Jan 2015.

[30] Daniel T. Gillespie. Stochastic Simulation of Chemical Kinetics. *Annu. Rev. Phys. Chem.*, 58(1):35–55, Apr 2007.

[31] Typed Memoryviews — Cython 3.0.0a9 documentation, Aug 2021. [Online; accessed 24. Aug. 2021].

[32] Basic Tutorial — Cython 3.0.0a9 documentation, Aug 2021. [Online; accessed 25. Aug. 2021].

[33] Barlow R. J. *Statistics*. John Wiley and Sons, July 1999.

[34] numpy.polynomial.polynomial.Polynomial.fit — NumPy v1.21 Manual, Jun 2021. [Online; accessed 30. Aug. 2021].

[35] Wigner E. Jordan, P. Über das paulische Äquivalenzverbot. *Z. Physik 47*, 47, 1928.

[36] Subir Sachdev. *Quantum Phase Transitions*. Cambridge University Press, 2 edition, 2011.

[37] Glen Bigan Mbeng, Angelo Russomanno, and Giuseppe E. Santoro. The quantum ising chain for beginners, 2020.

[38] A Yu Kitaev. Unpaired majorana fermions in quantum wires. *Physics-Uspekhi*, 44(10S):131–136, Oct 2001.

[39] Nico Leumer, Magdalena Marganska, Bhaskaran Muralidharan, and Milena Grifoni. Exact eigenvectors and eigenvalues of the finite kitaev chain and its topological properties. *Journal of Physics: Condensed Matter*, 32(44):445502, aug 2020.

[40] Yan He and Hao Guo. The boundary effects of transverse field ising model. *Journal of Statistical Mechanics: Theory and Experiment*, 2017(9):093101, Sep 2017.

[41] Elliott Lieb, Theodore Schultz, and Daniel Mattis. Two soluble models of an antiferromagnetic chain. *Annals of Physics*, 16(3):407 – 466, 1961.

[42] Robert Messer. *Linear Algebra*. Albion college, Polyteknisk Boghandel, September 2019.